UNIVERSITY OF SOUTHAMPTON

Dynamics of Spacecraft Formation Flight

by

Shankar Kumar Priya Balaji

Submitted for the degree of Doctor of Philosophy

Faculty of Engineering, Science and Mathematics

School of Engineering Sciences

Aerospace Engineering

June 2005

UNIVERSITY OF SOUTHAMPTON

ABSTRACT

Faculty of Engineering, Science and Mathematics
School of Engineering Sciences

Aerospace Engineering

Doctor of Philosophy

Dynamics of Spacecraft Formation Flight

by Shankar Kumar Priya Balaji

In recent years, the need for spacecraft flying formation has increased significantly. Its diverse applications range from synthetic aperture radar systems, like TechSat-21 to science missions such as EO-1 or LISA. Correspondingly, many studies have been performed on the relative motion of a spacecraft with respect to a reference orbit. Much of the literature, building on the early work of Clohessy and Wiltshire, is focused on solving the relative motion between spacecraft in two closely placed circular orbits.

Their solution works fairly well for low eccentricity missions. Recently, however, several missions have been proposed, designed or flown that need spacecraft flying in formation about a highly elliptical reference orbit. Most of these missions, such as the Cluster, have space physics science objectives, which involve at least four spacecraft moving in a "tetrahedron" configuration at apogee. The shape and the separation of the configuration are designed to resolve spatial and temporal variations. In order to be able to analyze the relative motion of such missions, a novel approach of analyzing spacecraft relative motion is proposed in this thesis. The new approach deals with the derivation of the relative coordinates of a deputy satellite with respect to a master satellite by a series of Euler transformations and a translation from the Earth-centered inertial frame to the spacecraft-centered rotating frame. The equations of relative coordinates derived in this thesis are precise and can be used to analyze orbits of any eccentricity and of any initial separation with or without the inclusion of orbit perturbations. For perturbed relative orbits, a modified version of the Gauss perturbation equations using equinoctial variables are used to model the dynamics. Several initial conditions are simulated using the developed mathematical model including practical cases like spacecraft having differential drag effects. Based on the simulation results, the amount of fuel required for formation and station keeping is estimated for different formation patterns. The problems associated with formation assembly are addressed and an algorithm to find the orbital elements from the knowledge of relative coordinates is proposed. The assessment of the relative motion due to perturbations is imperative for selecting the actuators for station keeping, designing control laws and deciding whether to use relative or absolute station-keeping methods.

Table of Contents

List of Figures

List of Tables

ACKNOWLEDGEMENTS

Life in the form of a human being has so far provided me with various opportunities to meet different people and visit different places. The most valuable of all meetings so far has been with my advisor Dr. Adrian Tatnall who with his patience and expertise has shown me the gateway to research and knowledge.

Although, I have not achieved anything like Einstein to be very proud of, the fact that I have contributed a few papers to the research community makes me feel happy and I owe this happiness to Dr. Tatnall. He has sometimes guided me like my father and helped me recover from difficult financial situations and I really appreciate his kindness and I am thankful to him.

I would also like to extend my gratitude to all my colleagues at the Astronautics Research group who with their Astro humour made me feel relaxed and entertained while pursuing my research. I am thankful to Professor Steve Gabriel and Dr. Anna Barney for helping me with references. I am also thankful to Dr. Craig Underwood of the University of Surrey for his very valuable comments on my thesis.

I owe my life and happiness to my parents and my younger brother who have always guided me in taking the right decisions including that of a doing a PhD. I will particularly never forget my stay in Southampton for the fact that both of my lovely sons were born here and I got promoted to a status of a Father. I thank my wife for making that promotion possible and also for her patience and understanding throughout my candidature.

NOMENCLATURE

a – semi-major axis

$\bar{a}_r$ – acceleration along the position vector r

$\bar{a}_t$ – acceleration in the velocity vector direction

$\bar{a}_z$ – acceleration in the normal direction

a_s – mean distance of the Earth from the sun

c – speed of light in vacuum

C_d – coefficient of drag

e – eccentricity

$\bar{e}_r$ – unit vector along the satellite orbit radius vector direction

$\bar{e}_t$ – unit vector along the local horizontal direction

$\bar{e}_z$ – unit vector along the orbit normal direction

F – solar energy flux at the spacecraft

h – angular momentum

i – inclination

J_2 – geo potential coefficient representing Earth's Oblateness, $J_2 = 1082.64 \times 10^{-6}$

m – mass of spacecraft

M – Mean anomaly

n – Mean motion

p – semilatus rectum

$\vec{R}$ – position vector of the satellite

r_e – Radius of earth, $r_e = 6371 \times 10^6 km$,

r_s - distance of the satellite from the sun

S – projected area of the spacecraft in the direction of motion

t – time

$\left[T_{ui\Omega}\right]_m$ – transformation matrix from frame $OXYZ$ to $OPQR$

$\left[T_{\Omega iu}\right]_d$ – transformation matrix from frame $(oxyz)_d$ to $OXYZ$

V_t, V_r, V_n – Spacecraft velocity in along-track, radial and orbit normal directions respectively

u – argument of latitude, $u = \theta + \omega$

Ω – right ascension of the ascending node

ω – argument of perigee

θ – true anomaly

μ – gravitational earth constant, $\mu = 3.986 \times 10^{14} m^3 / s^2$

ε – obliquity of the ecliptic

$\lambda_\odot$ – ecliptic longitude of the sun

ξ – constant of surface reflection

$\delta\alpha$ – Variation of variable α with respect to the chief orbit

Subscripts

d – refers to the deputy satellite
m – refers to the master satellite
0 – refers to the initial conditions

GRACE - Gravity Recovery and Climate Experiment

GPS - Global Positioning Systems

NASA- National Aeronautics and Space Administration

ESA- European Space Agency

MST- Micro Satellite Technology

ASO-Astronomical Search for Origins

SEC-Sun Earth Connections

SSE-Solar System Exploration

SEU- structure and Evolution of the Universe

CW- Clohessy-Wiltshire

XEUS - X-Ray Evolving Universe Spectroscopy Mission

Chapter 1
Introduction

1.1 Satellite Formation Flight

The concept of satellite formation flying has been a topic of considerable study for well over a decade. In fact, Visher[1] was given a patent for the concept in 1983. Formation flying can be defined as the co-ordinated motion control of a group of vehicles where the vehicle positions relative to each other are important. The reasons for using a satellite cluster or formation, as opposed to a single larger satellite, include providing on-orbit redundancy, reliability, survivability, reducing cost and improved performance (or possibly enabling performance that cannot be accomplished via a single satellite). An example demonstrates these gains easily. Imagine a satellite cluster comprised of ten satellites. Each satellite within the cluster contributes to the overall objective of the system. If one were to fail, the integrity of the system is not totally lost as the remaining nine can still function to achieve mission objectives. While the overall capability of the system may be temporarily diminished, it is not completely lost. Also, if the cluster is operating with more than the required number of elements to perform its objectives, the mission may not experience any degradation to its minimum advertised capability due to the on-orbit redundancy. The above example illustrated continued system performance during a failure, and thus improved reliability. A related concept to reliability is survivability. Survivability also implies continued performance after the infliction of damage due to on-orbit mishaps. Concisely, the advantages of a satellite cluster over a single large satellite are:

- Each spacecraft is smaller, lighter, simpler, and simpler to manufacture;
- Economies of scale enable a cluster of many satellites to be less expensive to manufacture than a single satellite;
- The cluster can adapt to the failure of any individual satellites, and failed satellites can be incrementally replaced;

- The cluster can reconfigure the orbits of the satellites in the cluster to optimize for different missions.

Formation flying of multiple spacecraft is an enabling technology for many future space missions. Earth and Space scientists are just beginning to understand the full potential of spacecraft formation flying. For example, the current complement of Earth Science missions perform somewhat infrequent measurements of targeted areas of the Earth using very large, expensive spacecraft platforms (e.g. Landsat-7 which takes 16 days to retrace its ground swath). In the future, swarms of inexpensive miniature space vehicles, flying in formation, will replace these expensive spacecraft platforms. These spacecraft formations will provide continuous measurements of the processes and events affecting the Earth. Space science will also be significantly impacted by formation flying technology. For example, the space science community' s ability to understand the events and processes that occur between the Sun and the Earth (the so called Sun-Earth connection) is limited to a just a few spacecraft in various Earth and Heliocentric orbits. A significant improvement in the understanding of the dynamics of the magnetosphere can be accomplished if these spacecraft were replaced by a constellation of miniature science probes flying around the Earth and Sun in a loose formation. Significant improvements in space-based interferometery can be accomplished by flying several spacecraft in formation, increasing the number of instruments comprising the system & eliminating the restrictions imposed by the use of physical structures to establish maintain, and control instrument separation and stability. The benefits of formation flying are countless and there is no doubt that it is currently one of the very interesting topics in the space industry.

1.2 Proposed Formation Flying Missions

Converting the Formation flying vision into reality is a formidable task and several research organizations are currently involved in developing new technologies for the successful realization of planned missions. In fact, the first successful Formation Flying mission, GRACE (Gravity Recovery and Climate Experiment) mission comprising of two identical satellites was successfully launched in March 2002 into a 500 km polar orbit with a satellite

separation of 220 km. The GRACE mission aims to map the Earth's gravity fields by making measurements of the distance between the two satellites, using GPS (Global Positioning Systems) and a microwave ranging system. According to the latest information from mission sources, the GRACE mission has provided much more information on the earth's gravitational field than what was gained in over 30 years of previous study.

Although most of the planned missions are funded by government organizations like NASA and ESA, a number of missions are now being planned and sponsored by various universities and private organizations like AeroAstro. One of such several planned Formation Flying programmes is the U.K. university-led technology demonstration programme proposed by Southampton University, Cranfield University and Astrium. The main objectives of the programme are to build and launch two identical satellites of approximately 10 kg mass each in to a 600 km, circular polar orbit, within a period of two years and demonstrate the use of MST (Micro Satellite Technology) in space and aspects of collaborative control. The programme also aims to demonstrate Formation Flight at very small distances, of the order of 100 meters or less. There are several other university led programmes proposed in the United States like the 3CS (Three CornerSat). This programme is a joint venture of three universities namely, The Colorado State University, Arizona State University and New Mexico State University. The 3CS mission has three primary objectives; Stereoscopic Imaging, Virtual-Formation Communications and Distributed and Automated Operations. A list of planned missions for this and the next decade is given in Table 1.1

Projected Launch Year	Mission Name	Mission Type
2007	Magnetospheric Multiscale (MMS)	Space Science/SEC
2007	Space Interferometry Mission (SIM)	Space Science/ASO
2007	Submillimeter Probe of the Evolution of Cosmic Structure (SPECS)	Space Science/SEU
2007	Cold Land Processes Research Mission (EX-7)	Earth Science
2007	Vegetation Recovery Mission (EX-6)	Earth Science

2007	Time-Dependent Gravity Field Mapping Mission (EX-5)	Earth Science
2007	Leonardo (GSFC)	Earth Science
2007	Soil Moisture and Ocean Salinity Observing Mission (EX-4)	Earth Science
2007	Global Precipitation Mission (EOS-9)	Earth Science
2007	Geospace Electrodynamic Connections (GEC)	Space Science/SEC
2008	Constellation-X	Space Science/SEU
2008	Magnetospheric Constellation (MC)	Space Science/SEC
2009	DARWIN Space Infrared Interferometer/European Space Agency	Space Science
2011	Laser Interferometric Space Antenna (LISA)	Space Science/SEU
2011	Terrestrial Planet Finder	Space Science/ASO
2011	Astronomical Low Frequency Array (ALFA)/Explorers	Space Science
2015	MAXIM X-ray Interferometry Mission	Space Science/SEU
2015	NASA Goddard Space Flight Center Earth Sciences Vision	Earth Science
2015	NASA Institute of Advanced Concepts/Very Large Optics for the Study	Space Science
2015	NASA Institute of Advanced Concepts /Structureless Extremely Large Yet Very Lightweight Swarm Array	Space Science
2015	NASA Institute of Advanced Concepts /Ultra-high Throughput X-Ray	Space Science

Table 1.1 - Representative List of Satellite Missions Utilizing Formation Flying Techniques

1.3 Formation Accuracy Requirements

Based on the required relative positional accuracy values, formation-flying missions can be categorized as

- Coarse Formation flying missions
- Precise Formation flying missions

The coarse formation flying missions are those that require relative positional accuracy of more than a few centimeters. One such formation-flying application is the formation of synthetic aperture radar such as the Astrium's TerraSAR-L [2]. These types of formations are typically considered in LEO remote sensing missions where each satellite is an individual element of a large, virtual antenna formed by the formation. By sharing the individual measurements, the resolution of the spacecraft cluster is potentially much higher then the resolution of any individual craft. Remaining in a close formation would allow the satellites to share information and computing ability among themselves. For such missions, it might be unnecessary to maintain extremely precise relative positions; rather, it might be sufficient to know the relative position accurately, and to remain in close enough proximity to allow intercraft communication. Another example of coarse formation-flying is a stereo imaging mission like the ThreeCornerSat[3]. For the mission to be accomplished the locations of the satellites will need to be " in range" and mutually known in order for each to support its portion of the mission, but physical proximity is not a requirement for the formation network. Stereo imaging only requires a nominal spacing of tens of kilometres. The accuracy requirements for such missions are in the order of few metres.

The Precise formation-flying missions are those, which require a relative positional tolerance of less than a millimeter to a few centimeters. Spaceborne optical stellar interferometry is one such example. Optical stellar interferometry involves the usage of mirrors to reflect the collected light (wavelengths 500-900 nanometers) from a distant body to one of the spacecraft that will also serve as the combiner. Because of the modest collecting area, the faintest measurable sources will have visual magnitudes in the range 10 to 12. The interferometric baselines may vary in length from perhaps 50-1000 m. In order to meet the mission goals of such a mission, the control system must maintain the distances between spacecraft to within 1-2 cm, and the relative orientations of the spacecraft within 1 arcminute per axis. Another example of a precise formation-flying mission is the proposed X-Ray spectroscopy mission, XEUS [4] that aims to study black holes & intergalactic medium. The mission proposes to use two spacecraft in LEO with a separation distance of 50 meters. Since the proposed relative separation also serves the purpose of the focal length of the onboard

mirrors, the relative positional accuracy has to be maintained with an accuracy of less than 1 millimetre.

The practical applications of formation-flying missions are open to both earth-based and deep space-based missions. For LEO formation flying missions requiring accuracy of less than centimeter, such as the X-ray spectroscopy mission and the optical interferometry mission, the limitations come in the form of mission lifetime. The deep space missions are also vulnerable to perturbative accelerations caused by solar wind, planetary attraction etc and the magnitude of the relative drift between the spacecraft depends on the spacecraft separation, distance from the sun etc. Therefore missions like spaceborne optical interferometry require very precise sensors and large amount of fuel to maintain the relative distance to an accuracy of few millimeters. The success of such missions depends on the development of new technologies in the field of precise orbit determination and control.

1.4 Problem Description /Objectives

The main motivation behind this thesis was the UK university-led Technology demonstration programme that aimed at building and launching two nano-satellites into a circular polar orbit of 600 km. Although this university-led nano-Satellite programme no longer exists at the time of writing this thesis, it was the main motivation behind this research on Formation Flight Dynamics. According to the original programme, it was planned to design and fly 2 spacecraft of 10 kg each at a separation distance of 100 meters and the universities involved in it were to share the tasks associated with mission design including relative trajectory analysis. The relative trajectory analysis was one of the first and foremost issues concerned with the mission design and at the time of proposal there was very little information about the stability and amount of fuel needed to maintain formation patterns. This motivated the author to pursue research on Formation flight Dynamics Analysis.

The main objective of this thesis is to analyze the dynamics of Formation flight and to address the issues concerned with formation stability, propellant utilization and orbit establishment. Analysis of the relative dynamics will help to plan the fuel budget, select the optimal orbital parameters and design the controller algorithm.

Spacecraft Formation flying is conceptually simple, but it can pose significant implementation challenges, because of the complex interrelationship of the principal design characteristics. Most formations are inherently unstable and will drift apart with time. Because of the perturbative forces and lack of any long-term stability, formation flying necessarily represents a compromise between formation structure, accuracy, long-term maintenance, and propellant utilization. One of the ways to understand the relationship between various design parameters is by analyzing the relative trajectory of the spacecraft in formation. The ability to control the formation with minimum resources requires a complete understanding of the behaviour of the formation in the presence of perturbative forces. The control accuracy has a great impact on the fuel budget and that in-turn has a great impact on the overall configuration of the spacecraft.

Arguably, the relative dynamics model is the most important part of a satellite formation's on-orbit estimator. Any inaccuracies in the dynamics model to predict the behavior of the formation will be returned in the form of perceived erratic behavior in the motion of the satellites by the filtering algorithm. On-board control mechanisms will then act upon this perceived erratic motion, resulting in the excessive use of station keeping fuel. This action would be especially unfortunate, as the erratic motion predicted may be nothing but harmless periodic motion. If left uncorrected this motion would show the satellites moving within a bounded envelope of space. With proper modeling to predict the movement of each spacecraft, this motion would be shown to not degrade the spacecraft's' mission and thus excessive maneuvering could be eliminated.

This thesis work will firstly focus on developing a novel model for relative trajectory analysis that is not based on the traditional Clohessy-Wiltshire (CW) method [5] and that can be used to analyze relative trajectories for any given condition. The method will be limitation free and support non-linear analysis of the formation flight problem. Secondly, with the help of the developed relative-trajectory model, the thesis will show how the orbit control requirements of the formation impose particular constraints on the overall spacecraft design.

To summarize. the thesis will

1. Develop a precise dynamical model of relative motion of formation-flying spacecraft.
2. Provide an insight into the relative motion of formation-flying spacecraft in the presence of all significant perturbative forces.
3. Identify and quantatize the secular drifts caused by the perturbative forces along all three axes with the developed dynamical model.
4. Investigate the rate of change of orbital elements and will find the ΔV requirements to compensate for the change in relative positions.
5. Study the behavior and stability of different formation-patterns.
6. Investigate the effects of altitude on the ΔV requirements of formation-flying spacecraft.
7. Investigate the effects of differential drag on cluster stability.
8. Identify the effects of initial separation on the control accuracy requirements.
9. Identify the practical technical issues concerned with Formation flight.
10. Address some of the system design issues related to formation-flight
11. Address the problem of orbit establishment

The organization and the contents of the different chapters of this thesis are shown below as a chart.

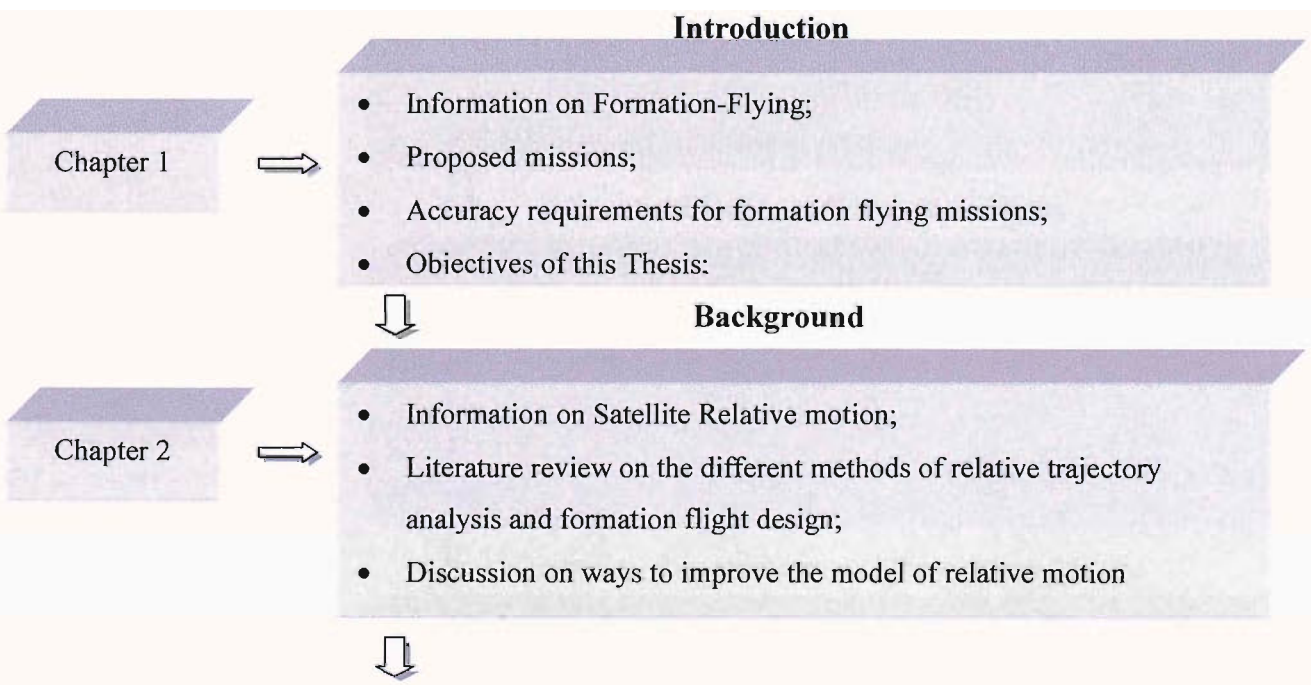

Methodology

Chapter 3 ⇨

- Authors attempt to model precise relative motion of satellites;
- Improvements to the model;
- Inclusion of various perturbative forces into the model;
- Relative trajectory simulation scheme;

⇩ **Properties of Spacecraft Orbits**

Chapter 4 ⇨

- Simulation of unforced and perturbed relative orbits;
- Effects of different initial conditions on the perturbed relative trajectory;
- Fuel consumption prediction;
- Comparison with CW equations and other methods

⇩ **Simulation of Other Test Cases**

Chapter 5 ⇨

- Analysis of different formation patterns;
- Effects of Differential drag on cluster stability;
- Fuel requirements for different test cases;

⇩ **Practical Issues of Formation Flight**

Chapter 6 ⇨

- Discussion on orbit establishment;
- Some practical system engineering issues concerned with spacecraft formation flight.

⇩ **Summary, Conclusions and Recommendations**

Chapter 7 ⇨

- Summary of the whole thesis
- Conclusions
- Ideas for possible future work

Chapter 2
Background

2.1 Spacecraft Relative motion

Relative spacecraft motion has long been a problem for mission analysts who plan rendezvous maneuvers. These planners look to the solution devised by Clohessy and Wiltshire[5] as their primary analysis tool. These two individuals reduced the problem of relative satellite motion to the familiar two-body problem by assuming circular orbits, linearizing the system, and then solving the resultant equations of motion. This problem was first looked at by Hill[6] in 1878, but it was revisited by Clohessy and Wiltshire in the 1960's and their work made it practical for engineers. While the original intent of these equations was to describe the relative motion of one closing spacecraft with respect to a target spacecraft, the Clohessy-Wiltshire (CW) solution has been the starting point of analysis for satellite formation dynamics.

2.1.1 Clohessy and Wiltshire Equations

Although the CW solution is not used for formation dynamics-analysis in this thesis, a brief description is warranted to highlight the reasons why it was necessary to develop a new method for relative trajectory analysis. As mentioned previously, the CW equations are the solution to the linearized circular orbit problem and in its simplest form, no perturbations are modeled. The differential form of the CW equations[5], for an earth-based scenario, is derived below;

Consider the situation in figure 2.1.1. The coordinate system $O-x-y-z$ moves with the origin (O) in a circular path at radius R with the axes so that x is along the radial direction and z is orthogonal to the orbit plane and y is in the along-track direction. The angular rate is related to the radial distance by $\omega^2 R^3 = \mu$.

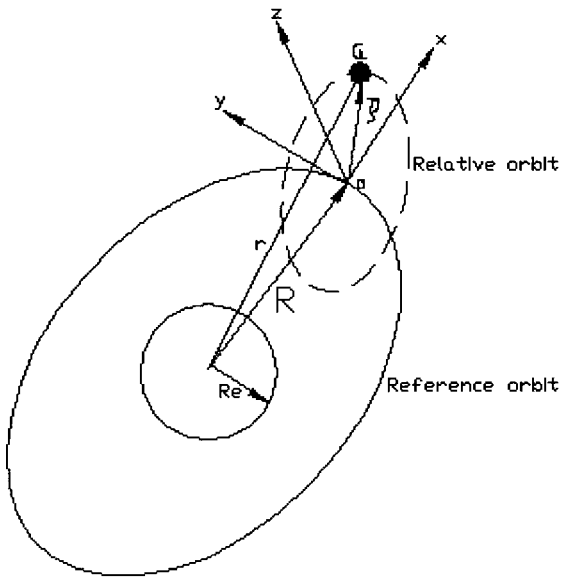

FIGURE 2.1.1 HILL FRAME

Now consider a master satellite, point *o*, moving in a circular orbit of radius *R* such that the *xyz* coordinate system moves along with it. In the *xyz* frame, *x* is the radial direction, *y* is the along-track direction of motion and *z* is perpendicular to the plane of orbit. The relative position of a deputy satellite *a* is

$$\vec{\rho} = x\vec{i} + y\vec{j} + z\vec{k} \tag{2.1.1.1}$$

The relative velocity is

$$\dot{\rho} = \dot{x}\vec{i} + \dot{y}\vec{j} + \dot{z}\vec{k} \tag{2.1.1.2}$$

The relative acceleration is

$$\ddot{\rho} = \ddot{x}\vec{i} + \ddot{y}\vec{j} + \ddot{z}\vec{k} \tag{2.1.1.3}$$

Now

$$\vec{R} = R\vec{i}$$

$$\ddot{\vec{R}} = -\omega^2 \vec{R} = -\omega^2 R\vec{i} \tag{2.1.1.4}$$

$$\ddot{\vec{r}} = \ddot{\vec{R}} + \ddot{\vec{\rho}} \tag{2.1.1.5}$$

Transformation of $\ddot{\vec{\rho}}$ yields

$$\vec{r} = \vec{R} + \vec{\rho} + 2\vec{\omega} \times \vec{\rho} + \vec{\omega} \times \vec{\rho} + \vec{\omega} \times (\vec{\omega} \times \vec{\rho})$$

$$= -R\omega^2 \vec{i} + \ddot{x}\vec{i} + \ddot{y}\vec{j} + \ddot{z}\vec{k} + 2\omega\vec{k} \times (\dot{x}\vec{i} + \dot{y}\vec{j} + \dot{z}\vec{k}) + \omega\vec{k} \times [\omega\vec{k} \times (x\vec{i} + y\vec{j} + z\vec{k})]$$

$$\ddot{\vec{r}} = (\ddot{x} - x2\omega\dot{y} - \omega^2 x - R\omega^2)\vec{i} + (\ddot{y} + 2\omega\dot{x} - \omega^2 y)\vec{j} + \ddot{z}\vec{k} \tag{2.1.1.6}$$

Now the equation of motion for a two-body problem in the inertial frame is

$$\ddot{\vec{r}} = -\frac{\mu}{r^3}\vec{r} + \vec{f}(t)$$

From the geometry of the problem

$$\ddot{\vec{r}} = \ddot{\vec{R}}(t) + \ddot{\vec{\rho}}(t) = -\frac{\mu}{\left\|R(t) + \rho(t)\right\|^3}\left[\vec{R}(t) + \vec{\rho}(t)\right] + \vec{f}(t) \tag{2.1.1.7}$$

$$\left\|\vec{R}(t) + \vec{\rho}(t)\right\|^{-3} = ([\vec{R}(t) + \vec{\rho}(t)].[\vec{R}(t) + \vec{\rho}(t)])^{-3/2}$$

$$= \left([\vec{R}.\vec{R}] + 2[\vec{R}.\vec{\rho}] + [\vec{\rho}.\vec{\rho}]\right)$$

$$= \frac{1}{R^3}\left(1 + \frac{[\vec{R}.\vec{\rho}]}{R^2} + \frac{[\vec{\rho}.\vec{\rho}]}{R^2}\right)^{-3/2}$$

$$r^{-3} = R^{-3}\left(1 + 1 + \frac{[\vec{R}.\vec{\rho}]}{R^2} + \frac{[\vec{\rho}.\vec{\rho}]}{R^2}\right)^{-3/2}$$

Expanding the left hand side of the expression by binomial theorem yields

$$r^{-3} = R^{-3}\left(1-\frac{3}{2}[2\frac{[\vec{R}.\vec{\rho}]}{R^2}+\frac{[\vec{\rho}.\vec{\rho}]}{R^2}]+.....\right)$$

Since $R >> \rho$

$$r^{-3} = R^{-3}\left(1-3\frac{[\vec{R}.\vec{\rho}]}{R^2}+.....\right)$$

Substitution of the above equation in equation 2.1.1.7 yields,

$$\ddot{\vec{r}} = \ddot{\vec{R}}(t)+\ddot{\vec{\rho}}(t) = -\frac{\mu}{R^3}\left[\vec{R}(t)+\vec{\rho}(t)-\frac{3}{R^2}(\vec{R}.\vec{\rho})\vec{R}+.....\right]+\vec{f}(t) \qquad (2.1.1.8)$$

Assuming the reference orbit to be circular

$$\ddot{\vec{R}} = -\frac{\mu}{R^3}\vec{R} = -\omega^2 R\vec{i} \qquad (2.1.1.9)$$

Substitution of equation 2.1.1.9 in equation 2.1.1.8 and then comparing it with equation 2.1.1.6, gives

$$(\ddot{x}-x2\omega\dot{y}-\omega^2 x)\vec{i}+(\ddot{y}+2\omega\dot{x}-\omega^2 y)\vec{j}+\ddot{z}\vec{k} = -\omega^2\left[\vec{\rho}(t)-\frac{3}{R^2}(\vec{R}.\vec{\rho})\vec{R}+..\right]+\vec{f}(t)$$

$$(\ddot{x}-x2\omega\dot{y}-\omega^2 x)\vec{i}+(\ddot{y}+2\omega\dot{x}-\omega^2 y)\vec{j}+\ddot{z}\vec{k} = -\omega^2\left[\vec{\rho}(t)-\frac{3}{R^2}(\vec{R}.\vec{\rho})\vec{R}+.....\right]+\vec{f}(t)$$

$$(\ddot{x}-x2\omega\dot{y}-\omega^2 x)\vec{i}+(\ddot{y}+2\omega\dot{x}-\omega^2 y)\vec{j}+\ddot{z}\vec{k} = -\omega^2\left(x\vec{i}+y\vec{j}+z\vec{k}-\frac{3}{R^2}R^2 x\vec{i}\right)+\vec{f}(t)$$

$$(\ddot{x}-x2\omega\dot{y}-\omega^2 x)\vec{i}+(\ddot{y}+2\omega\dot{x}-\omega^2 y)\vec{j}+\ddot{z}\vec{k} = -\omega^2\left(y\vec{j}+z\vec{k}-2x\vec{i}\right)+\vec{f}(t)$$

(2.1.1.10)

The acceleration term $\vec{f}(t)$ in equation 2.1.1.10 can be due to thrust force, aerodynamic force or a gravitational force from a third body.

Comparing *i*, *j* and *k* components on both the sides, the components of relative motions are

$$\ddot{x}-2\omega\dot{y}-3\omega^2 x = f_x \qquad (2.1.1.11a)$$

$$\ddot{y} + 2\omega\dot{x} - 3\omega^2 y = f_y \tag{2.1.1.11b}$$

$$\ddot{z} + \omega^2 z = f_z \tag{2.1.1.11c}$$

where ω is the mean motion $\omega = \sqrt{\frac{\mu_\oplus}{R_{radius}^{\ 3}}}$

and R_{radius} is the distance from the center of the earth to the target vehicle in circular orbit. The standard reference frame is a radial, orbit normal, and in-track frame (Figure 2.1.1). Any perturbations to be included within this set of equations would be modeled as acceleration terms on the right hand side of equations 2.1.1.11a, 2.1.1.11b and 2.1.1.11c.

If these equations are set to zero (i.e. no non-central force effects), then the resultant motion can be described as free motion. These equations can either be solved via the standard eigenvalue-eigenvector approach or through a simpler approach if one utilizes simple harmonic motion[5]. The unforced solutions to equations 2.1.1.11a-2.1.1.11c are

$$x(t) = 2(2x_0 + \frac{\dot{y}_0}{\omega}) - (3x_0 + \frac{2\dot{y}_0}{\omega})\cos\omega t + \frac{\dot{x}_0}{\omega}\sin\omega t \tag{2.1.1.12a}$$

$$y(t) = (y_0 - \frac{2\dot{x}_0}{\omega}) - 3(2x_0 + \frac{\dot{y}_0}{\omega})\omega t + \frac{2\dot{x}_0}{\omega}\cos\omega t + 2(3x_0 + 2\frac{\dot{y}_0}{\omega})\sin\omega t \tag{2.1.1.12b}$$

$$z(t) = z_0\cos\omega t + \frac{\dot{z}_0}{\omega}\sin\omega t \tag{2.1.1.12c}$$

The coefficients x_0, $\dot{x}_0$, etc in (2.1.1.12a-2.1.1.12c) represent initial values of position and velocity.

The Clohessy-Wiltshire equations were developed for the rendezvous problem that is of short duration and has frequent thruster firings. Consequently, the long-term accuracy of the equations of motion is not as important in the rendezvous problem as in the formation-flying problem. However, CW equations are derived with assumptions like the reference orbit is circular, the Earth is spherically symmetric, and the target orbit is very close to the reference orbit such that there is no external perturbing force and the nonlinear terms in the relative motion can be neglected. The assumptions made in the derivation of the solution deteriorate

the usefulness of the same and result in errors that are unacceptable for an accurate prediction of relative motion needed for formation flying satellites. A precise analytic solution for the relative motion of and formation flying satellites is needed to minimize fuel consumption and maximize lifetime. Also, the CW solution is being used for purposes other than its original intent. Thus, improvement in the relative dynamics model is key in the effort to find fuel-optimized solutions for satellite formation flight.

2.2 Improvement of the Relative Motion Equations

The CW equations have been the basis of study of relative dynamics of satellites since 1960. Several authors have since then proposed their own methods of analysis or have tried to make the CW equations more precise and useful. In this section, the work of several authors in connection to this problem will be reviewed.

London[7] improved the CW method by assuming that the satellites were influenced by a quadratic gravity field. His method of successive approximations was based on the approximation of the non-linear CW differential equations and the linear solutions to the CW equations. The resulting solutions were more accurate than the linearized solutions but were only accurate enough for a few orbits of the reference satellite. This was due to the presence of secular terms in the solutions that limited the time interval of integration.

Anthony[8] further improved the work of London by solving the relative equations of motion with slight eccentricity. Again a quadratic gravity field, similar to that used by London was considered and any higher order terms of eccentricity were ignored while solving the equations. A similar approach was used in solving the non-linear equations and the resultant solutions were only accurate for a few orbital revolutions.

Werlwas[9] also obtained solutions to the linearized equations of motion. His solutions differed to those obtained by others for the fact that he considered the reference frame to be in the satellite rather than a point on a reference orbit. The equations of motion were linearized with

respect to this configuration. This formulation lead to a complicated, although accurate solution. A limitation of the solution was that there could be no initial out of plane displacement, although an initial velocity out of plane is allowable. The form of the solution also depends on the initial conditions, which is a disadvantage as well.

Berreen [10] improved the CW equations by considering the relative motion of a satellite with reference to an elliptical reference orbit. The solutions, he obtained to the linearized equations were based on the assumption that the two orbits were coplanar. However, most applications of interest, such as intercept or rendezvous, will in general have two vehicles in non-coplanar orbits, so this restriction is a disadvantage when considering practical problems.

Garrison[11] also derived solutions to the relative motion of a satellite with reference to an elliptical orbit. The linearized solutions were plotted for several sets of initial conditions and were found to be accurate for up to two revolutions of the reference orbit. However the results were not as good for large separations of the satellites. A study was also conducted to understand the error induced by the linear representation of the dynamics as well as the effects of a non-spherical central body and other perturbations that were ignored in the model. It was determined that the error made by the linearization is much greater than that of the perturbations over the course of two revolutions of the reference orbit.

Melton[12] developed a linear set of relative motion equations for an elliptical reference orbit. The equations developed included second order eccentricity terms in approximation. The solution was also give as a function of time and not as a function of true anomaly unlike previous solutions for the case of elliptical reference orbits. The solution was presented in both rectangular and cylindrical co-ordinates, and can include the effects of certain forms of perturbations through a convolution integral. The cylindrical co-ordinate representation was found to be more accurate than the rectangular co-ordinate solution. Secular terms are present which limits the time interval over which the solution will be valid.

Recently, Gim and Alfriend [13] proposed a method for relative position analysis known as the Geometry method. Based on the transformation and the state transition matrix for the relative orbital elements, the geometric method gives a precise solution in closed form to 1st order for the non-circular reference orbit with mean and osculating orbital elements under the existence of the gravitational perturbation J_2. In the geometric method, the relationship between the state vector and relative variables is obtained in matrix form instead of directly solving the differential equations of relative motion. The state vector of the relative position and the relative velocity for a satellite, called the Deputy, and a set of equinoctial orbital elements for a reference satellite, called the Chief, are defined as $e=(a,\theta,i,q_1,q_2,\Omega)^T$ and $X=(x,\dot{x},y,\dot{y},z,\dot{z})^T$. By a Taylor series expansion about the chief [13], the relative variables for the deputy are represented by δe

The Geometric transformation is then given by

$$X(t)=[\bar{A}(t)+\alpha\bar{B}(t)]\delta\bar{e}(t)$$

where $\alpha=3J_2R_e^2$ and R_e is the radius of earth, $A(t)$ and $B(t)$ are the transitional matrices.

The general idea is to represent the relative motion in 2 parts, one having the J_2 term ($B(t)$) and the other without ($A(t)$). The same approach was used by Garrison [11] with a different set of variables but without J_2.

The general relation ship between $X(t)$ and $\delta\bar{e}(t)$ is [12]

$$\begin{bmatrix} x \\ y \\ z \end{bmatrix} = \begin{bmatrix} \frac{R}{a}\delta a+\left(\frac{R^2}{p}(q_1\sin\theta-q_2\cos\theta\right)\delta\theta-\left(\frac{2Raq_1}{p}+\frac{R^2\cos\theta}{p}\right)\partial q_1-\left(\frac{2Raq_2}{p}+\frac{R^2\sin\theta}{p}\right)\partial q_2 \\ R\partial\theta+R\cos i\partial\Omega \\ R(\sin\theta\partial i-\cos\theta\sin i\partial\Omega) \end{bmatrix} \tag{2.2.1}$$

where

Where $q_1=e\cos\omega$ and $q_2=e\sin\omega$

The effects of J_2 in equation 2.2.1 can be represented through the variations in orbital elements due to J_2. Gim[12] describes the derivation of the above equations in a detailed manner. Although the geometry method provides a precise solution to the relative dynamics problem with the inclusion of reference satellite eccentricity and J_2 dynamics, it does possess some limitations[12]. Due to the neglected nonlinear terms, the relative positional errors have been found to increase with the increase in the magnitude of spacecraft separation and orbit eccentricity. The equation of relative coordinates for an unperturbed orbit is given as[13]

$$\begin{bmatrix} x \\ y \\ z \end{bmatrix} = \begin{bmatrix} \delta R \\ R_d \delta\theta + R_d \cos i_m \delta\Omega \\ R_d (\sin\theta_d \delta i - \cos\theta_d \sin i_m \delta\Omega) \end{bmatrix} \tag{2.2.2}$$

In the above equation θ is the argument of lattitude and not the true anomaly. In this thesis, the argument of latitude is represented as u

Another recent development is the COWPOKE (Cluster Orbits With Perturbations of Keplerian Elements) equations developed by Sabol[14]. The COWPOKE equations also use the differences in the orbital elements of two satellites to determine their relative motion and support analysis of elliptical reference orbits. According to Sabol[14], the equations should provide sufficient accuracy for low-fidelity simulation applications, although they are inadequate for high precision analyses. The cowpoke equations are also derived as a solution to the geometry of the formation-flying problem but in a different way. Sabol[14] uses the geometry of the formation to find the angle between the deputy spacecraft and the master spacecraft with respect to the center of earth. Once this angle is found, it is then multiplied with the projection of the radius in the required plane to yield the arc length. The x, y and z coordinates are quite precise for a close formation where the angles between the spacecraft are very small. The COWPOKE equations are given as[14]

$$\begin{bmatrix} \delta r \\ \alpha \\ \beta \end{bmatrix} = \begin{bmatrix} x \\ \frac{y}{r} \\ \frac{z}{r} \end{bmatrix} = \begin{bmatrix} \frac{(a+\delta a)(1-(e+\delta e)^2)}{1+(e+\delta e)\cos(M+2e\sin(M)+\delta v)} - \frac{a(1-e^2)}{1+e\cos(v)} \\ [(\delta\omega+\delta v)\cos(\delta i)+\delta\Omega\cos(i)] \\ [-2\sin\frac{\delta\Omega}{2}\sin(i)\cos(\omega+\frac{\delta\omega}{2}+M+2e\sin(M)+\frac{\delta v}{2})+\delta i\sin(\omega+\delta\omega+M+2e\sin(M)+\delta v)] \end{bmatrix} \quad (2.2.3)$$

where $\delta r, \alpha$ and β correspond to radial, along-track and cross-track angular separations and r is the position vector of the spacecraft and v is the true anomaly. All other orbital elements are same as the classical orbital elements defined in the nomenclature of this thesis. In the above equations, the orbital elements of the deputy spacecraft are represented as sum of the orbital elements of the master and the difference in the orbital elements. For example the RAAN (ascending node) would be represented as $\Omega_d = \Omega + \delta\Omega$ where Ω is the RAAN of the master spacecraft and $\delta\Omega$ is the difference in the ascending node. Also the true anomaly is represented as $\upsilon = M + 2e\sin(M)$.

Rewriting Equation 2.2.3 in terms of x, y and z and the orbital elements of the master and the deputy yields

$$\begin{bmatrix} x \\ y \\ z \end{bmatrix} = \begin{bmatrix} R_d - R_m \\ R_d\left[(\delta\omega+\delta v)\cos(\delta i)+\cos(i_m)\delta\Omega\right] \\ R_d(-2\sin\left(\frac{\delta\Omega}{2}\right)\sin(i_m)\cos\left((\omega_m+v_m)+\frac{(\delta\omega+\delta v)}{2}\right)+\delta i\sin(\omega_d+v_d)) \end{bmatrix}$$

Substitution of $R_d - R_m = \delta R$ and $\delta\omega + \delta v = \delta u$, the argument of latitude in the above equation and assumption of $\cos\delta i \approx 1$ for small separation distances reduces the x and y coordinates of the above equation to the following; $x = \delta R$ and $y = R_d\delta u + R_d\cos i_m\delta\Omega$

Similarly for small separation distances $\sin\frac{\Omega}{2} \approx \frac{\Omega}{2}$ and $\cos u_d \approx \cos(u_m + \frac{\delta u}{2})$. This reduces the z coordinate to $z \approx R_d(\sin u_d\delta i - \cos u_d \sin i_m\delta\Omega)$.

The COWPOKE equations then become

$$\begin{bmatrix} x \\ y \\ z \end{bmatrix} = \begin{bmatrix} \delta R \\ R_d \delta u + R_d \cos i_m \delta\Omega \\ R_d (\sin u_d \delta i - \cos u_d \sin i_m \delta\Omega) \end{bmatrix} \tag{2.2.4}$$

It can be seen that the COWPOKE equations (equation 2.2.3) with some modifications (equation 2.2.4) are similar to the Gim and Alfriend Equations (2.2.2) although the derivations are different. So both the methods converge well when the relative separation between the spacecraft is very small (a few hundred meters).

2.3 Relative Motion Equations and Satellite Formation Flight

Relative motion equations have been useful in the design and optimization of satellite formation geometry, as well as for developing control algorithms to maintain these formations. Sabol [15] analyzed different formation patterns with the help of the CW equations. He used the DSST orbit propagator to simulate different formation patterns and estimated the fuel requirements of different formations based on the results of the simulation. He found out that the Circular and projected formation patterns were very costly in terms of fuel and orbit maintenance.

Badesha[16] modified the CW equations to include atmospheric drag forces to investigate the deployment and initialization of a cluster of six satellites in an in-track formation. The investigation focused on determining possible collision scenarios between the satellites during the deployment phase and the effects of error in the deployment velocity as well as error in the time spacing between subsequent deployments. No study was conducted to determine the effect of error in the deployment direction. A procedure was outlined for determining the amount of fuel needed to initialize the formation.

Chichka[17] used a relative motion solution to characterize the relative orbits of satellite formations that appear to have a constant distribution from an observer located on the planetary surface. A more detailed study was then conducted in order to ascertain the error made in the linearized study.

Schweighart[18] analyzed the effects of J_2 on a spacecraft relative motion by adding a linearized form of J_2 onto the right-hand side of the Hill's equations. The linear equations were compared against the mean variation of the orbital elements, where the linear equations captured the variation in 5 out of 6 elements. The missing variation was due to the fact that the linearized equations did not incorporate the geometry of the orbital planes.

A technique for controlling satellite formations, based on relative motion equations, is found in Vadali [19]. This technique used the relative motion equations to design periodic relative orbits of a deputy with respect to a chief. A control was then developed in order to cancel a simple gravity perturbation model in such a way that the average fuel consumption of each satellite is minimized.

2.4 Conclusions

The review of literature on relative trajectory analysis shows that all existing methods of analysis have certain types of limitations like limitation on orbit eccentricity, simulation duration, initial separation of satellites etc. These limitations are a consequence of several assumptions made in the derivation of the relative motion equations. The geometric method by Gim[12] was found to be more precise than the CW method but has limitations on spacecraft separation. There exists no method that is valid for all conditions. The purpose of the research described in this thesis is to develop a generalized method that is not based on the traditional CW method and that can be used to analyze relative trajectories for any given condition. The method should be with the minimum of limitations and support non-linear analysis of the formation flight problem.

The research work presented in this thesis has also been presented as published papers[20,21,22,23,24]. In the following chapters, a dynamical model to analyze relative trajectory of spacecraft in elliptical orbits for any initial separation will be developed. This model will be then used to study the dynamics of spacecraft formation flight as discussed in the objectives of this thesis.

Chapter 3
Methodology

3.1 Introduction

The purpose of this chapter to develop a precise method to analyze the relative motion of satellites that is valid for any type of Formation pattern without the limitations of the CW method. Firstly, the preliminary method developed during the initial stages of this research work is presented. The final method is a further development of the preliminary method that can be only used to analyze one of the basic configurations of formation flight, the Leader-Follower formation pattern.

3.2 The preliminary method

The motivation behind this thesis was the UK-University led programme that aimed to design and develop two satellites of 10 kg mass each and launch them into a leader follower formation pattern with a separation distance of 100 meters. To understand the relative dynamics of such a formation, the author initially developed a method based on the geometry of the problem and then used low-propulsion flight theory[25] to understand the dynamics of such a formation. This method will be hereafter referred to as the Preliminary method. With the new model, it was possible to analyze elliptical reference orbits, a feature that the CW equations fail to provide. But the disadvantage of the model was that it could be only used to analyze planar cases and any out of plane motion had to be ignored. This was not a problem for designs like Leader-Follower configuration but was certainly a big issue for other types of Formation patterns that had satellites in all planes. Also, the initial method had low-propulsion flight theory as the basis of relative dynamics analysis, which made modeling of perturbative forces, normal to the orbit, very difficult to accomplish. The idea behind incorporating the low-propulsion theory was that the perturbative forces were assumed to be of a very small magnitude and constant in nature. By assuming the perturbative accelerations to be similar to that of the effect of a low thrust propulsion system like plasma thrusters, one can get a picture of the dynamics of the satellites in a perturbative field. But the main

drawback of the low-thrust propulsion theory is that it assumes constant micro thrust acting on the spacecraft whereas in a real scenario the spacecraft would experience different perturbative accelerations in different points of the orbit due to different perturbative accelerations like J_2 and Solar Radiation Pressure. However the low-propulsion flight model can be used to model atmospheric drag by assuming that the acceleration caused by atmospheric drag remains constant for the same altitude, which is only true for a small change in altitude.

The drawbacks of the preliminary method led to the advent of a new approach that could accommodate analysis of any perturbative accelerations acting on any type formation pattern.

3.2.1 Mathematical modeling of the leader-follower pattern using the preliminary method

The most basic configuration in which spacecraft can fly in formation is that of leader and follower shown in Fig.3.2.1. In this configuration, the orbital elements of each spacecraft are identical except for the true anomaly, meaning that the spacecraft follow the same orbital path at different times.

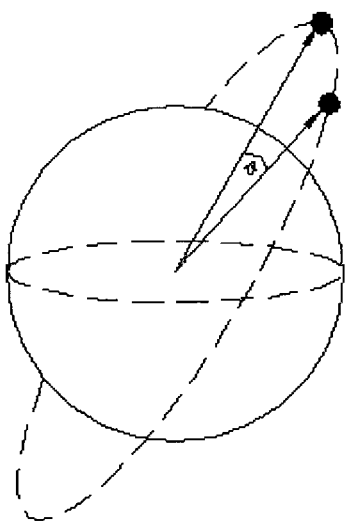

FIGURE 3.2.1 LEADER-FOLLOWER FORMATION

An example of Leader-follower formation of two spacecraft (namely *A* and *B*) separated by a distance of 100 meters and located at an altitude of 600 kilometers is considered and is shown in fig.3.2.2. The orbits of the spacecraft are assumed to be circular and only the planar case shall be investigated. It can be seen further in this thesis that orbits with eccentricity could also be subjects of such a model.

The equations of motion are derived as a solution to the geometry of the system, where the origin of the system *O* coincides with the earth's centre. The *OY* axis lies along the line that connects the center of the earth with the equator and *OX* axis lies along the line that connects the center of earth with its north pole as shown in figure 3.2.2. Firstly, the *OXY* system is transformed to system *OPQ* by rotating the axis by θ_A to align with the local co-ordinate system of the reference spacecraft. In our case, spacecraft *A* will act as the reference spacecraft. Then the origin of the *OPQ* system is translated to the centre of mass of the reference spacecraft *oxy* from the centre of earth. In the new system, *x*-axis is the radial

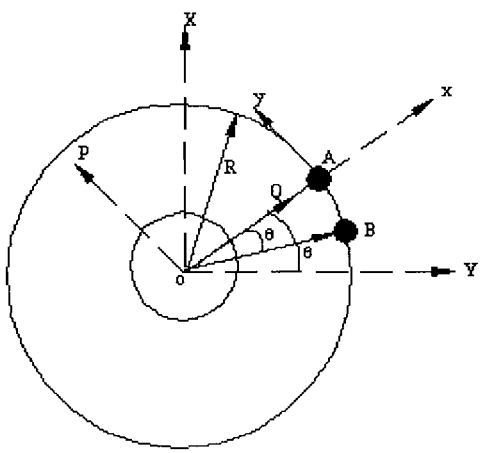

FIGURE 3.2.2 RELATIVE MOTION OF SATELLITES IN POLAR CO-ORDINATES

direction of motion of the spacecraft with respect to the centre of earth and *y*-axis points in the direction of the velocity vector.

The coordinates of spacecraft *B* in *OPQ* frame can be mathematically represented as

$$\begin{bmatrix} P_B \\ Q_B \end{bmatrix} = T_{\theta_A} \begin{bmatrix} X_B \\ Y_B \end{bmatrix} \tag{3.2.1.1}$$

Where T_{θ_A} is the transformation matrix and is given as

$$T_{\theta_A} = \begin{bmatrix} \cos\theta_A & \sin\theta_A \\ -\sin\theta_A & \cos\theta_A \end{bmatrix} \tag{3.2.1.2}$$

θ_A is the true anomaly of spacecraft A. Further, co-ordinates X_B, Y_B can be represented as

$$\begin{bmatrix} X_B \\ Y_B \end{bmatrix} = T_{\theta_B} \begin{bmatrix} r_B \\ 0 \end{bmatrix} \tag{3.2.1.3}$$

$$\text{Where } T_{\theta_B} = \begin{bmatrix} \cos\theta_B & -\sin\theta_B \\ \sin\theta_B & \cos\theta_B \end{bmatrix} \tag{3.2.1.4}$$

θ_B is the true anomaly of spacecraft B. Substituting equations 3.2.1.3 in 3.2.1.1 gives

$$\begin{bmatrix} P_B \\ Q_B \end{bmatrix} = \begin{bmatrix} \cos\theta_A & \sin\theta_A \\ -\sin\theta_A & \cos\theta_A \end{bmatrix} \begin{bmatrix} \cos\theta_B & -\sin\theta_B \\ \sin\theta_B & \cos\theta_B \end{bmatrix} \begin{bmatrix} r_B \\ 0 \end{bmatrix} \tag{3.2.1.5}$$

Now translating frame OPQ to Oxy gives us the coordinates in the spacecraft body-centered frame

$$\begin{bmatrix} x \\ y \end{bmatrix} = \begin{bmatrix} \cos\theta_A & \sin\theta_A \\ -\sin\theta_A & \cos\theta_A \end{bmatrix} \begin{bmatrix} \cos\theta_B & -\sin\theta_B \\ \sin\theta_B & \cos\theta_B \end{bmatrix} \begin{bmatrix} r_B \\ 0 \end{bmatrix} - \begin{bmatrix} r_A \\ 0 \end{bmatrix} \tag{3.2.1.6}$$

Expansion of equation 3.2.1.6 gives

$$\begin{bmatrix} x \\ y \end{bmatrix} = \begin{bmatrix} (\cos(\theta_A)\cos(\theta_B) + \sin(\theta_A)\sin(\theta_B)) \cdot r_B - r_A \\ (-\sin(\theta_A)\cos(\theta_B) + \cos(\theta_A)\sin(\theta_B)) \cdot r_B \end{bmatrix} \tag{3.2.1.7}$$

In the above equations r_A , r_B are the position vectors of spacecraft A and B respectively

Equation (3.2.1.7) can be used to analyze reference orbits of elliptical nature as the equations are given as a function of the position vector r. There is no relative drift if both the spacecraft experience perturbative accelerations of the same magnitude as the orbits of both

the spacecraft decay at the same rate. However, If the pertubative accelerations differ in magnitude, the orbits decay at different rates and there arises a relative drift due to the difference in positions of both the spacecraft. In the next subsection force models will be included in equation (3.2.1.7).

3.2.2 Equations of Motion in a Perturbative Field

It is possible to simulate the dynamics of relative motion in the presence of perturbative forces using equation 3.2.1.7 if the evolution of the position vectors r_a and r_b with time due to disturbances is known. One of the methods is the Low propulsion method by Ehricke[25]. His method gives an analytical expression for finding the position vector of spacecraft in circular or elliptical orbits acted upon by perturbative forces with respect to time. In his method, as described in *Spacecraft Dynamics*[25], he derives analytical expressions for position vector and velocity assuming the perturbative forces to be of constant magnitude for a short period of time (a few orbits). The perturbative forces are treated as micro-thrust forces accelerating or decelerating the spacecraft.

Ehricke, in his method, assumes the perturbative forces to be of very small magnitude, compared to the local gravitational force, and applies the so-called "small perturbation method"[25].

If the tangential force is a small thrust F that can accelerate or decelerate then the position vector as a resultant of the perturbative forces, for departure from a slightly elliptical orbit by Ehricke's method is given as,

$$r(t) = r_0 \pm \frac{\mu / r_0}{v_0^{\,2}}\left[2\frac{F}{m}\frac{r_0}{\mu / r_0^{\,2}}(\omega_0 t - \sin\omega_0 t) + \left(\frac{v_0^{\,2}}{\mu / r_0^{\,2}} - r_0\right)(1-\cos\omega_0 t)\right] \qquad (3.2.2.1)$$

Where the subscript 0 refers to the initial orbit, ω_0 is the angular velocity of the original orbit and v_0 is the initial orbital velocity of the spacecraft.

The Velocity as a function of time is given as

$$v(t) = v_0 + \frac{\mu / r_0}{v_0^2}\{\frac{F}{m}\frac{r_0}{v_0}[(\frac{v_0^2}{\mu / r_0} - 2)\omega_0 t + 2\sin\omega_0 t] - v_0(1 - \frac{\mu / r_0}{v_0^2})(1 + \cos\omega_0 t)\} \quad (3.2.2.2)$$

It is also imperative to derive the relation between the angular velocity of the spacecraft and the pertubative acceleration acting on it to simulate the dynamics in equation 3.2.1.7.

From the energy equation we have

$$\frac{v(t)^2}{2} - \frac{\mu}{r} = -\frac{\mu}{2a} \quad (3.2.2.3)$$

Rearranging and observing that $v_0^2 = \frac{\mu}{r}$,

$$\frac{r}{a} = 2 - \left(\frac{v(t)}{v_0}\right)^2 \quad (3.2.2.4)$$

From kepler's third law $T^2 \propto a^3$. Thus the period of given ratio $v(t) / v_o$ is

$$\frac{T(t)}{T_0} = \left[2 - \left(\frac{v(t)}{v_0}\right)^2\right]^{-\frac{3}{2}} \quad (3.2.2.5a)$$

Where T_o is the Time period of the initial orbit. So, if $v(t) = v_o - \Delta v$, then

$$T(t) = \left[2 - \left(\frac{v(t)}{v_0}\right)^2\right]^{-\frac{3}{2}} T_0 \quad (3.2.2.5b)$$

The angular velocity $\omega(t) = \frac{2\pi}{T(t)}$

$$\omega(t) = \frac{2\pi}{\left[2 - \left(\frac{v(t)}{v_0}\right)^2\right]^{\frac{3}{2}} T_0} \quad (3.2.2.6)$$

And the true anomaly $\theta(t)$ is $\theta(t) = \theta_0 + \int \omega(t) dt$

$$\theta(t) = \theta_0 + \int \frac{2\pi}{\left[2 - \left(\frac{v(t)}{v_0}\right)^2\right]^{-\frac{3}{2}} T_0} dt \tag{3.2.2.7a}$$

$$\theta(t) = \theta_0 + \int \frac{2\pi}{\left[2 - \left(\frac{v(t)}{v_0}\right)^2\right]^{-\frac{3}{2}} T_0} dt \tag{3.2.2.7b}$$

Where θ_o is the initial position of the spacecraft and $v(t)$ as given in equation 3.2.2.2. The true anomaly at any point t is found by numerically integrating equation 3.2.2.7b with a step size of dt to epoch time t.

Now, having all these results, it wouldn't be difficult to model the specific case of motion where the formation flying spacecraft are in a Leader follower formation as shown in figure.3.2.2 and are initially separated by distance d.

If the spacecraft are acted upon by external forces which oppose their motion, then the velocity of spacecraft A and B at any time t can be written as $v_a(t)$ and $v_b(t)$. The true anomalies of spacecraft A and B at any time can be written as

$$\theta_a(t) = \theta_{a0} + \int \omega_a(t) \cdot dt \tag{3.2.2.8a}$$

$$\theta_b(t) = \theta_{b0} + \int \omega_b(t) \cdot dt \tag{3.2.2.8b}$$

Substituting for $\omega_a(t)$ and $\omega_b(t)$,

$$\theta_a(t) = \theta_{a0} + \int \frac{2\pi}{\left(2 - \left[\frac{v_a(t)}{v_0}\right]^2\right)^{-\frac{3}{2}} T_{a0}} dt \tag{3.2.2.9}$$

$$\theta_b(t) = \theta_{b0} + \int \frac{2\pi}{\left(2 - \left[\frac{v_b(t)}{v_0}\right]^2\right)^{-\frac{3}{2}} T_{b0}} dt \tag{3.2.2.10}$$

The position of spacecraft *A* and *B* at any time *t* from equation (3.2.2.1) can be written as

$$r_a(t) = \frac{\mu / r_{a0}}{v_{a0}^2}[2\frac{F}{m}\frac{r_{a0}}{\mu / r_{a0}^2}(\omega_{a0}t - \sin\omega_{a0}t) + (\frac{v_{a0}^2}{\mu / r_{a0}^2} - r_{a0})(1 - \cos\omega_{a0}t)] \quad (3.2.2.11)$$

$$r_b(t) = \frac{\mu / r_{b0}}{v_{b0}^2}[2\frac{F}{m}\frac{r_{b0}}{\mu / r_{b0}^2}(\omega_{b0}t - \sin\omega_{b0}t) + (\frac{v_{b0}^2}{\mu / r_{b0}^2} - r_{b0})(1 - \cos\omega_{b0}t)] \quad (3.2.2.12)$$

Where the subscripts *a0* and *b0* refer to initial conditions of spacecraft *A* and spacecraft *B* respectively.

The perturbed relative co-ordinates of spacecraft *B* with respect to spacecraft *A* can then be found by substituting equations (3.2.2.9), (3.2.2.10), (3.2.2.11) and (3.2.2.12) in equation (3.2.1.7). The resultant equation is given in Appendix B

3.2.3 Advantages and Discrepancies of the Preliminary method

The method developed in the preceding sections is a closed form solution to the relative motion problem for planar case of a formation-flying scenario. Equation 3.2.1.7 that is represented as

$$\begin{bmatrix} x \\ y \end{bmatrix} = \begin{bmatrix} (\cos(\theta_A)\cos(\theta_B) + \sin(\theta_A)\sin(\theta_B)) \cdot r_B - r_A \\ (-\sin(\theta_A)\cos(\theta_B) + \cos(\theta_A)\sin(\theta_B)) \cdot r_B \end{bmatrix}$$

is a direct solution to the relative motion problem based on the geometry of the formation. Moreover, since the equations have the position vector, the inclusion of eccentricity becomes a very easy task. This allows us to study relative orbits that are elliptical in nature. This is a significant development as no other method allows treatment of elliptical reference orbits precisely. The methods that allow treatment of elliptical orbits like Melton[26], Berreen[10] have truncated eccentricity terms of higher order that make them valid for only small eccentricity values. Also there is no limitation on the initial spacecraft separation like in the traditional CW method where the spacecraft separation is assumed to be very small when compared to the radius of earth. The above equations also can be derived as a function of time by representing the true anomaly as a function of time[27].

$$\theta(t) = M(t) + 2e(t)\sin(M(t)) + \frac{5}{4}e^2(t)\sin(2M(t)) + \frac{1}{12}e^3(t)(13\sin(3M(t)) - 3\sin(M(t)))$$

Although the preliminary method was helpful to model forces like drag with the help of low propulsion flight theory, it was not helpful where modeling of radial and out of plane forces was essential. Also the incorporation of J_2 in to the relative co-ordinate equations was very difficult. It was still possible to analyze some issues like differential drag effects with the above model. Figure 3.2.3 shows the effect of differential drag on a formation of two satellites one following the other. The trailing satellite is assumed to have 10% more surface area than the leading satellite. Figure 3.2.3 was plotted with some approximations made on the time dependent terms in equation 3.2.2.2. This was to ease the burden of the program used for numerical integration.

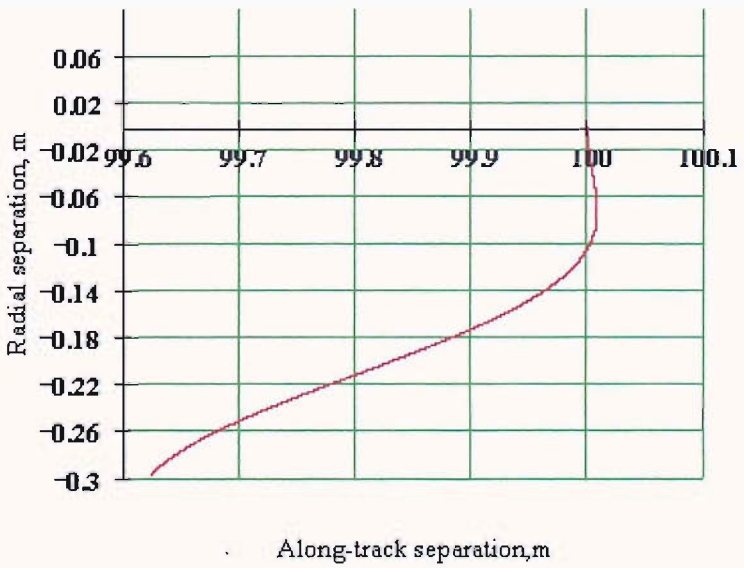

FIGURE 3.2.3 - EFFECTS OF DIFFERENTIAL DRAG AREA OF 10% SIMULATED FOR 1 ORBIT AT 600-KM ALTITUDE

The explanation to the figure is as follows. Dissipation of kinetic energy into heat through drag decreases the orbital velocities of the both the spacecraft, causing them to slow initially. But as the spacecraft enter a circular inward spiral trajectory, their angular velocities increase thereby causing them to approach slowly but steadily. Since the trailing satellite has more drag area than leading satellite, It loses height more rapidly and as a result, the offset in the x

(radial) direction increases. At the same time, there is also a steady increase of the offset in the y (along-track) direction.

3.3 Improved method

The equations for the relative coordinates are again derived as a precise solution to the formation geometry problem with the definition of orbital frames and orbital elements as shown in Figure 3.3.1[28]. The reference satellite will be considered as the master satellite (subscript m) and the satellite to be observed as the deputy (subscript d) hereafter. It should be noted that there could be many deputy spacecraft for a specific mission. But in our case it will be assumed that the formation consists of only two spacecraft namely the master and the deputy.

The origin of the spacecraft centered co-ordinate system is assumed to be at the master satellite's centre of mass. The origin of the coordinate system $OXYZ$ is at the center of the earth with the XY plane coinciding with the Earth's equatorial plane and X-axis pointing in the direction of vernal eqinox γ. The Z-axis points in the direction of the North Pole and the Y-axis is normal to the XZ plane and completes the right-handed frame of system.

The origin of the system $OPQR$ also lies at the center of the earth with the P axis pointing in the direction of the master satellite's Centre-of-Mass.

The unit vector of P is defined as

$$P = \frac{r}{|\mathrm{r}|} \tag{3.3.1}$$

where r is the radius vector of the spacecraft

The P-axis originates from the center of earth and lies along the points that connect the center of earth with the center of mass of the spacecraft, R-axis also originates from the center of earth, lies in the orbital plane and is perpendicular to the P-axis and Q axis originates from the center of the earth and lies perpendicular to the orbital plane.

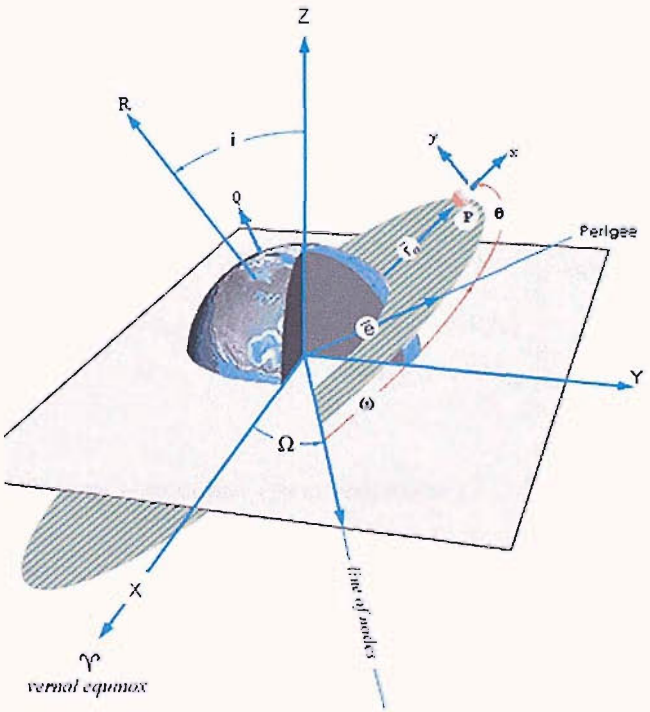

FIGURE 3.3.1 – ORBITAL FRAMES AND ELEMENTS

The origin of the *oxyz* system lies at the master satellite's center of mass and its unit vectors are

$$x = P, \qquad y = Q, \qquad z = R \tag{3.3.2}$$

From Figure 3.3.1, *XYZ* axes can be transformed to *PQR* axes by 3 successive rotations as follows:

1. Rotation about the *Z* axis by + Ω
2. Rotation about the *X* axis by + i
3. Rotation about the Z axis by + u $(u = \omega + \theta)$

All the greek symbols and the italicized alphabets are standard notations for the orbital elements namely θ representing the true anomaly, Ω representing right ascension of ascending node (RAAN), ω representing argument of perigee, u representing the argument of latitude and i the inclination.

The new coordinates can now be represented as

$$\begin{bmatrix} P \\ Q \\ R \end{bmatrix} = \left[T_{ui\Omega}\right]_m \begin{bmatrix} X \\ Y \\ Z \end{bmatrix} \tag{3.3.3}$$

Where

$$\left[T_{ui\Omega}\right]_m = \begin{bmatrix} \cos u_m & \sin u_m & 0 \\ -\sin u_m & \cos u_m & 0 \\ 0 & 0 & 1 \end{bmatrix} \begin{bmatrix} 1 & 0 & 0 \\ 0 & \cos i_m & \sin i_m \\ 0 & -\sin i_m & \cos i_m \end{bmatrix} \begin{bmatrix} \cos \Omega_m & \sin \Omega_m & 0 \\ -\sin \Omega_m & \cos \Omega_m & 0 \\ 0 & 0 & 1 \end{bmatrix} \tag{3.3.4}$$

The coordinates of the deputy spacecraft (from equation (3.3.3) in the *OPQR* system are

$$\begin{bmatrix} P_d \\ Q_d \\ R_d \end{bmatrix} = \left[T_{ui\Omega}\right]_m \begin{bmatrix} X_d \\ Y_d \\ Z_d \end{bmatrix} \tag{3.3.5}$$

The Coordinates X_d, Y_d, Z_d can also be represented by the Matrix as given below

$$\begin{bmatrix} X_d \\ Y_d \\ Z_d \end{bmatrix} = \left[T_{\Omega iu}\right]_d \begin{bmatrix} R_d \\ 0 \\ 0 \end{bmatrix} \tag{3.3.6}$$

Where $\left[T_{\Omega iu}\right]_d = \begin{bmatrix} \cos \Omega_d & -\sin \Omega_d & 0 \\ \sin \Omega_d & \cos \Omega_d & 0 \\ 0 & 0 & 1 \end{bmatrix} \begin{bmatrix} 1 & 0 & 0 \\ 0 & \cos i_d & -\sin i_d \\ 0 & \sin i_d & \cos i_d \end{bmatrix} \begin{bmatrix} \cos u_d & -\sin u_d & 0 \\ \sin u_d & \cos u_d & 0 \\ 0 & 0 & 1 \end{bmatrix}$ (3.3.7)

Substituting equation (3.3.6) in equation.(3.3.5) yields the Coordinates X_d, Y_d, Z_d in the *OPQR* frame as

$$\begin{bmatrix} P_d \\ Q_d \\ R_d \end{bmatrix} = \left[T_{ui\Omega}\right]_m \left[T_{\Omega iu}\right]_d \begin{bmatrix} R_d \\ 0 \\ 0 \end{bmatrix} \tag{3.3.8}$$

Now shifting the origin of the *OPQR* frame to the master satellite's Centre-of-mass gives the relative coordinates of the deputy spacecraft with respect to the master spacecraft in the *oxyz* frame.

$$\begin{bmatrix} x \\ y \\ z \end{bmatrix} = \left[T_{ui\Omega}\right]_m \left[T_{\Omega iu}\right]_d \begin{bmatrix} R_d \\ 0 \\ 0 \end{bmatrix} - \begin{bmatrix} R_m \\ 0 \\ 0 \end{bmatrix} \tag{3.3.9}$$

Combining the two transformations in to one then gives

$$\begin{bmatrix} x \\ y \\ z \end{bmatrix} = \left[A\right] \begin{bmatrix} R_d \\ 0 \\ 0 \end{bmatrix} - \begin{bmatrix} R_m \\ 0 \\ 0 \end{bmatrix} \tag{3.3.10}$$

where $\left[A\right] = \left[T_{ui\Omega}\right]_m \bullet \left[T_{\Omega iu}\right]_d$ and $\left[A\right] = \begin{bmatrix} A_{11} & A_{12} & A_{13} \\ A_{21} & A_{22} & A_{23} \\ A_{31} & A_{32} & A_{33} \end{bmatrix}$

$$\begin{aligned} A_{11} &= cu_m \cdot c\Omega_m \cdot c\Omega_d \cdot cu_d - cu_m \cdot c\Omega_m \cdot s\Omega_d \cdot ci_d \cdot su_d - su_m \cdot ci_m \cdot s\Omega_m \cdot c\Omega_d \cdot cu_d \\ &+ su_m \cdot ci_m \cdot s\Omega_m \cdot s\Omega_d \cdot ci_d \cdot su_d + cu_m \cdot s\Omega_m \cdot s\Omega_d \cdot cu_d + cu_m \cdot s\Omega_m \cdot c\Omega_d \cdot ci_d \cdot su_d \\ &+ su_m \cdot ci_m \cdot c\Omega_m \cdot s\Omega_d \cdot cu_d + su_m \cdot ci_m \cdot c\Omega_m \cdot c\Omega_d \cdot ci_d \cdot su_d + su_m \cdot si_m \cdot si_d \cdot su_d \end{aligned}$$

$$\begin{aligned} A_{12} &= -cu_m \cdot c\Omega_m \cdot c\Omega_d \cdot su_d - cu_m \cdot c\Omega_m \cdot s\Omega_d \cdot ci_d \cdot cu_d + su_m \cdot ci_m \cdot s\Omega_m \cdot c\Omega_d \cdot su_d \\ &+ su_m \cdot ci_m \cdot s\Omega_m \cdot s\Omega_d \cdot ci_d \cdot cu_d - cu_m \cdot s\Omega_m \cdot s\Omega_d \cdot su_d + cu_m \cdot s\Omega_m \cdot c\Omega_d \cdot ci_d \cdot cu_d \\ &- su_m \cdot ci_m \cdot c\Omega_m \cdot s\Omega_d \cdot su_d + su_m \cdot ci_m \cdot c\Omega_m \cdot c\Omega_d \cdot ci_d \cdot cu_d + su_m \cdot si_m \cdot si_d \cdot cu_d \end{aligned}$$

$$\begin{aligned} A_{13} &= c\Omega_m \cdot s\Omega_d \cdot si_d \cdot cu_m - s\Omega_d \cdot si_d \cdot su_m \cdot ci_m \cdot s\Omega_m - c\Omega_d \cdot s\Omega_m \cdot si_d \cdot cu_m \\ &- c\Omega_d \cdot si_d \cdot su_m \cdot ci_m \cdot c\Omega_m + su_m \cdot si_m \cdot ci_d \end{aligned}$$

$$A_{21} = -su_m \cdot c\Omega_m \cdot c\Omega_d \cdot cu_d + su_m \cdot c\Omega_m \cdot s\Omega_d \cdot ci_d \cdot su_d - cu_m \cdot ci_m \cdot s\Omega_m \cdot c\Omega_d \cdot cu_d$$
$$+cu_m \cdot ci_m \cdot s\Omega_m \cdot s\Omega_d \cdot ci_d \cdot su_d - su_m \cdot s\Omega_m \cdot s\Omega_d \cdot cu_d - su_m \cdot s\Omega_m \cdot c\Omega_d \cdot ci_d \cdot su_d$$
$$+cu_m \cdot ci_m \cdot c\Omega_m \cdot s\Omega_d \cdot cu_d + cu_m \cdot ci_m \cdot c\Omega_m \cdot c\Omega_d \cdot ci_d \cdot su_d + cu_m \cdot si_m \cdot si_d \cdot su_d$$

$$A_{22} = su_m \cdot c\Omega_m \cdot c\Omega_d \cdot su_d + su_m \cdot c\Omega_m \cdot s\Omega_d \cdot ci_d \cdot cu_d + cu_m \cdot ci_m \cdot s\Omega_m \cdot c\Omega_d \cdot su_d$$
$$+cu_m \cdot ci_m \cdot s\Omega_m \cdot s\Omega_d \cdot ci_d \cdot cu_d + su_m \cdot s\Omega_m \cdot s\Omega_d \cdot su_d - su_m \cdot s\Omega_m \cdot c\Omega_d \cdot ci_d \cdot cu_d$$
$$-cu_m \cdot ci_m \cdot c\Omega_m \cdot s\Omega_d \cdot su_d + cu_m \cdot ci_m \cdot c\Omega_m \cdot c\Omega_d \cdot ci_d \cdot cu_d + cu_m \cdot si_m \cdot si_d \cdot cu_d$$

$$A_{23} = -c\Omega_m \cdot s\Omega_d \cdot si_d \cdot su_m - s\Omega_d \cdot si_d \cdot cu_m \cdot ci_m \cdot s\Omega_m + c\Omega_d \cdot s\Omega_m \cdot si_d \cdot su_m$$
$$-c\Omega_d \cdot si_d \cdot cu_m \cdot ci_m \cdot c\Omega_m + cu_m \cdot si_m \cdot ci_d$$

$$A_{31} = si_m \cdot s\Omega_m \cdot c\Omega_d \cdot cu_d - si_m \cdot s\Omega_m \cdot s\Omega_d \cdot ci_d \cdot su_d - si_m \cdot c\Omega_m \cdot s\Omega_d \cdot cu_d$$
$$-si_m \cdot c\Omega_m \cdot c\Omega_d \cdot ci_d \cdot su_d + su_d \cdot si_d \cdot ci_m$$

$$A_{32} = -si_m \cdot s\Omega_m \cdot c\Omega_d \cdot su_d - si_m \cdot s\Omega_m \cdot s\Omega_d \cdot ci_d \cdot cu_d + si_m \cdot c\Omega_m \cdot s\Omega_d \cdot su_d$$
$$-si_m \cdot c\Omega_m \cdot c\Omega_d \cdot ci_d \cdot cu_d + cu_d \cdot si_d \cdot ci_m$$

$$A_{33} = si_m \cdot s\Omega_m \cdot s\Omega_d \cdot si_d + si_m \cdot c\Omega_m \cdot c\Omega_d \cdot si_d + ci_d \cdot ci_m$$

where the sine and cosine functions are represented as ***s*** and ***c*** for simplicity.

The equations of the coordinates of the deputy spacecraft relative to the master spacecraft in *xyz* frame are

$$x = (cu_m \cdot c\Omega_m \cdot c\Omega_d \cdot cu_d - cu_m \cdot c\Omega_m \cdot s\Omega_d \cdot ci_d \cdot su_d - su_m \cdot ci_m \cdot s\Omega_m \cdot c\Omega_d \cdot cu_d$$
$$+su_m \cdot ci_m \cdot s\Omega_m \cdot s\Omega_d \cdot ci_d \cdot su_d + cu_m \cdot s\Omega_m \cdot s\Omega_d \cdot cu_d + cu_m \cdot s\Omega_m \cdot c\Omega_d \cdot ci_d \cdot su_d$$
$$+su_m \cdot ci_m \cdot c\Omega_m \cdot s\Omega_d \cdot cu_d + su_m \cdot ci_m \cdot c\Omega_m \cdot c\Omega_d \cdot ci_d \cdot su_d + su_m \cdot si_m \cdot si_d \cdot su_d) \cdot R_d - R_m$$

(3.3.11a)

$$y = (-su_m \cdot c\Omega_m \cdot c\Omega_d \cdot cu_d + su_m \cdot c\Omega_m \cdot s\Omega_d \cdot ci_d \cdot su_d - cu_m \cdot ci_m \cdot s\Omega_m \cdot c\Omega_d \cdot cu_d$$
$$+cu_m \cdot ci_m \cdot s\Omega_m \cdot s\Omega_d \cdot ci_d \cdot su_d - su_m \cdot s\Omega_m \cdot s\Omega_d \cdot cu_d - su_m \cdot s\Omega_m \cdot c\Omega_d \cdot ci_d \cdot su_d$$
$$+cu_m \cdot ci_m \cdot c\Omega_m \cdot s\Omega_d \cdot cu_d + cu_m \cdot ci_m \cdot c\Omega_m \cdot c\Omega_d \cdot ci_d \cdot su_d + cu_m \cdot si_m \cdot si_d \cdot su_d) \cdot R_d$$

(3.3.11b)

$$z = (si_m \cdot s\Omega_m \cdot c\Omega_d \cdot cu_d - si_m \cdot s\Omega_m \cdot s\Omega_d \cdot ci_d \cdot su_d - si_m \cdot c\Omega_m \cdot s\Omega_d \cdot cu_d$$
$$-si_m \cdot c\Omega_m \cdot c\Omega_d \cdot ci_d \cdot su_d + su_d \cdot si_d \cdot ci_m) \cdot R_d \qquad (3.3.11b)$$

The above three equations are the generalized form of the coordinates of the deputy spacecraft with respect to master satellite. Substitution of $R_m = \frac{a_m \cdot (1 - e_m^2)}{1 + e_m \cdot \cos\theta_m}$ and $R_d = \frac{a_d \cdot (1 - e_d^2)}{1 + e_d \cdot \cos\theta_d}$ in equations (3.3.11a – 3.3.11c) yields a set of equations with the orbital properties of both the master and deputy satellites including the master satellite eccentricity, a parameter that was neglected in the CW equations. This resultant equation is given as

$$x = (cu_m \cdot c\Omega_m \cdot c\Omega_d \cdot cu_d - cu_m \cdot c\Omega_m \cdot s\Omega_d \cdot ci_d \cdot su_d - su_m \cdot ci_m \cdot s\Omega_m \cdot c\Omega_d \cdot cu_d$$
$$+su_m \cdot ci_m \cdot s\Omega_m \cdot s\Omega_d \cdot ci_d \cdot su_d + cu_m \cdot s\Omega_m \cdot s\Omega_d \cdot cu_d + cu_m \cdot s\Omega_m \cdot c\Omega_d \cdot ci_d \cdot su_d$$
$$+su_m \cdot ci_m \cdot c\Omega_m \cdot s\Omega_d \cdot cu_d + su_m \cdot ci_m \cdot c\Omega_m \cdot c\Omega_d \cdot ci_d \cdot su_d + su_m \cdot si_m \cdot si_d \cdot su_d) \cdot \frac{a_d \cdot (1 - e_d^2)}{1 + e_d \cdot \cos\theta_d}$$
$$- \frac{a_m \cdot (1 - e_m^2)}{1 + e_m \cdot \cos\theta_m}$$

$$y = (-su_m \cdot c\Omega_m \cdot c\Omega_d \cdot cu_d + su_m \cdot c\Omega_m \cdot s\Omega_d \cdot ci_d \cdot su_d - cu_m \cdot ci_m \cdot s\Omega_m \cdot c\Omega_d \cdot cu_d$$
$$+cu_m \cdot ci_m \cdot s\Omega_m \cdot s\Omega_d \cdot ci_d \cdot su_d - su_m \cdot s\Omega_m \cdot s\Omega_d \cdot cu_d - su_m \cdot s\Omega_m \cdot c\Omega_d \cdot ci_d \cdot su_d$$
$$+cu_m \cdot ci_m \cdot c\Omega_m \cdot s\Omega_d \cdot cu_d + cu_m \cdot ci_m \cdot c\Omega_m \cdot c\Omega_d \cdot ci_d \cdot su_d + cu_m \cdot si_m \cdot si_d \cdot su_d) \cdot \frac{a_d \cdot (1 - e_d^2)}{1 + e_d \cdot \cos\theta_d}$$

$$z = (si_m \cdot s\Omega_m \cdot c\Omega_d \cdot cu_d - si_m \cdot s\Omega_m \cdot s\Omega_d \cdot ci_d \cdot su_d - si_m \cdot c\Omega_m \cdot s\Omega_d \cdot cu_d$$
$$-si_m \cdot c\Omega_m \cdot c\Omega_d \cdot ci_d \cdot su_d + su_d \cdot si_d \cdot ci_m) \cdot \frac{a_d \cdot (1 - e_d^2)}{1 + e_d \cdot \cos\theta_d} \qquad (3.3.12)$$

Equation 3.3.12, can be used to analyze any type of formation pattern with any number of satellites acting as the deputy.

3.3.1 Verification of the Results

To verify the consistency of the derived relative co-ordinate equations, simulations are performed for different initial conditions. The technique behind the verification procedure is as follows.

For verifying the consistency of the x co-ordinate that represents the radial direction, all the orbital elements of the master satellite and the deputy satellite except for the altitude of the orbit are assumed to be the same. If the derivation for x is consistent with the derived equations then the simulation should start with an initial value of x that represents the difference in altitudes. Also because of the difference in altitudes the y co-ordinate should be expected to change for the simulated time due to the difference in the orbital periods. The value of the z co-ordinate should remain zero throughout the simulated time.

For verifying the consistency of the y co-ordinate, all the orbital elements of the master and the deputy satellites except for the true anomaly are assumed to be the same. If the derivation for y is consistent with the derived equations then the simulation should start with an initial value of y that equals the product of the radius of the orbit and the difference in true anomaly. This is illustrated in figure 3.3.2. Also the values of the other coordinates namely x and z should remain zero throughout the simulated time.

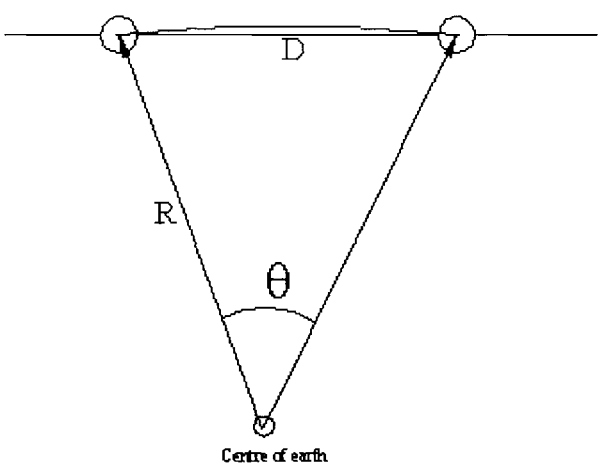

FIGURE 3.3.2 RELATIONSHIP BETWEEN THE ANGLE SUBTENDED AND THE DISTANCE OF SEPARATION

For verifying the consistency of the z co-ordinate, two different simulations are performed. In both the simulations the equator is considered as the starting point of the simulation. In the first simulation, the value of all other orbital elements of the master satellite and the deputy satellite except for the inclination are assumed to be the same. If the derivation of the z co-ordinate is consistent then the simulation should start with zero value of z and should increase progressively for one fourth of the orbit and then decrease to zero at exactly half of the orbital revolution. This is because of the plane of the orbits intersecting at the equator. In the other simulation, the value of all other orbital elements except for the RAAN is assumed to be the same. If the derivation of the z co-ordinate is consistent then the simulation should start with value of z that is equal to the product of the difference in RAAN and the radius of the orbit. It should then decrease progressively for one fourth of the orbit and then increase to its initial value at exactly half of the orbital revolution. This is because of the plane of the orbits intersecting at the poles.

The results of the simulations are shown in figures 3.3.3 - 3.3.6 Figure 3.3.3 shows the result of the first simulation, where the consistency of the x co-ordinate is verified. The satellites are assumed to be in two different altitudes with a difference in altitude of 100 m. All the other orbital elements are assumed to be the same. The value of the x co-ordinate is 100 meters in the simulation and therefore indicates that the derivation for x is consistent with the derivation. The increasing y value is due to the difference in time periods that arises as a result in the difference of altitude. The value of z is zero throughout the simulation.

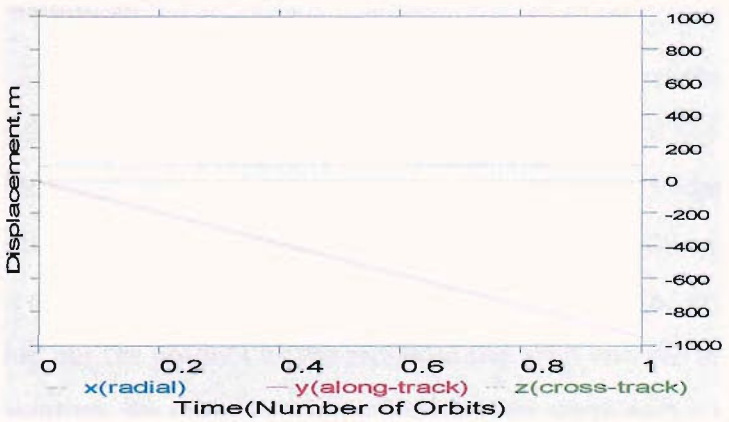

FIGURE 3.3.3 SIMULATION TO CHECK THE CONSISTENCY OF X CO-ORDINATE

Figure 3.3.4 shows the result of the second simulation, where the consistency of the y co-ordinate is verified. In this simulation, the satellites are assumed to have a small difference in true anomalies. All the other orbital elements are assumed to be the same. The value of the difference in true anomaly is selected as 8.219×10^{-4}. This corresponds to an initial separation of 100 meters for a 600-km altitude orbit.

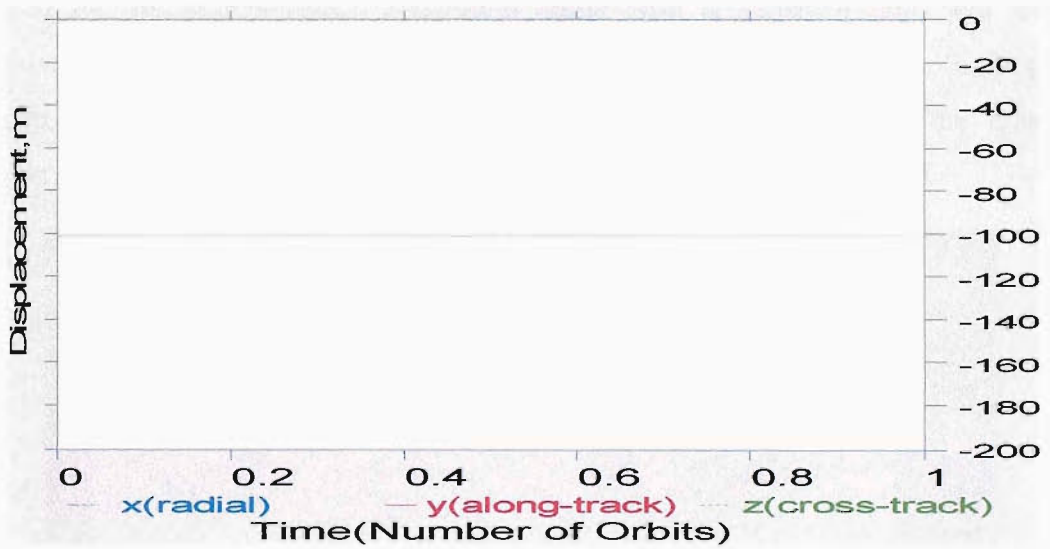

FIGURE 3.3.4 SIMULATION TO CHECK THE CONSISTENCY OF Y CO-ORDINATE

As expected, the simulation starts with a value of the y that is a product of the difference in true anomaly and the radius of the orbit. The negative sign indicates that the deputy satellite is 100 meters behind the master and remains at that distance. This proves the consistency of the y co-ordinate derivation. The other coordinates namely x and z remain at a zero value throughout the simulation.

Figures 3.3.5 and 3.3.6 show the results of the third simulation, where the consistency of the z co-ordinate is verified. For figure 3.3.5, all the orbital elements of the satellites are same except for the difference in RAAN that is chosen to be 0.005 degrees. This should correspond to an initial cross-track separation of approximately 608 meters for a 600-km altitude orbit if the z co-ordinate were to be correct. This is because the cross-track separation in this case is nothing but the product of the radius of the orbit and the difference in RAAN. Note that in the simulation, the initial cross-track separation starts with a value of 608 meters and decreases progressively to zero value. This point corresponds to the point of intersection

of the orbital planes of the satellites as discussed earlier. And then the cross-track separation starts to increase until it reaches the maximum value of 608 meters at exactly half of the orbit. For figure 3.3.6, all the orbital elements of the satellites are same except for the difference in inclination that is chosen to be 0.005 degrees. This corresponds to an initial cross-track separation of zero as the orbital planes intersect at the equator. Note that in the simulation the initial cross-track separation starts with a value of zero and increases progressively to a value of approximately 608 meters. This point corresponds to the point of maximum separation of the orbital planes of the satellites. And then the cross-track separation starts to decrease until it reaches the zero at exactly half of the orbit.

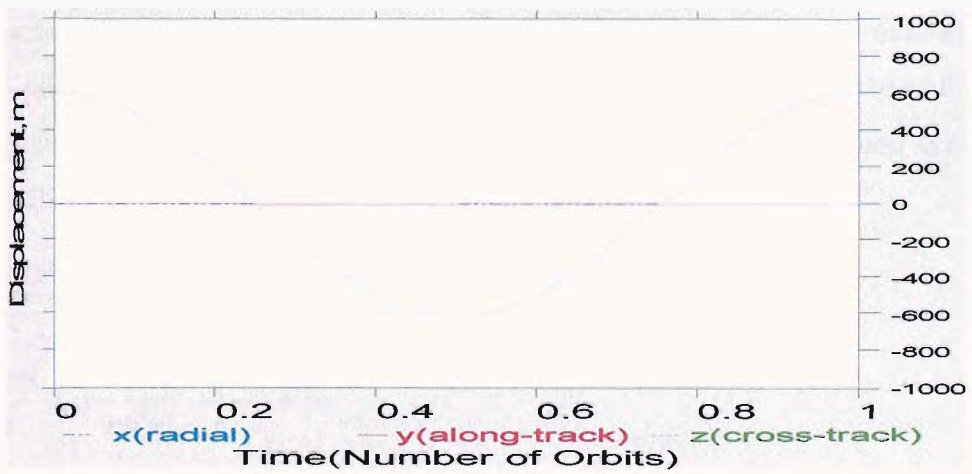

FIGURE 3.3.5 SIMULATION TO CHECK THE CONSISTENCY OF Z CO-ORDINATE BY CHANGING THE RAAN

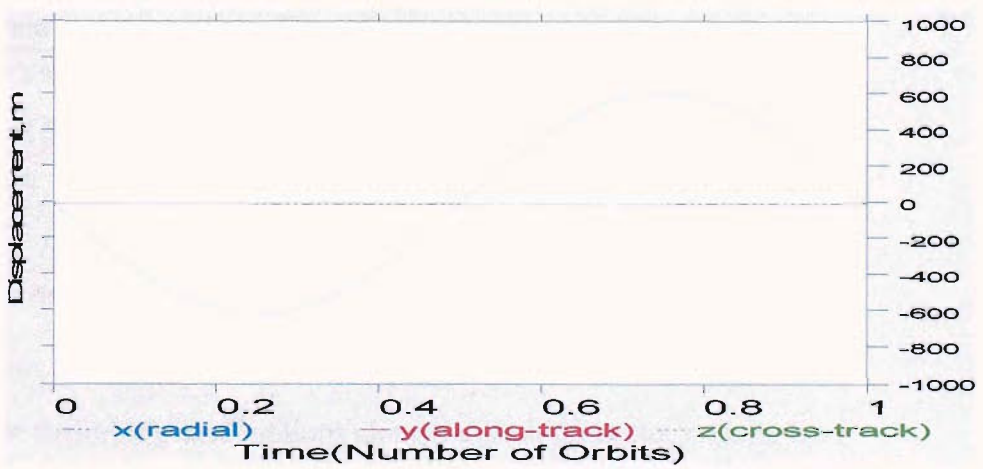

FIGURE 3.3.6 SIMULATION TO CHECK THE CONSISTENCY OF Z CO-ORDINATE BY CHANGING THE INCLINATION

3.3.2 Dynamical Modeling of Perturbative Forces using Gauss Equations

The equations for the relative coordinates derived in the previous section contain all the orbital properties of both the master and the deputy spacecraft making it a very useful tool in predicting the exact relative trajectory in the presence of external forces, if the rate of change of the orbital elements is known.

In the earlier developed preliminary method, the low-propulsion flight theory was used to study the dynamical behavior of the relative motion equations. Now, the Gauss perturbation equations will be used to study the rate of change of orbital elements. The Gauss perturbation equations are a group of equations that describe the change of all orbital elements with time in the presence of perturbations. They are well suited to study long-term evolution of orbital elements under perturbation influence[29]. The Gauss equations can also be used to study the effect of perturbative forces in all three directions making it a better method than the low-propulsion flight method. The Gauss perturbation equations are given as[29]

$$\frac{da}{dt} = \frac{2e\sin\theta}{nx} a_r + \frac{2ax}{nr} a_t$$

$$\frac{de}{dt} = \frac{x\sin\theta}{na} a_r + \frac{x}{na^2 e}\left(\frac{a^2x^2}{r} - r\right) a_t$$

$$\frac{di}{dt} = \frac{r\cos u}{na^2 x} a_z$$

$$\frac{d\Omega}{dt} = \frac{r\sin u}{na^2 x\sin i} a_z$$

$$\frac{d\omega}{dt} = \frac{x\cos\theta}{nae} a_r + \frac{p}{eh}\left[\sin\theta\left(1+\frac{1}{1+e\cos\theta}\right)\right] a_t - \frac{r\cot i\sin u}{na^2 x} a_z$$

$$\frac{dM}{dt} = n - \frac{1}{na}\left(\frac{2r}{a} - \frac{x^2}{e}\cos\theta\right) a_r - \frac{x^2}{nae}\left(1+\frac{r}{ax^2}\right)\sin\theta a_t \qquad (3.3.2.1)$$

where

a_r, a_t, a_z = Perturbing accelerations along the position vector r, along the velocity vector direction and normal to the orbit plane respectively.

θ= True anomaly, n = mean motion, $x = \sqrt{1-e^2}$, $u = \omega + \theta$, $p = a(1-e^2), h = \sqrt{\mu p}$

The Gauss perturbation equations can be used to study the effects of perturbations for long time intervals if the perturbing forces are small compared to those that produce the two body motion [30].

3.3.3 Improved Version of the Gauss equations

The Gauss's Perturbation equations [29], defined with the classical orbital elements in the above subsection, can be used to find the variation of orbital elements only for orbits without zero eccentricity and zero inclination as one or more equations have eccentricity and inclination terms in the denominator. To remove the singularities for circular and equatorial orbits one can use non-singular equinoctial elements. The equinoctial orbital element set is defined by Battin[27] as the semi major axis, a, unnamed elements, P_1, P_2, Q_1, and Q_2, and the mean longitude, l. Some authors refer to these elements as a, h, k, p, q and λ. The non-singular equinoctial elements are defined in terms of the classical elements as [27]:

$$\begin{aligned} a &= a \\ P_1 &= e\sin\varpi \\ P2 &= e\cos\varpi \\ Q_1 &= \tan(i/2)\sin\Omega \\ Q_2 &= \tan(i/2)\cos\Omega \\ l &= \varpi + M \end{aligned} \qquad (3.3.2.2)$$

where ϖ, the longitude of pericenter, is defined as

$$\varpi = \Omega + \omega$$

In addition to the mean longitude, l, the true longitude, L, is defined as

$$L = \varpi + \theta$$

The reverse transformation is given by:

$$a = a$$

$$e = (P_1^2 + P_2^2)^{1/2}$$

$$i = 2\tan^{-1}(Q_1^2 + Q_2^2)^{1/2}$$

$$\Omega = \tan^{-1}(Q_1/Q_2)$$

$$\omega = \tan^{-1}(P_1/P_2) - \tan^{-1}(Q_1/Q_2)$$

$$M = 1 - \tan^{-1}(P_1/P_2) \qquad (3.3.2.3)$$

The Gauss Perturbation equations in terms of the non-singular equinoctial orbital elements then become [31]:

$$\frac{da}{dt} = \frac{2a^2}{h}\left[\left(P_2 \sin L - P_1 \cos L\right)a_r + \frac{p}{r}a_t\right]$$

$$\frac{dP_1}{dt} = \frac{r}{h}\left\{-\frac{p}{r}\cos L a_r + \left[P_1 + \left(1+\frac{p}{r}\right)\sin L\right]a_t - P_2\left(Q_1 \cos L - Q_2 \sin L\right)a_z\right\}$$

$$\frac{dP_2}{dt} = \frac{r}{h}\left\{-\frac{p}{r}\sin L a_r + \left[P_2 + \left(1+\frac{p}{r}\right)\cos L\right]a_t - P_1\left(Q_1 \cos L - Q_2 \sin L\right)a_z\right\}$$

$$\frac{dQ_1}{dt} = \frac{r}{2h}\left(1+Q_1^2+Q_2^2\right)\sin L a_z$$

$$\frac{dQ_2}{dt} = \frac{r}{2h}\left(1+Q_1^2+Q_2^2\right)\cos L a_z$$

$$\frac{dl}{dt} = n - \frac{r}{h}\left\{\begin{array}{l}\left[\frac{a}{a+b}\left(\frac{p}{r}\right)\left(P_1 \sin L + P_2 \cos L\right) + \frac{2b}{a}\right]a_r + \frac{a}{a+b}\left(1+\frac{p}{r}\right)\cdot \\ \left(P_1 \cos L - P_2 \sin L\right)a_t + \left(Q_1 \cos L - Q_2 \sin L\right)a_z\end{array}\right\}$$

(3.3.2.4)

where b is the semi minor axis and

$$h = nab$$

$$b = a\sqrt{1 - P_1^2 - P_2^2}$$

$$\frac{p}{r} = 1 + P_1 \sin L + P_2 \cos L$$

$$\frac{r}{h} = \frac{h}{\mu\left(1 + P_1 \sin L + P_2 \cos L\right)}$$

and a_r, a_t, a_z as defined in equation 3.3.2.1

The relative trajectory equations can similarly be modified with the equinoctial variables to make it compatible with the Gauss's equation with equinoctial variables. This can be done by substituting the classical orbital elements in the relative motion equations (3.3.11a - 3.3.11c) with their respective equinoctial variable substitutes from equation (3.3.2.3).

3.3.4 Relative Trajectory Simulation Scheme

The Gauss perturbation equations relate the change of the orbital elements with time in the presence of any acceleration components. The components of the perturbative accelerations if substituted in the Gauss equations should provide the value of the rate of change of elements with time. So at any time *t*, the value of any orbital element can be found out from the following equations.

$$a(t) = a(t_0) + \int_{t_0}^{t} \frac{da}{dt} \cdot dt \qquad e(t) = e(t_0) + \int_{t_0}^{t} \frac{de}{dt} \cdot dt \qquad i(t) = i(t_0) + \int_{t_0}^{t} \frac{di}{dt} \cdot dt$$

$$\Omega(t) = \Omega(t_0) + \int_{t_0}^{t} \frac{d\Omega}{dt} \cdot dt \qquad \omega(t) = \omega(t_0) + \int_{t_0}^{t} \frac{d\omega}{dt} \cdot dt \qquad M(t) = M(t_0) + \int_{t_0}^{t} \frac{dM}{dt} \cdot dt$$

(3.3.4.1)

In the above equations, the subscript '0' refers to the initial conditions. The initial values depend on the type of formation pattern and the altitude of the formation. Equations (3.3.4.1) can be either evaluated for the master or the deputy with the respective subscripts and then when substituted in Equations (3.3.11a - 3.3.11c) yield the relative coordinates of the deputy spacecraft, at any time *t*, in the presence of the perturbative forces. The relative coordinates generalized for *n* spacecraft is given below The first subscript *m* denotes the master spacecraft and the second subscript *d* denotes the deputy spacecraft.

$$
\begin{aligned}
x_{md}(t) = (&cu_m(t)\cdot c\Omega_m(t)\cdot c\Omega_d(t)\cdot cu_d(t) - cu_m(t)\cdot c\Omega_m(t)\cdot s\Omega_d(t)\cdot ci_d(t)\cdot su_d(t)\\
&-su_m(t)\cdot ci_m(t)\cdot s\Omega_m(t)\cdot c\Omega_d(t)\cdot cu_d(t) + su_m(t)\cdot ci_m(t)\cdot s\Omega_m(t)\cdot s\Omega_d(t)\cdot ci_d(t)\cdot su_d(t)\\
&+cu_m(t)\cdot s\Omega_m(t)\cdot s\Omega_d(t)\cdot cu_d(t) + cu_m(t)\cdot s\Omega_m(t)\cdot c\Omega_d(t)\cdot ci_d(t)\cdot su_d(t)\\
&+su_m(t)\cdot ci_m(t)\cdot c\Omega_m(t)\cdot s\Omega_d(t)\cdot cu_d(t) + su_m(t)\cdot ci_m(t)\cdot c\Omega_m(t)\cdot c\Omega_d(t)\cdot ci_d(t)\cdot su_d(t)\\
&+su_m(t)\cdot si_m(t)\cdot si_d(t)\cdot su_d(t))\cdot R_d(t) - R_m(t)
\end{aligned}
$$

$$
\begin{aligned}
y_{md}(t) = (&-su_m(t)\cdot c\Omega_m(t)\cdot c\Omega_d(t)\cdot cu_d(t) + su_m(t)\cdot c\Omega_m(t)\cdot s\Omega_d(t)\cdot ci_d(t)\cdot su_d(t)\\
&-cu_m(t)\cdot ci_m(t)\cdot s\Omega_m(t)\cdot c\Omega_d(t)\cdot cu_d(t) + cu_m(t)\cdot ci_m(t)\cdot s\Omega_m(t)\cdot s\Omega_d(t)\cdot ci_d(t)\cdot su_d(t)\\
&-su_m(t)\cdot s\Omega_m(t)\cdot s\Omega_d(t)\cdot cu_d(t) - su_m(t)\cdot s\Omega_m(t)\cdot c\Omega_d(t)\cdot ci_d(t)\cdot su_d(t)\\
&+cu_m(t)\cdot ci_m(t)\cdot c\Omega_m(t)\cdot s\Omega_d(t)\cdot cu_d(t) + cu_m(t)\cdot ci_m(t)\cdot c\Omega_m(t)\cdot c\Omega_d(t)\cdot ci_d(t)\cdot su_d(t)\\
&+cu_m(t)\cdot si_m(t)\cdot si_d(t)\cdot su_d(t))\cdot R_d(t)\\
z_{md}(t) = (&si_m(t)\cdot s\Omega_m(t)\cdot c\Omega_d(t)\cdot cu_d(t) - si_m(t)\cdot s\Omega_m(t)\cdot s\Omega_d(t)\cdot ci_d(t)\cdot su_d(t)\\
&-si_m(t)\cdot c\Omega_m(t)\cdot s\Omega_d(t)\cdot cu_d(t) - si_m(t)\cdot c\Omega_m(t)\cdot c\Omega_d(t)\cdot ci_d(t)\cdot su_d(t)\\
&+su_d(t)\cdot si_d(t)\cdot ci_m(t))\cdot R_d(t)
\end{aligned}
$$

(3.3.4.2)

In the above equations $m,d = 1..n \quad \& \quad m \neq d$

and $R_m(t) = \dfrac{a_m(t)\cdot(1-e_m(t)^2)}{1+e_m(t)\cdot\cos\theta_m(t)}$, $R_d(t) = \dfrac{a_d\cdot(1-e_d{}^2(t)^2)}{1+e_d\cdot\cos\theta_d}$

represent the radius vectors at any time t and

$$u_d(t) = \theta_d(t) + \omega_d(t)$$

$$u_m(t) = \theta_m(t) + \omega_m(t)$$

are the equations for the argument of latitude.

Equation 3.3.4.2 is the same as 3.3.11 except that it is represented as a function of time and generalized for *n* number of master or deputy spacecraft.

The true anomaly can be found from the solutions of Kepler's equations[27]

$$\theta_m(t) = M_m(t) + 2e_m(t)\sin(M_m(t)) + \frac{5}{4}e_m{}^2(t)\sin(2M_m(t)) + \frac{1}{12}e_m{}^3(t)(13\sin(3M_m(t)) - 3\sin(M_m(t)))$$

$$\theta_d(t) = M_d(t) + 2e_d(t)\sin(M_d(t)) + \frac{5}{4}e_d{}^2(t)\sin(2M_d(t)) + \frac{1}{12}e_d{}^3(t)(13\sin(3M_d(t)) - 3\sin(M_d(t)))$$

It should be noted that the above solutions to the Kepler's equations work well for only small values of eccentricities because they contain values of eccentricity only up to the third order. For large eccentricity values (e>0.001), the higher order terms should also be considered [27]. In the actual simulations that accompany the discussions in this thesis the Kepler's solutions have 6th order eccentricity terms.

For a Keplerian case, only u ($\theta + \omega$) is a function of time. All other orbital elements are constants. For perturbed orbits, all the orbital elements become functions of time. The change in each orbital element for every step size simulated is calculated by the Gauss Perturbation equations. These orbital elements are updated every second and hence we see the evolution of x, y, z as a function of time.

In a real formation flying mission, equations 3.3.4.2 can be used for finding the relative trajectory of the deputy with respect to master by using onboard Global Positioning Satellite (GPS) receivers. With the help of GPS receivers, fitted on the deputy and the master spacecraft, the position and the velocity of the satellites can be found in the Geo-Centric frame of reference. This can be converted to the Orbital elements with a standard transformation[29] and once the orbital elements are calculated, they can be substituted in equations 3.3.4.2 to calculate the instantaneous positions in the master spacecraft frame of reference.

There are two main properties associated with relative orbits considered in the Master satellite's frame of reference. They are

1. $\Pi_{md} = \Pi_{ij} + \Pi_{jn}$ $(i \neq j)$

2. $\Pi_{md} = -\Pi_{dm}$

where $\Pi \equiv x, y, z$

This means that if we consider an array of 5 spacecraft in the Master satellite's frame of reference,, the along-track separation distance between spacecraft 1 and spacecraft 5 can be written as

$$y_{15} = y_{13} + y_{35} = y_{12} + y_{23} + y_{34} + y_{45} = -y_{51}$$

Similarly the radial separation and the cross-track separation can be written as

$$x_{15} = x_{13} + x_{35} = x_{12} + x_{23} + x_{34} + x_{45} = -x_{51}$$

$$z_{15} = z_{13} + z_{35} = z_{12} + z_{23} + z_{34} + z_{45} = -z_{51}$$

3.3.5 Orbit Integrator and Numerical integration

Runge-Kutta Fehlberg (6^{th} order method) has been used to numerically integrate the Gauss perturbation equations. This method was found to be 10^2 –10^3 times more accurate than the traditional Runge Kutta method. This was found by comparing the error estimates that they yield for various step sizes. The Runge-Kutta Fehlberg method and also has an optimum step size control for any assigned tolerance. This means that the Runge-Kutta Fehlberg Algorithm continuously checks the errors and decreases the step size automatically to match with the assigned tolerance value. The decrease in step size is done by decrements of 0.1 sec. The step size used in all simulations is 1 second. In the simulations, the tolerance control value was assigned as 10^{-4}. This was to effectively reduce the simulation time. The total time taken for 1 complete orbital simulation clocked at an average of 15 minutes for a perturbed case and 2 minutes for a Keplerian case. MathConnex, a visual simulation program, has been used to perform the simulations. Mathconnex is a product of MathCad that has many inbuilt functions and is being used by many millions of people worldwide. The product is known for its simplicity, flexibility and accuracy of its inbuilt functions. The best feature of Mathconnex is its ability to check the compatibility of units within the terms of a general equation.

The whole mathematical model was optimized for accuracy and not for the time of simulations. Efforts were taken to decrease the loss of accuracy in the simulations by using a standard 4 decimal input and output format for both the master and deputy's orbital elements.

This is also true for any constants declared in the initial conditions. This considerably helps to reduce the loss of accuracy due to rounding errors. This was particularly important with the calculation of the true anomaly of the master and the deputy spacecraft as different input/output formats would result in an unwanted secular drift caused due to the difference in evolution of the absolute orbits. The simulation code is written to accommodate zero eccentricities and zero inclinations by converting all the classical orbital elements to modified equinoctial elements. The effects of perturbative forces like Atmospheric drag, Solar radiation pressure, J_2, J_3, J_4 and J_5 have been effectively modeled into the simulation algorithm. The mathconnex interface allows the user to select or disengage any force component during the simulation process. The effect of these perturbative forces is discussed in section 4.3 of the next chapter. The algorithm for the Runge-Kutta Fehlberg method is given in Appendix A.

Chapter 4

Properties of Spacecraft Relative Orbits

The first part of this chapter deals with orbits of an unforced nature (without perturbations) and the second part deals with orbits with various perturbations.

4.1 Equations of Relative Coordinates For Closely Placed Formation Flying Spacecraft

Firstly, the equations for relative coordinates for a closely placed Formation-Flying scenario using equations (3.3.11a - 3.3.11c) will be derived. For closely placed Formation-Flying spacecraft $\delta\Omega = \Omega_m - \Omega_d$, $\delta i = i_m - i_d, \delta u = u_m - u_d$ and $\delta i, \delta u$ and $\delta\Omega$ are very small and so it can be assumed that the sine's of the angles $\delta i, \delta u$ and $\delta\Omega$ are equivalent to their argument and their cosines equivalent to one.

By rearranging the terms in equation (3.3.11a) and by considering $\delta\Omega = \Omega_m - \Omega_d$

$$x = cu_m \cdot (cu_d \cdot c\delta\Omega + ci_d \cdot su_d \cdot s\delta\Omega) + su_m \cdot (si_m \cdot si_d \cdot su_d + ci_m \cdot (ci_d \cdot su_d \cdot c\delta\Omega - cu_d \cdot s\delta\Omega)) \cdot R_d - R_m$$
$$\Rightarrow x = (cu_m \cdot cu_d + su_m \cdot su_d \cdot si_m \cdot si_d + su_m \cdot su_d \cdot ci_m \cdot ci_d) \cdot R_d - R_m$$
$$\Rightarrow x = c\delta u \cdot R_d - R_m = R_d - R_m = \delta R \Rightarrow x = \delta R \qquad (4.1.1)$$

Similarly equation (3.3.11b) becomes

$$y = (-su_m \cdot cu_d \cdot c\Omega_d - ci_m \cdot cu_m \cdot (cu_d \cdot s\delta\Omega - ci_d \cdot su_d \cdot c\delta\Omega) + su_d \cdot (si_m \cdot si_d \cdot cu_m - ci_d \cdot su_m \cdot s\delta\Omega)) \cdot R_d$$
$$\Rightarrow y = (-su_m \cdot cu_d - ci_m \cdot cu_m \cdot cu_d \cdot \delta\Omega + ci_m \cdot cu_m \cdot ci_d \cdot su_d + su_d \cdot si_m \cdot si_d \cdot cu_m - su_d \cdot ci_d \cdot su_m \cdot \delta\Omega) \cdot R_d$$

Assumption of $\cos i_m \approx \cos i_d$ yields

$$\Rightarrow y = (-su_m \cdot cu_d + cu_m \cdot su_d \cdot c\delta i + ci_m \cdot \delta\Omega \cdot c\delta u) \cdot R_d$$
$$\Rightarrow y = (\sin\delta u + \cos i_m \cdot \delta\Omega \cdot \cos\delta u) \cdot R_d \qquad (4.1.2)$$

and finally equation (3.3.11c) can be written as

$$z = (su_d \cdot si_m \cdot ci_d - cu_d \cdot si_m \cdot \delta\Omega - ci_m \cdot su_d \cdot si_d) \cdot R_d$$
$$\Rightarrow z = (\sin u_d \cdot \delta i - \sin i_m \cdot \cos u_d \cdot \delta\Omega) \cdot R_d \qquad (4.1.3)$$

So for a Close Formation flying scenario, the relative coordinates of the deputy spacecraft can be represented as

$$\begin{bmatrix} x \\ y \\ z \end{bmatrix} = \begin{bmatrix} \cos\delta u \cdot R_d - R_m \\ (\sin\delta u + \cos i_m \cdot \delta\Omega \cdot \cos\delta u) \cdot R_d \\ (\sin u_d \cdot \delta i - \sin i_m \cdot \cos u_d \cdot \delta\Omega) \cdot R_d \end{bmatrix} \tag{4.1.4}$$

or assuming $\cos\delta u \approx 1$ and $\sin\delta u \approx \delta u$ for small values of δu and $R_d - R_m = \delta R$

$$\begin{bmatrix} x \\ y \\ z \end{bmatrix} = \begin{bmatrix} \delta R \\ (\delta u + \cos i_m \cdot \delta\Omega) \cdot R_d \\ (\sin u_d \cdot \delta i - \sin i_m \cdot \cos u_d \cdot \delta\Omega) \cdot R_d \end{bmatrix} \tag{4.1.5}$$

It is interesting to note that the above equation for relative coordinates is the same as equation (2.2.2) for an unperturbed orbit derived by Gim[12] using a transformation matrix and expanding it with Taylor series. It should be noted that $\delta\theta = \delta u$ in equation 2.2.2.

4.1.1 Validity of the results for the Close formation flying Scenario

Equation 4.1.5, for a closely placed formation-flying scenario, was derived from the general relationship for the relative coordinates namely equations (3.3.12). Since the derivation involved many simplifications, it is obvious that the resultant formulae are only valid for a closely placed formation-flying scenario. Now the unanswered question is how close should the satellite formation be to obtain errors of insignificant magnitude? To answer this question and to understand the accuracy of the derived formulae, a strategy was developed. According to the strategy, it was decided to gradually increase the satellite separation using one of the orbital elements, namely the right ascension of the ascending node (RAAN) and then find the difference in the relative coordinates using equations (3.3.12) and the equation 4.1.5 for different separation distances. Theoretically, the difference is nothing but the error arising as a result of the assumptions and simplifications made in equation 4.1.5. A very small error in the order of a few millimeters indicates that the equation 4.1.5 is still accurate and valid for

that separation distance. For all the simulations, the spacecraft altitude was assumed to be 600 km.

Plots 4.1.1 – 4.1.3 show the variation of errors for three different values of separation distance. The orbital elements used in both the methods are the same. Figure 4.1.1 is plotted for 100 orbits and for a difference in RAAN of $5x10^{-5}$ degrees. The corresponding cross-track separation distance is 6.08 meters. The errors are in the order of 10^{-6} m in the radial direction, 10^{-8} m in the along-track direction and 10^{-13} m in the cross-track direction over 100 orbits. . Figure 4.1.2 is plotted for 100 orbits and for a difference in RAAN of $5x10^{-3}$ degrees. The corresponding cross-track separation distance is approximately 608 meters. The errors are in the order of 10^{-2} m in the radial direction, 10^{-3} m in the along-track direction and 10^{-7} m in the cross-track direction over 100 orbits.

Figure 4.1.3, like figures 4.1.1 and 4.1.2 is plotted for 100 orbits and for a difference in RAAN of 10^{-1} degrees. The corresponding cross-track separation distance is 61 km. The errors are in the order of approximately 265 m in the radial direction, 10 m in the along-track direction and 0.7 m in the cross-track direction over 100 orbits.

It is evident from the simulations that the accuracy of equation 4.1.5 deteriorates with time and the initial separation distance due to the simplifications made in the derivations.. For a 60-km cross-track separation, the errors of predicting the initial relative coordinates were found to be hundreds of meters for the radial direction and tens of meters for the along-track. However, the errors were in the magnitude of 10^{-7}m – 10^{-9} m for very closely placed spacecraft. Therefore it is wise to conclude that the usage of equation 4.1.5 is only limited to very closely placed spacecraft where the initial displacement is in the order of a few tens or hundred of meters. For accurate prediction of relative coordinates for any separation, equations (3.3.12) should be used instead.

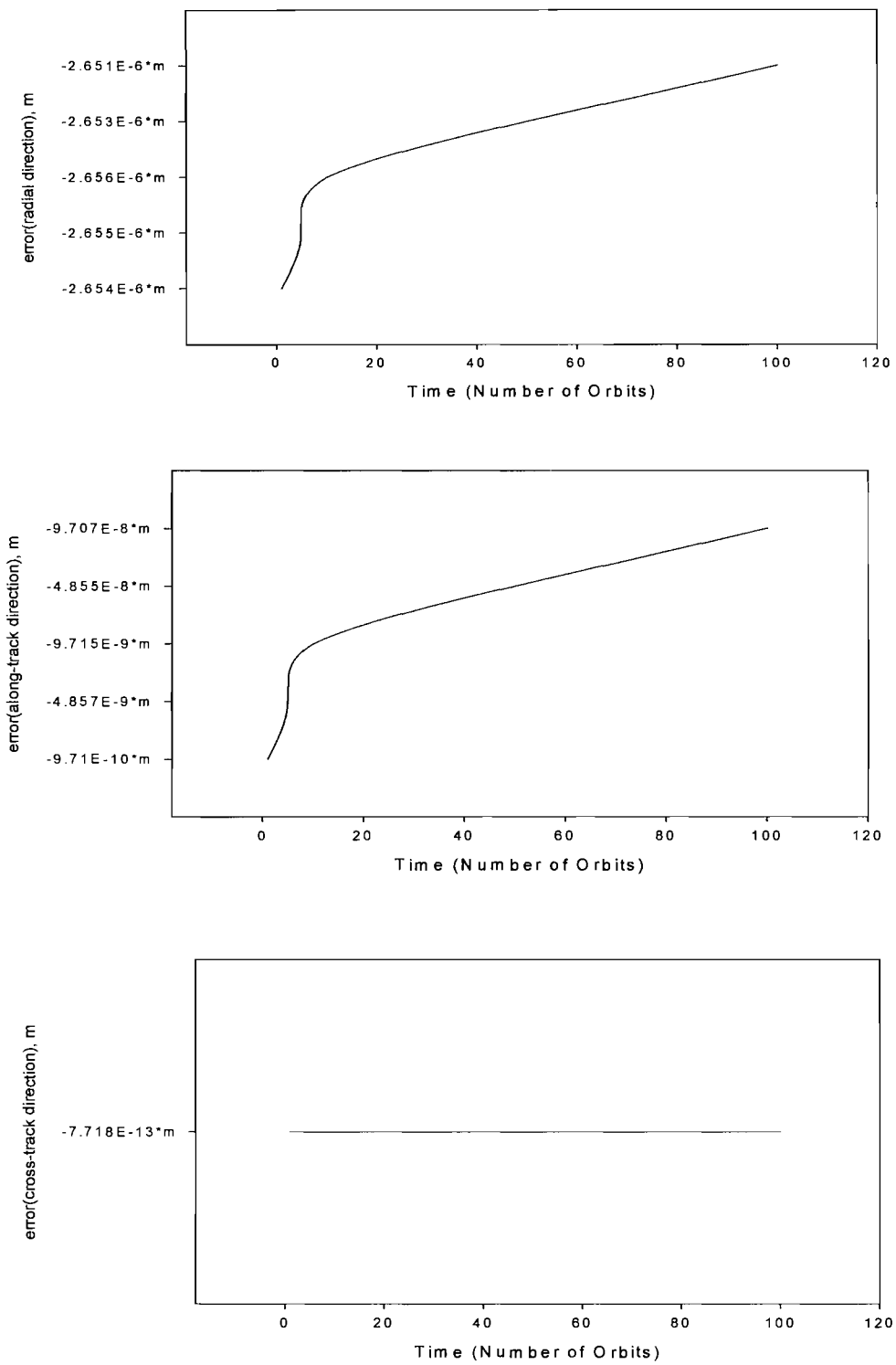

FIGURE 4.1.1 ERRORS IN THE RELATIVE COORDINATES GENERATED BY THE GEOMETRY METHOD FOR A DIFFERENCE IN RAAN OF $5X10^{-5}$ DEGREES

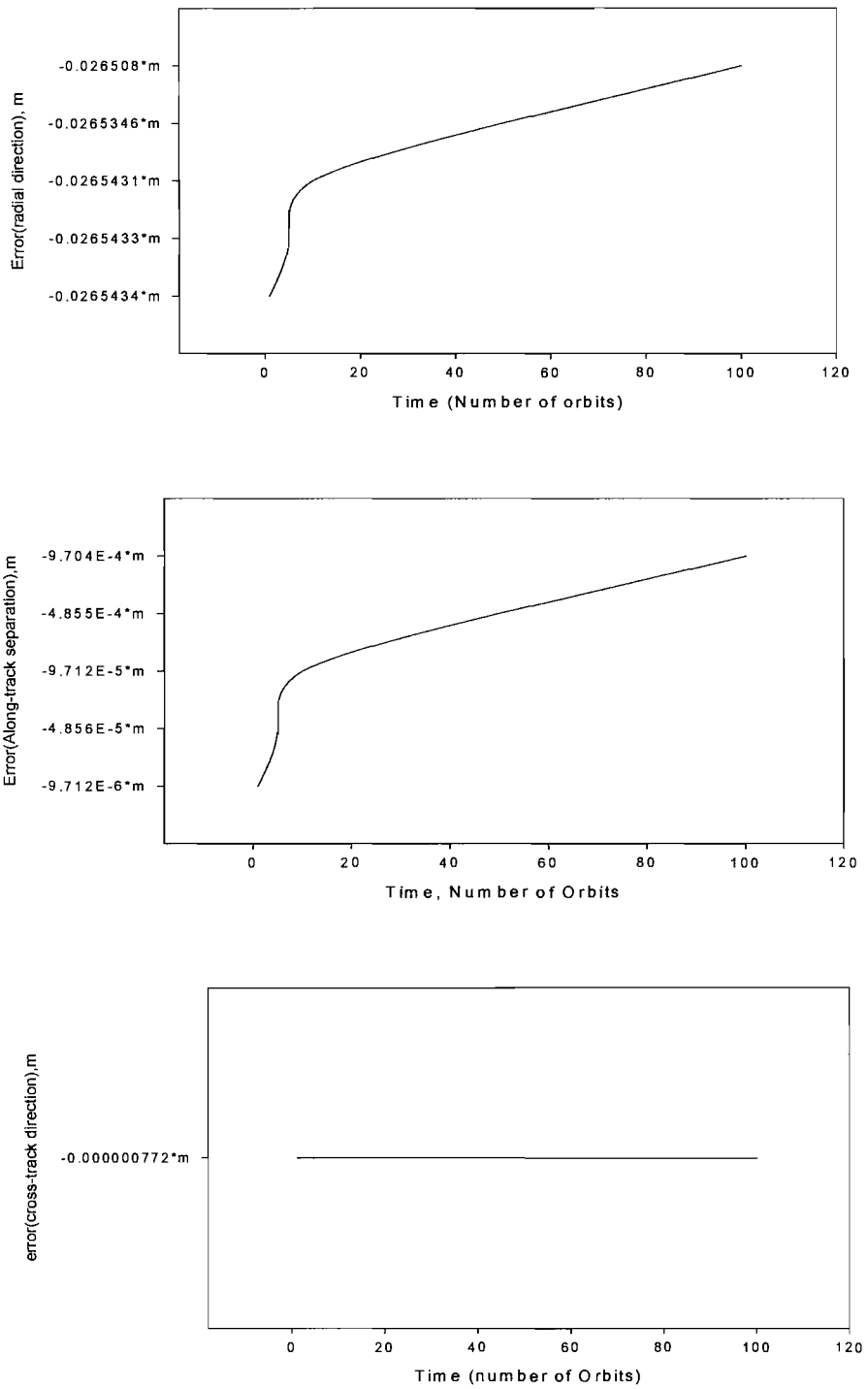

FIGURE 4.1.2 ERRORS IN THE RELATIVE COORDINATES GENERATED BY THE GEOMETRY METHOD FOR A DIFFERENCE IN RAAN OF $5X10^{-3}$ DEGREES

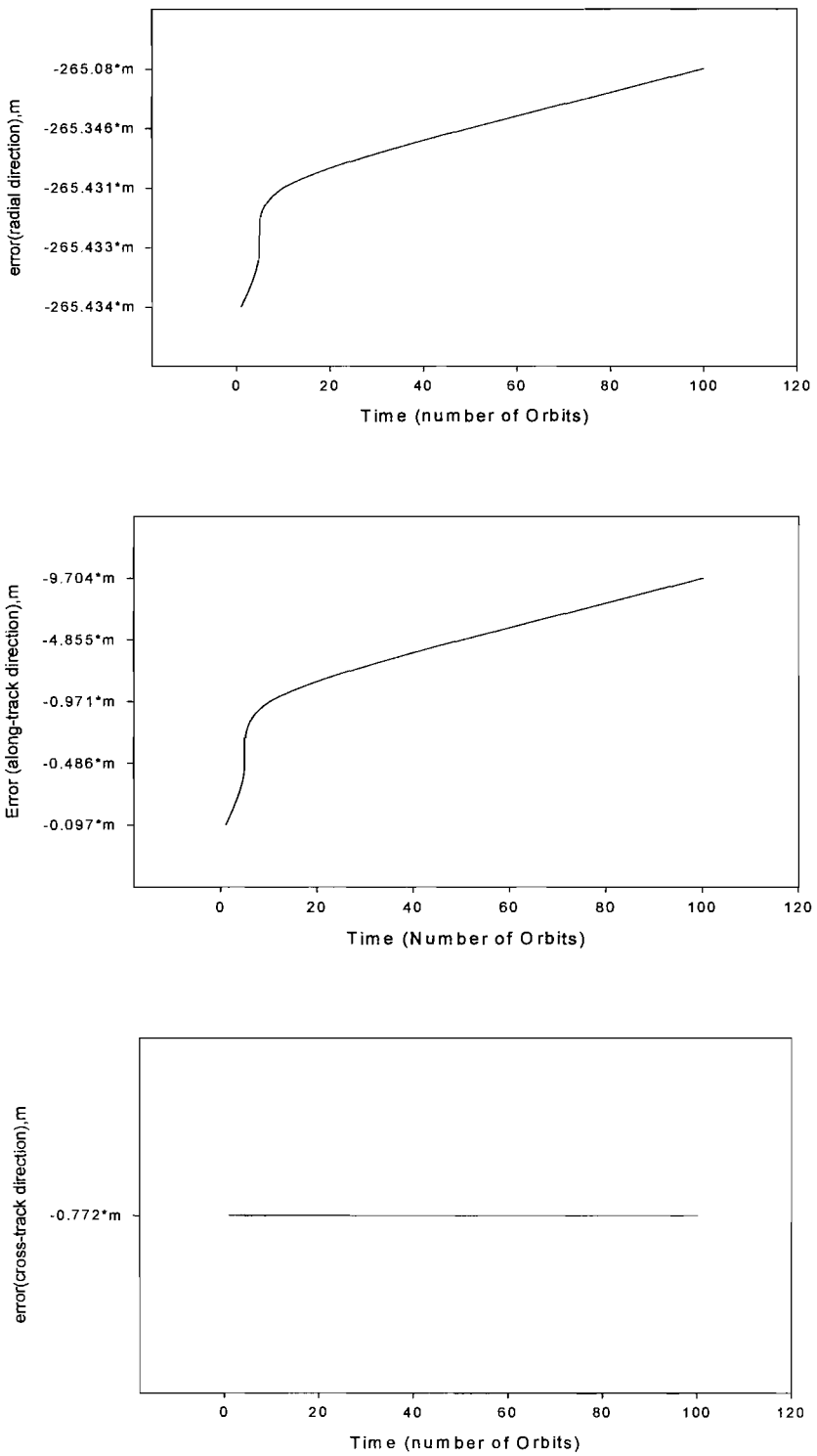

FIGURE 4.1.3 ERRORS IN THE RELATIVE COORDINATES GENERATED BY THE GEOMETRY METHOD FOR A DIFFERENCE IN RAAN OF $5x10^{-1}$ DEGREES

4.2 Free Spacecraft Relative Orbits

In this section, the dynamics of satellite relative motion will be studied for the case when the motion of satellites is purely keplerian. i.e., no perturbative forces disturb the orbits. To start with, a case is considered where the satellites are in the same plane, i.e. $\delta\Omega = 0$, $\delta i = 0$.

Equation (4.1.4) then becomes

$$\begin{bmatrix} x \\ y \\ z \end{bmatrix} = \begin{bmatrix} \cos\delta u \cdot R_d - R_m \\ \sin\delta u \cdot R_d \\ 0 \end{bmatrix} \tag{4.2.1}$$

From the above equation, it is clear that

$$\left(\frac{x + R_m}{R_d}\right)^2 + \left(\frac{y}{R_d}\right)^2 = 1 \tag{4.2.2}$$

From equation 4.2.2, it is evident that the relative trajectory is a circle if R_m and R_d are constant throughout, i.e. when the orbits of the master and deputy are circular with equal or different altitudes. On the other hand, when both R_m and R_d are variable, i.e. when the orbits of the master and deputy are elliptical, the relative trajectory is a moving circle placed in a circular band of variable radii This is because the origin and the radius of the circle changes periodically. To test this and other possible conditions, the following test cases are simulated;

1. Both Master and Deputy satellites are in a circular orbit and

- The orbits have same/different altitudes and
    - Lie in the same plane
    - Lie in different planes

2. Both Master and Deputy satellites have elliptical orbits and the orbits
    - Lie in the same plane

The corresponding orbital elements for the different graphs plotted based on the above defined conditions of simulation are given in table (4.2.2) below.

	Fig. 4.2.1	**Fig. 4.2.2**	**Fig. 4.2.3**
a_m, **km**	6971	6971	6971
Ω_m, **deg**	10	10	10
i_m, **deg**	90	90	90
ω_m, **deg**	0	0	0
e_m	0	0	0.005
a_d, **km**	6981	6971	6971
Ω_d, **deg**	10	10.005	10
i_d, **deg**	90	90	90
ω_d, **deg**	0	0	0
e_d	0	0	0.001

Table 4.2.1 Simulation conditions for the master and the deputy for the unforced case

Figure 4.2.1 corresponds to a case where there is an initial radial separation of 10km. There is no along-track or cross-track separation. Figure 4.2.2 corresponds to a case where there is an initial cross-track separation due to a difference in RAAN of 0.005 degrees. There are no initial radial or along-track separations. Figure 4.2.3 corresponds to a case where both the master and the deputy have elliptical orbits of different eccentricities and both the spacecraft have no initial separation in all the three directions. The first of the plots shows the simulation of relative orbits with only radial separation and is given in the next page.

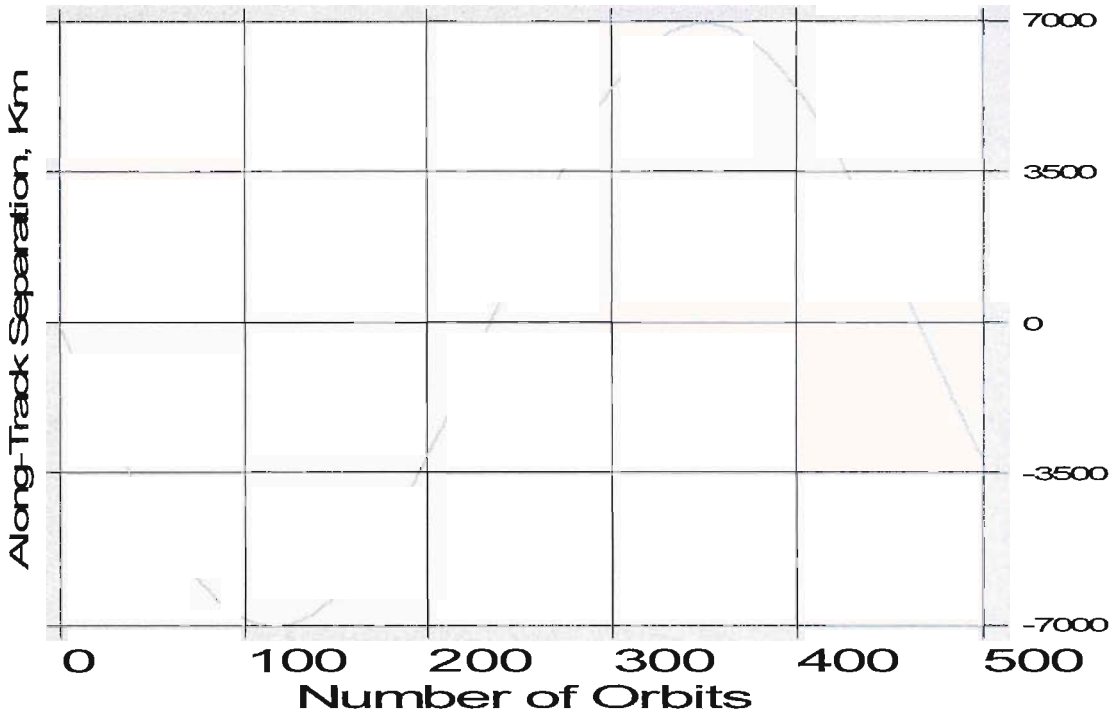
Along-Track Separation, Km
7000
3500
0
-3500
-7000
0
100
200
300
400
500
Number of Orbits

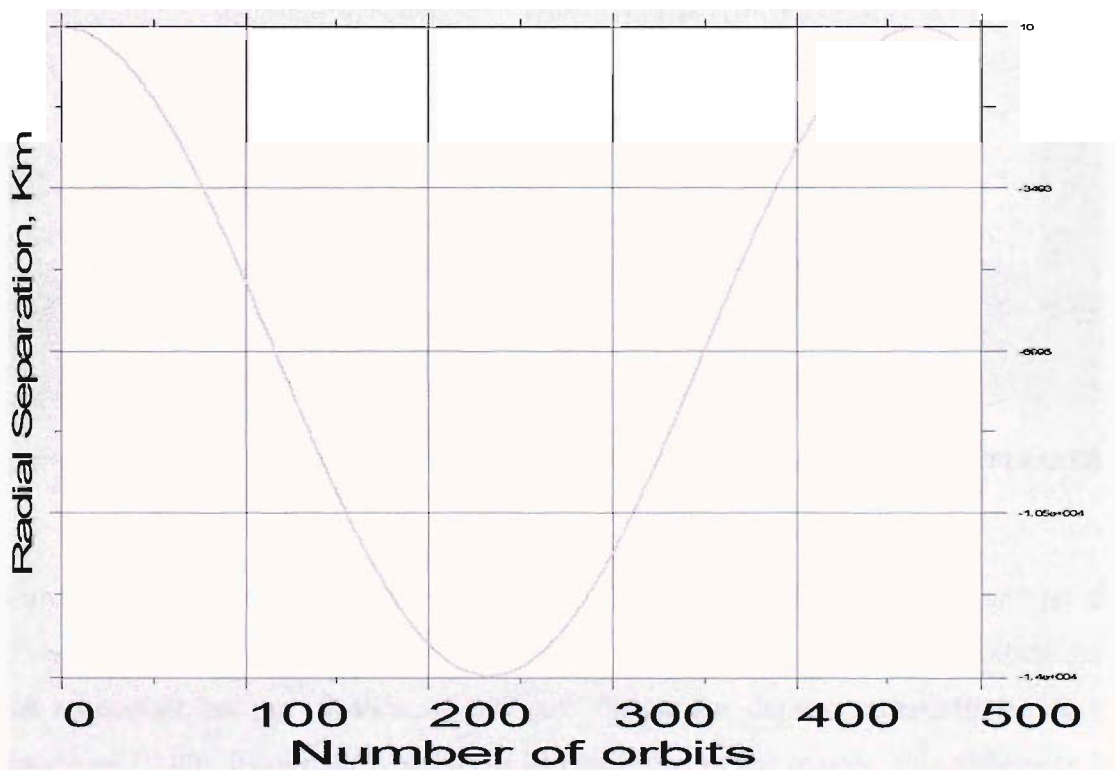
Radial Separation, Km
10
-3493
-6995
-1.05e+004
-1.4e+004
0
100
200
300
400
500
Number of orbits

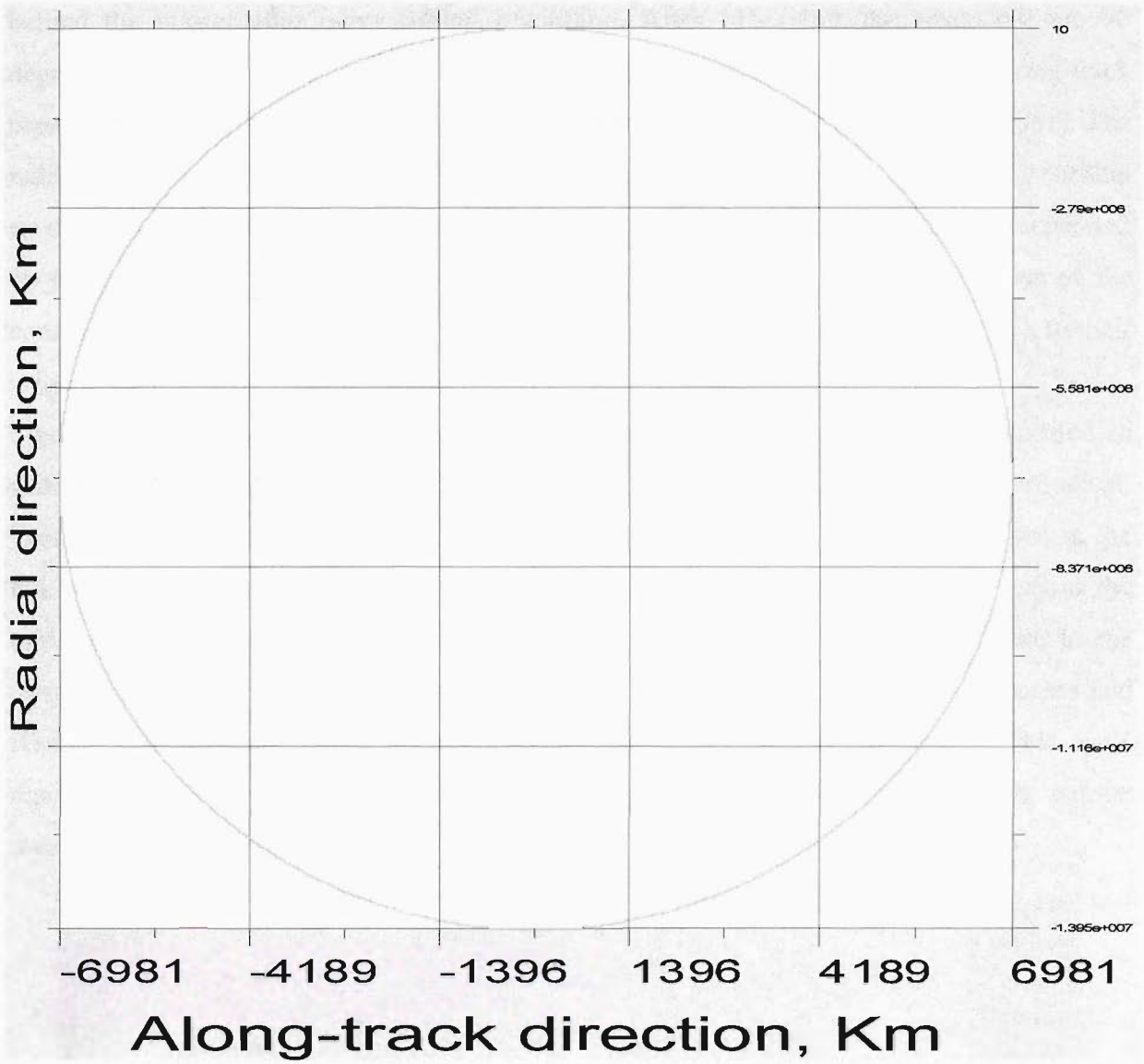

FIGURE 4.2.1 EVOLUTION OF RELATIVE TRAJECTORY FOR MASTER AND DEPUTY SEPERATED BY 10 KM RADIAL SEPERATION

In figure 4.2.1, the deputy spacecraft has an initial radial separation of 10 km and no along-track separation. Both the master and the deputy spacecraft are in circular orbits and the master spacecraft has an altitude of 600 km. Since the deputy spacecraft has a radial separation of 10 km, its circular velocity is less than that of the master. The difference in the orbital velocities results in a difference of time period of the master and the deputy spacecraft by 12.47 seconds. This difference of orbital time periods causes the deputy spacecraft to fall

behind the master after every orbital revolution. After 115 orbits the spacecraft are 90 degrees apart with respect to the center of the earth and this is the maximum along-track separation distance (radius of the spacecraft + separation distance = 6971 +10 == 6981). The radial separation distance also increases in the negative direction. After 230 orbital revolutions, the spacecraft are 180 degrees apart from one another and so they are separated by the distance of their radiuses whereas the along-track direction is zero because of the considered frame of reference. The whole cycle repeats and the spacecraft come back to their original positions after 460 orbits.

Figure 4.2.2 shows the evolution of relative trajectory of a formation that is located in different orbital planes for 1 orbit. The trajectory in the cross-track direction is periodical. This is due to the intersection of the orbital planes at the poles. A small difference in the RAAN results in an initial cross-track separation. This cross-track separation decreases as the orbit progresses and becomes zero at exactly one fourth of the orbital period due to the intersection of the orbital planes at the poles. The cross-track separation then increases and reaches the maximum value, the same as the initial separation at the equator. This cycle repeats as the spacecraft move towards the poles again. The values of the along-track and the radial separations remain constant.

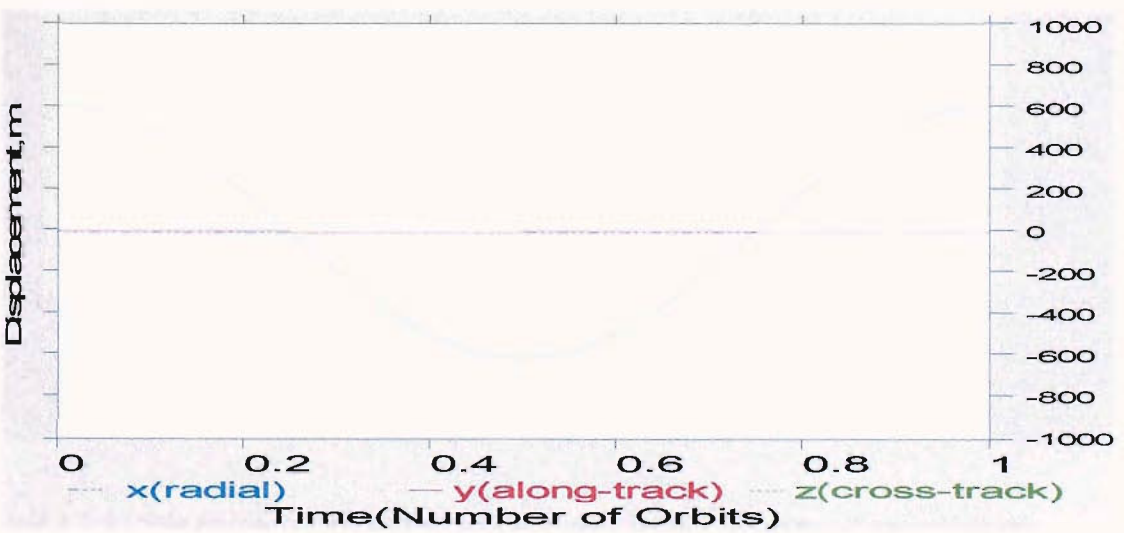

FIGURE 4.2.2 EVOLUTION OF RELATIVE TRAJECTORY FOR MASTER AND DEPUTY LOCATED IN DIFFERENT ORBITAL PLANES

Figure 4.2.3 shows the relative trajectory evolution when both the master and deputy are in elliptical orbits with different eccentricities. The relative trajectory is circle of periodically varying radii. This can be predicted from equation 4.2.2. It can be seen that the spacecraft return back to the same initial position after several orbital revolutions, if not perturbed by external forces.

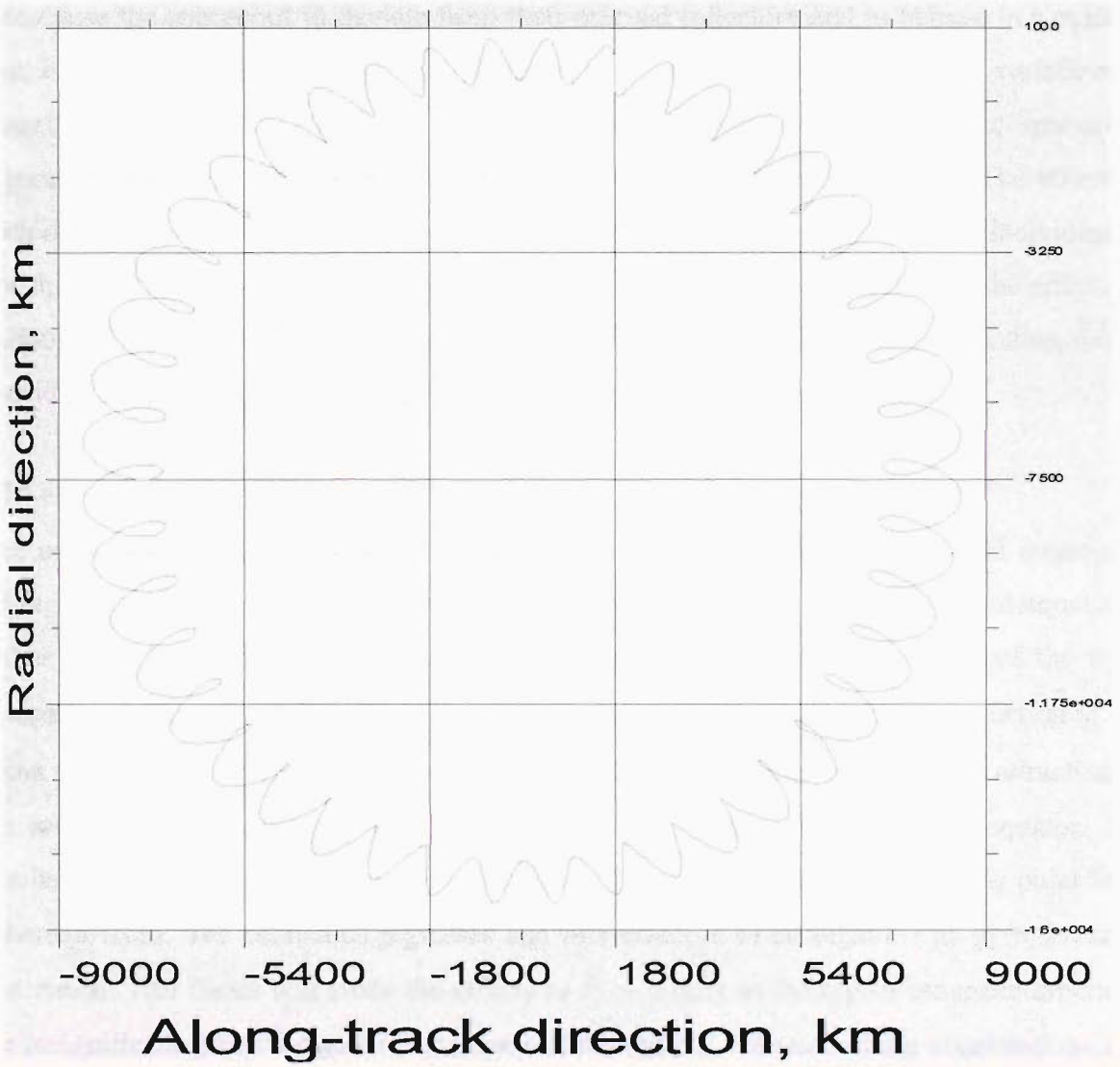

FIGURE 4.2.3 EVOLUTION OF RELATIVE TRAJECTORY WITH THE DEPUTY AND MASTER SATELLITES BOTH IN ELLIPTICAL ORBITS OF DIFFERENT ECCENTRICITIES

4.3 Perturbed Formation-Flying Orbits

The simulations generated with the relative motions equations in the previous section were for the unforced case in which the formation flying spacecraft were considered to follow keplerian motion. But in a real scenario, each spacecraft in a formation would experience perturbations of different magnitudes, in different directions, from several forces. This would then cause the spacecraft to deviate from their original trajectory and to behave in a manner that is directly dictated by the magnitude of the perturbation forces. The variation in magnitudes of forces experienced by the spacecraft depends on factors like spacecraft separation, orbit altitude, spacecraft orientation and formation configuration. The effect of each of the above said factors on spacecraft relative motion will be investigated individually. For this, a simple case like the Leader-Follower pattern will be considered and the effects of various forces with different test conditions will be simulated. The main perturbation forces considered for simulation are discussed in the following subsections.

4.3.1 J_2 Perturbations

The most significant of gravity harmonics is J_2. J_2 is related to Earth equatorial oblateness through earth rotation, and the estimated difference between the polar radius and equatorial radius is 22 km. The zonal harmonic J_2 is responsible for the secular rates of the right ascension of the ascending node Ω, the argument of perigee ω, and a small correction to the mean motion of the orbit. The motion of the node Ω occurs because of the added attraction of the earth's equatorial bulge, which introduces a force component towards the equator. The resultant acceleration causes the satellite to reach the equator short of the crossing point for a spherical earth. The orbit thus regresses and this effect is often regarded as gyro dynamic precession. This thesis will study the effects of $J_2 \sim J_5$ only as the higher order perturbations are insignificant given the general accuracy of the model. The perturbing accelerations due to J_2 may be given in the spherical coordinate system as [29].

$$\bar{a}_{j_2} = -\frac{3J_2\mu r_e^4}{r^4}[\bar{e}_r(0.5-1.5\sin^2 i\sin^2 u)+\bar{e}_t \sin^2 i\sin u\cos u+\bar{e}_z \sin i\cos i\sin u] \qquad (4.3.1.1)$$

where $\mu = 3.986 \times 10^{14} m^3/s^2$ is the gravitational earth constant, $J_2 = 1082.64 \times 10^{-6}$, $r_e = 6371 \times 10^6 km$, r is the distance between the satellite and earth-center, $\bar{e}_r$ is the unit vector along the satellite orbit radius vector direction, $\bar{e}_t$ is the unit vector along the local horizontal direction and $\bar{e}_z$ is the unit vector along the orbit normal direction.

It can be seen from Equation (4.3.1.1) that the J_2 perturbation acceleration has components along all three directions of the spacecraft trajectory. Since the components of the J_2 perturbation acceleration are dependent on the values of u, the argument of latitude, and i, the inclination of the spacecraft, any difference of these values between the master and the deputy spacecraft results in a relative motion along all the three coordinates. Generally, one can calculate the earth non-sphere perturbation accelerations by differentiating the corresponding disturbing potentials.

The perturbation acceleration can be found as follows[32]

$$\bar{a}_{J_n} = \forall U_n = \left(\frac{\partial U_n}{\partial r} + \frac{\partial U_n}{\partial Z} \sin i \sin\theta \right) \cdot \bar{e}_r + \frac{\partial U_n}{\partial Z} \sin i \cos\theta \cdot \bar{e}_t + \frac{\partial U_n}{\partial Z} \cos i \cdot \bar{e}_z \qquad (4.3.1.2)$$

where $n = 3, 4, 5..$

for $n = 3$

$$U_3 = -\frac{\mu J_3 R_e^3}{2} \cdot \left(5\frac{Z^3}{r^7} - 3\frac{Z}{r^5} \right)$$

$$\frac{\partial U_3}{\partial r} = -\frac{\mu J_3 r_e^2}{2} \left(-35 Z^3 r^{-8} + 15 Z r^{-6} \right)$$

$$\frac{\partial U_3}{\partial Z} = -\frac{\mu J_3 r_e^2}{2} \left(15 Z^2 r^{-7} - 3 r^{-5} \right)$$

$Z = r \sin i \sin\theta$ and $J_3 = -2.5 \times 10^{-6}$

The perturbation acceleration expressions for J_4 and J_5 can be found in a similar way. For J_4

$$U_4 = -\frac{\mu J_4 R_e^4}{8} \cdot \left(35\frac{Z^4}{r^9} - 30\frac{Z^2}{r^7} + 3\frac{1}{r^5} \right) \qquad (4.3.1.3)$$

where $J_4 = -1.6 \times 10^{-6}$

$$\frac{\partial U_4}{\partial r} = -\frac{\mu J_4 r_e^4}{8}\left(-315Z^4 r^{-10} + 210Z^2 r^{-8} - 15r^{-6}\right)$$

$$\frac{\partial U_4}{\partial Z} = -\frac{\mu J_4 r_e^4}{8}\left(140Z^3 r^{-9} - 60Zr^{-7}\right)$$

For J_5

$$U_5 = -\frac{\mu J_5 R_e^5}{8}\cdot\left(63\frac{Z^5}{r^{11}} - 70\frac{Z^3}{r^9} + 15\frac{Z}{r^7}\right) \tag{4.3.1.4}$$

where J_5 = -0.23 x 10^{-6}

$$\frac{\partial U_5}{\partial r} = -\frac{\mu J_5 r_e^5}{8}\left(-693Z^5 r^{-12} + 630Z^3 r^{-10} - 105Zr^{-8}\right)$$

$$\frac{\partial U_5}{\partial Z} = -\frac{\mu J_5 r_e^5}{8}\left(315Z^4 r^{-11} - 210Z^2 r^{-9} + 15r^{-7}\right)$$

Substituting the above results in equation (4.3.1.2), one gets J_3, J_4 and J_5 perturbation accelerations

4.3.2 Solar Radiation Pressure

The perturbing acceleration of an earth satellite due to solar radiation pressure effects can be computed with the following equation.

$$a_{SRP} = \xi\frac{A}{m}SRP\left(\frac{a_s}{r_s}\right)^2 \tag{4.3.2.1}$$

where:

ξ is a constant whose value depends upon the reflective properties of the surface

r_s is the distance of the satellite from the sun,

a_s is the mean distance of the Earth from the sun,

S is the area of the satellite,

m is the mass of the satellite.

$$SRP = \frac{F}{c}$$

F is the solar energy flux at the spacecraft

and c is the speed of light

The components of Solar-radiation pressure can be expressed as [33].

$$\begin{aligned}\left\{\frac{S_0(\theta)}{T_0(\theta)}\right\} = &\cos^2\frac{i}{2}\cos^2\frac{\varepsilon}{2}\left\{\frac{\cos}{\sin}\right\}(\lambda_\odot - u - \Omega) - \sin^2\frac{i}{2}\sin^2\frac{\varepsilon}{2}\left\{\frac{\cos}{\sin}\right\}(\lambda_\odot - u + \Omega)\\ &-\frac{1}{2}\sin i\sin\varepsilon\left[\left\{\frac{\cos}{\sin}\right\}(\lambda_\odot - u) - \left\{\frac{\cos}{\sin}\right\}(-\lambda_\odot - u)\right]\\ &-\sin^2\frac{i}{2}\cos^2\frac{\varepsilon}{2}\left\{\frac{\cos}{\sin}\right\}(-\lambda_\odot - u + \Omega) - \cos^2\frac{i}{2}\sin^2\frac{\varepsilon}{2}\left\{\frac{\cos}{\sin}\right\}(-\lambda_\odot - u - \Omega)\end{aligned}$$

$$W_0 = \sin i\cos^2\frac{\varepsilon}{2}\sin(\lambda_\odot - \Omega) - \sin i\sin^2\frac{\varepsilon}{2}\sin(\lambda_\odot + \Omega) - \cos i\sin\varepsilon\sin\lambda_\odot \qquad (4.3.2.2)$$

$S = a_{srp}S_0(\theta)$, $T = a_{srp}T_0(\theta)$ and $W = a_{srp}W_0$

where $S_0(\theta)$, $T_0(\theta)$ and W_0 are direction cosines in the satellite orbit radius vector direction, local horizontal direction and orbit normal direction respectively. The parameters, i, u and Ω are orbital elements, ε denotes the obliquity of the ecliptic, and $\lambda_\odot$, the ecliptic longitude of the sun. The quantities ε, $\lambda_\odot$ and a_s/r_s (in equation.(4.3.2.2) can be computed with sufficient accuracy from the expressions [30]

$d = MJD - 15019.5$

$\varepsilon = 23^\circ.44$

$M_\odot = 358^\circ.48 + 0^\circ.98560027d$

$\lambda_\odot = 279^\circ.70 + 0^\circ.9856473d + 1^\circ.92\sin M_\odot$

$a_s / r_s = [1 + 0.01672\cos(M_\odot + 1^\circ.92\sin M_\odot)]/0.99972$

where MJD is the modified Julian day. The modified Julian day = Julian day- 2400000.5

The effects of SRP can then be studied by substituting the direction cosines in the following equations.

$$S = a_{srp} S_0(\theta),\ T = a_{srp} T_0(\theta) \text{ and } W = a_{srp} W_0 \tag{4.3.2.3}$$

4.3.3 Aerodynamic Drag

When the orbit perigee height is below 1000 km, the atmospheric drag effect becomes important. Drag, unlike other perturbative forces, is a non-conservative force and will continuously take energy away from the orbit. Thus the orbit semi major axis and the period gradually decrease because of the effect of drag. This causes the orbital velocity to increase in order to satisfy the kepler's law ($\mu = n^2 a^3 = const$). This is sometimes known, as the 'Drag Paradox': the effect of atmospheric friction is to speed up the motion of the satellite as it spirals inward.

The aerodynamic drag, D, of a satellite orbiting the earth is given by equation:

$$D = \frac{1}{2} \cdot \rho \cdot V^2 \cdot S \cdot C_d \tag{4.3.3.1}$$

Where ρ is the density of the atmosphere, V is the velocity of the spacecraft, C_d is the coefficient of drag, and S the projected area of the spacecraft in the direction of motion.

The drag deceleration a, may be written as

$$a = \frac{C_d \cdot S \cdot \rho \cdot V^2}{2.\ m} \tag{4.3.3.2}$$

where m is the mass of the spacecraft.

Unlike other perturbative forces, Drag force has components only along the negative velocity vector direction.

4.4 Forced Spacecraft Relative Orbits

As discussed in section 3.3.4, the relative trajectories of spacecraft with the effects of orbit perturbations can be modeled with the aid of the Gauss perturbation equations. These equations help to evaluate the rates of change of orbital elements of individual spacecraft acted upon by perturbations. The values of rates of change of orbital elements can then be used to find the values of the actual orbital elements which when substituted in the relative motion equations will provide the coordinates of the deputy spacecraft in consideration. This technique will be used to analyze the Leader-Follower formation pattern for 600-km circular orbit altitude with an initial separation of 100 meters. This follows from the motivation by the UK University-led Technology demonstration programme that proposed to build and launch two identical satellites of approximately 10 kg mass each in to a 600 km, circular orbit. The Leader-Follower formation pattern will be considered as the case study for the relative motion analysis.

The most basic configuration in which spacecraft can fly in formation is that of leader and follower shown in figure (4.4.1). In this configuration, the orbital elements of each spacecraft are identical except for the true anomaly, meaning that the spacecraft follow the same orbital path at different times one behind the other. To understand the dynamics of such a formation, simulations were performed with the use of the newly developed Orbital element method with the inclusion of all significant perturbative forces. The simulation conditions for the test case are given in Table (4.4.1)

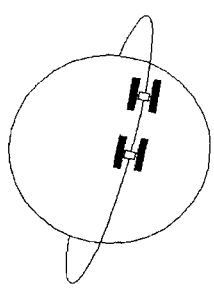

FIGURE 4.4.1. LEADER FOLLOWER FORMATION PATTERN

Parameter	Master Spacecraft	Deputy Spacecraft
Perigee Altitude, km	600	600
Eccentricity	0.0001	0.0001
Inclination, deg	98	98
RAAN, deg	10	10
Argument of perigee, deg	0	0
True anomaly, deg	8.219×10^{-4}	0
Initial separation, m	100 (Deputy Spacecraft behind)	

Table 4.4.1. Initial conditions for the Master and Deputy Spacecraft for Leader-Follower Pattern

In the calculations for drag and solar radiation pressure the normal drag-area of the satellites is taken as 0.0625 m^2 (25 cm x 25 cm) and the drag coefficient C_d =1.8. Both the Master and the Deputy satellites are assumed to be identical and weighing 10 kg each. The value of atmospheric density is taken as 10^{-13} kg/m^3 for 600 km altitude and is assumed to be the same for small changes in altitude. The solar flux incident on the spacecraft is assumed to be constant and the shadow conditions are not taken into account. The integration step size is 1 second and the simulations are performed for a few successive orbits.

In table 4.4.1 all the orbital elements have arbitrary values except for the true anomalies that depend on the assigned along-track separation distance. For a given along-track initial separation distance, the true anomalies of the master and the deputy spacecraft are calculated using the equations that are given below. The method of finding the correct true anomalies of the master and the deputy satellites is very important for the correct prediction of evolution of relative motion. It is imperative that the resultant orbits are energy matched as a small difference in the energy of the orbits of the master and the deputy satellites will lead to a drift in the separation distance. For the Leader-Follower case, Equation 4.2.1 is used to calculate

the orbital elements. Equation 4.2.1 was specially derived for a planar case and is only valid for orbits in the same plane. If the orbits are not coplanar then equation 6.2.1.1c should be used that is derived for a general case.

From equation 4.2.1, $y = R_d \sin \partial u$

$$\partial u = \sin^{-1} \frac{y}{R_d} \tag{4.4.1}$$

$$\partial u = \sin^{-1} \frac{y(1 + e_d \cos \theta_d)}{a_d (1 - e_d^{\,2})} \tag{4.4.2}$$

Expanding the Left-hand side of equation 4.4.2 gives

$$\theta_d - \theta_m = \sin^{-1} \frac{y(1 + e_d \cos \theta_d)}{a_d (1 - e_d^{\,2})} + \omega_m - \omega_d \tag{4.4.3}$$

$$\theta_m = \theta_d - \sin^{-1} \frac{y(1 + e_d \cos \theta_d)}{a_d (1 - e_d^{\,2})} - \omega_m + \omega_d \tag{4.4.4}$$

Equation 4.4.4 is the general equation to calculate the initial true anomaly of the master spacecraft from the given initial data that includes the along-track separation distance y, the initial true anomaly of the deputy, semi major axis of the deputy spacecraft, argument of perigees of the master and the deputy spacecraft.

For selecting energy matched orbits this is the only condition that should be satisfied;

$$a_m = a_d$$

This follows from the Energy equation that is given as $E = -\frac{\mu}{2a}$. In the simulations that follow this discussion, the same technique is used to calculate the initial true anomaly values for any specified initial along-track separation distance.

In a real Leader-follower formation-flying scenario, there are possibilities to have slight differences of the semi-major axis of the master and the deputy satellites. This can be due to the spacecraft having small differences in the velocities after separation or due to the effects

of perturbations. The first of the above said causes can be avoided by careful planning of the spacecraft separation procedure and by using active control techniques. The effects of perturbations also cause differences in semi-major axis and depend on the various factors like initial separation distance, spacecraft dimensions, shadow conditions, etc. For example, the magnitude of the J_2 acceleration is dependent on the latitude of the sub-satellite point. So spacecraft separated by a distance will experience different magnitudes of gravitational acceleration that will in turn change the time period of the orbits thereby causing a difference in the semi-major axis.

The simulation interface is designed in such a way that relative orbits can be analyzed with or without the effects of perturbations. For the Keplerian case (without perturbations), the initial orbital elements of the master and the deputy spacecraft are entered and the progression of time is set through the changing true anomaly of the master and the deputy spacecraft. For the perturbed case, once the initial orbital elements are entered and the simulation started, the effects of the perturbations based on the different factors like initial separation distance, spacecraft dimensions, type of orbit etc are calculated and applied from the first second of simulation. The effects are modeled through the change in orbital elements that the perturbations produce and these updated orbital elements are fed to the main equations (equations 3.3.4.2) to find the relative position of the deputy spacecraft with respect to the master spacecraft.

The simulations with perturbations in the thesis are performed for osculating elements as the short-term effects of perturbations can be visualized better with osculating elements than with the mean elements. The short-term effects are particularly interesting for formation flying as they help us to assess the magnitude of oscillations within one orbital period and thereby providing a better understanding of the control accuracy requirements. Mean elements could also be used with the orbital element method and they are helpful in determining the long-term evolution of relative orbits.

Before starting the actual simulations, the Leader follower formation pattern as given in table 4.4.1 was simulated for 100 orbits for a Keplerian case. This was to ensure that the master and the deputy spacecraft had same energy orbits. The plots are given below as figures 4.4.2.

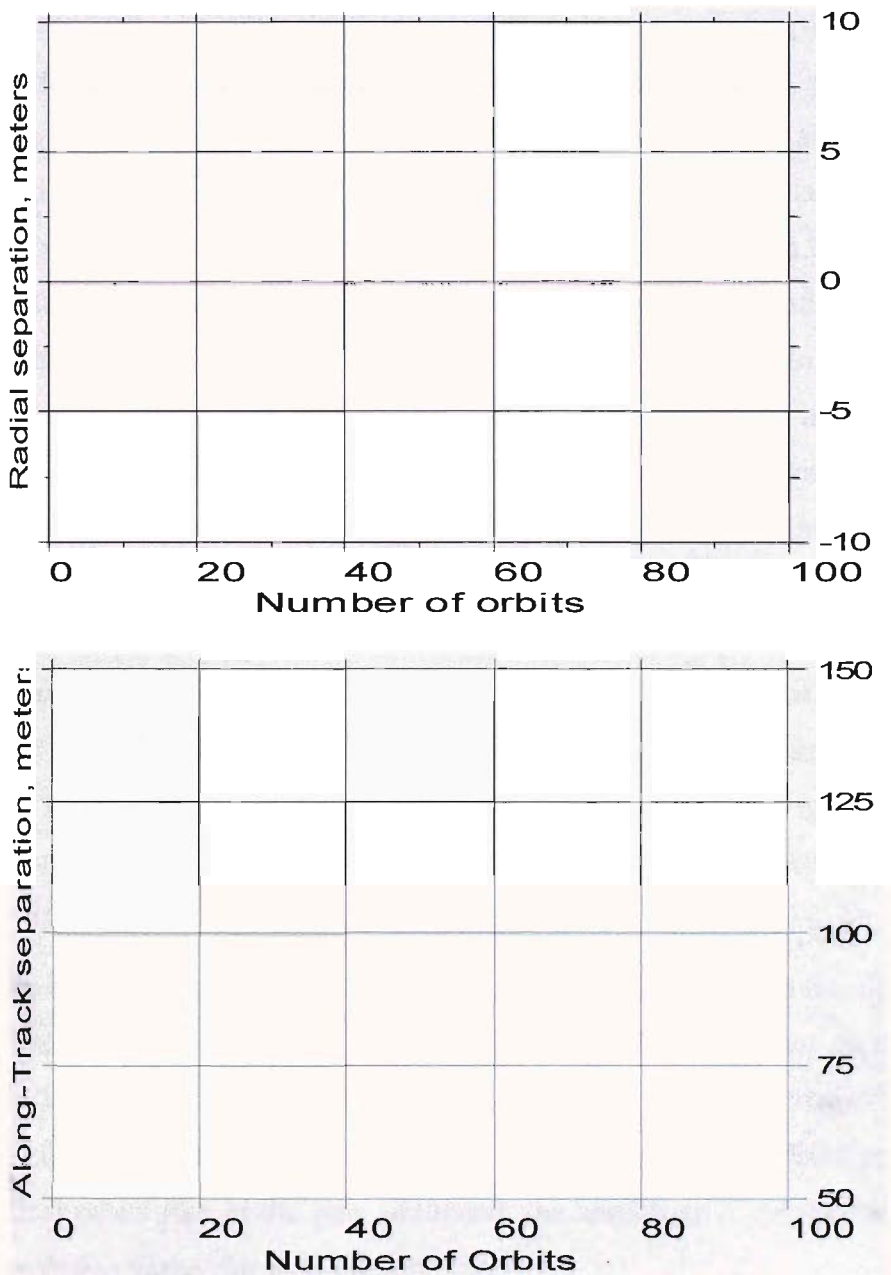

FIGURE 4.4.2 SIMULATION OF THE LEADER-FOLLOWER FORMATION PATTERN AT 600 KM SEPARATION AND 100 METERS SEPARATION FOR A KEPLERIAN CASE

4.4.1 Simulation Results

Figure 4.4.2 shows the results of simulation of the Leader-Follower formation pattern in the presence of drag, solar radiation pressure and J_2 to J_5. The drifts caused by the perturbative forces are plotted against the number of orbital revolutions for 30 orbits with a step size of 1

second. The magnitude of secular drifts induced by all forces including J_2 was found to be approximately 0.06 m/orbit in the along-track direction. There was no secular drift in the radial direction and the cross-track direction. Periodic oscillations were also recorded in the along-track and the radial directions. The maximum amplitude of oscillation in the Along-track direction was 0.25 m/orbit. The periodic variations of amplitude in the radial direction seem to increase with time and were only 0.05 cm after 30 orbital revolutions but there were no secular drifts recorded. The increase of amplitude in the radial direction can be attributed to the secular drift caused by J_2 in the along-track direction. The main cause of the oscillations and secular drifts were found to be due to earth's oblateness and this was verified by running the simulations without $J_2 - J_5$. For an oblate shaped earth, the magnitude of the gravitational acceleration is dependent on latitude and longitude of the sub satellite point. Hence satellites passing different locations at the same time experience different magnitudes of the gravitational acceleration. This in turn causes minor changes in the orbital period and therefore causes oscillations. Apart from these oscillations, the J_2 perturbations cause a secular drift in the longitude of the ascending node and argument of perigee and change the mean anomaly rate. The differential change in the mean anomaly rate causes relative drift in the velocity vector direction.

A careful examination of the plots will reveal 2 cycles of oscillations in the along-track and radial directions. This is because the gravitational acceleration decreases as the spacecraft move from the equator to the poles and the gravitational acceleration increases as they move from the poles to the equator. This cycle repeats again within one full orbital revolution. For slightly elliptical orbits like in the case simulated, the amplitude of oscillations within one full orbital revolution varies due to the eccentricity.

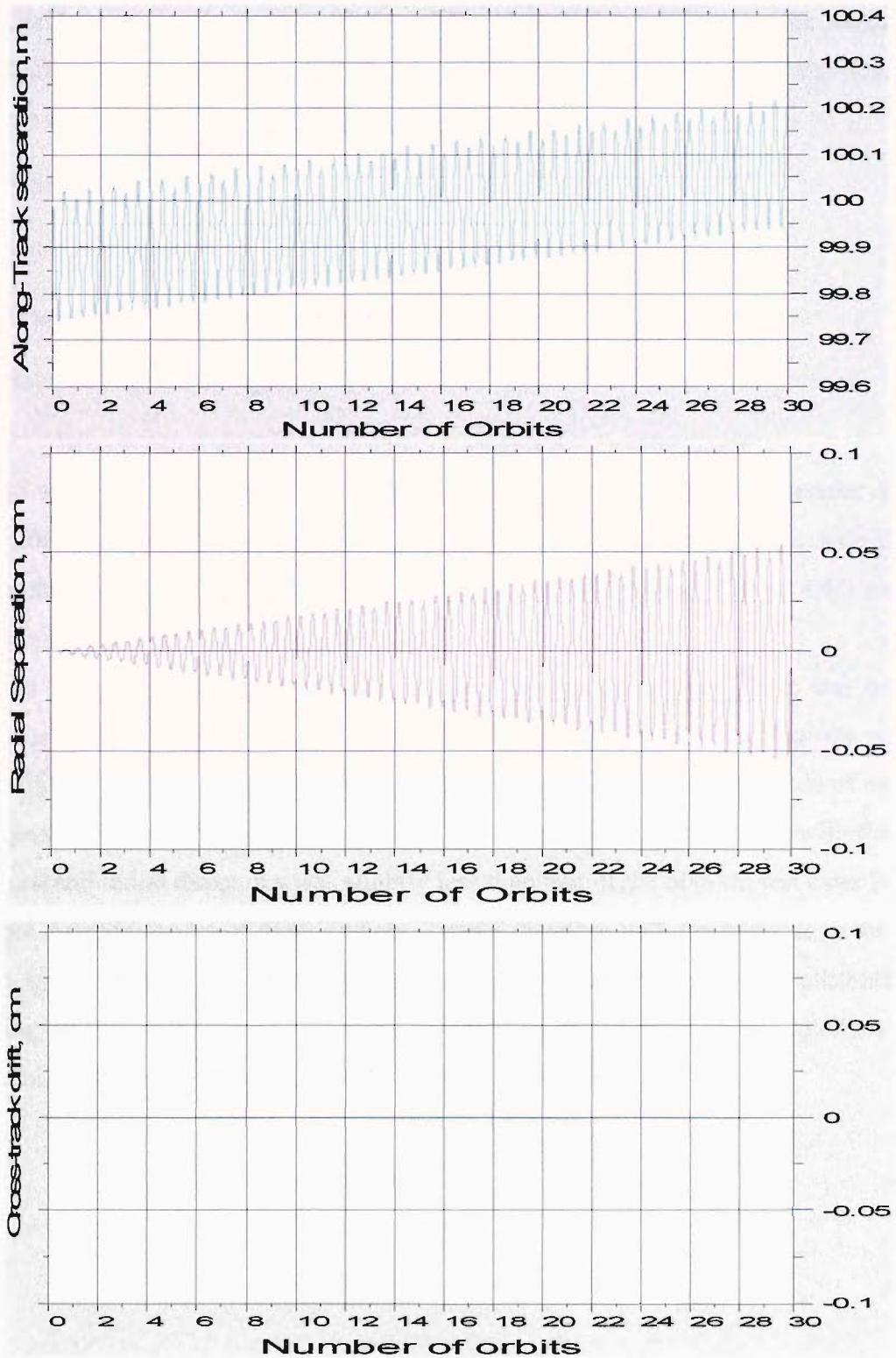

FIGURE 4.4.2 ALONG-TRACK, RADIAL AND CROSS-TRACK OFFSETS FOR LEADER-FOLLOWER FORMATION AT 600 KM POLAR ORBIT AND 100-M INITIAL SEPARATION

It was decided to investigate the effect of different initial conditions on the magnitude of secular drifts and the amplitude of oscillations induced by earth's oblateness and possible test cases were identified for analysis, in particular,

- Altitude of the orbit
- Satellite separation
- Type of orbit (Circular or elliptical)
- Nature of the orbit (Equatorial, Polar, etc.)

Firstly, to understand the effect of altitude of the orbit on the magnitude of secular drifts and the amplitude of oscillations, a test case was simulated for 800-km altitude with the same orbital elements and the initial separation of the previous test case. Figure 4.4.3 shows the results of simulation for the 800-km test case.

There was a secular drift of 0.05 m/orbit in the along-track direction. There was no secular drift in the radial direction and the cross-track direction. Periodic oscillations were also recorded in the along-track and the radial directions. The maximum amplitude of oscillation in the Along-track direction was 0.24 m/orbit. The maximum amplitude of oscillations in the along-track and radial directions was slightly less than that of the 600-km test case. So, it was found that the magnitudes of drifts and oscillations decrease with the increase in the altitude of orbits for the same initial separation and inclination of orbits. This can be attributed to the decreasing magnitude of the gravitational acceleration experienced by the satellites and the differential J_2 effect decreases with the increase in altitudes.

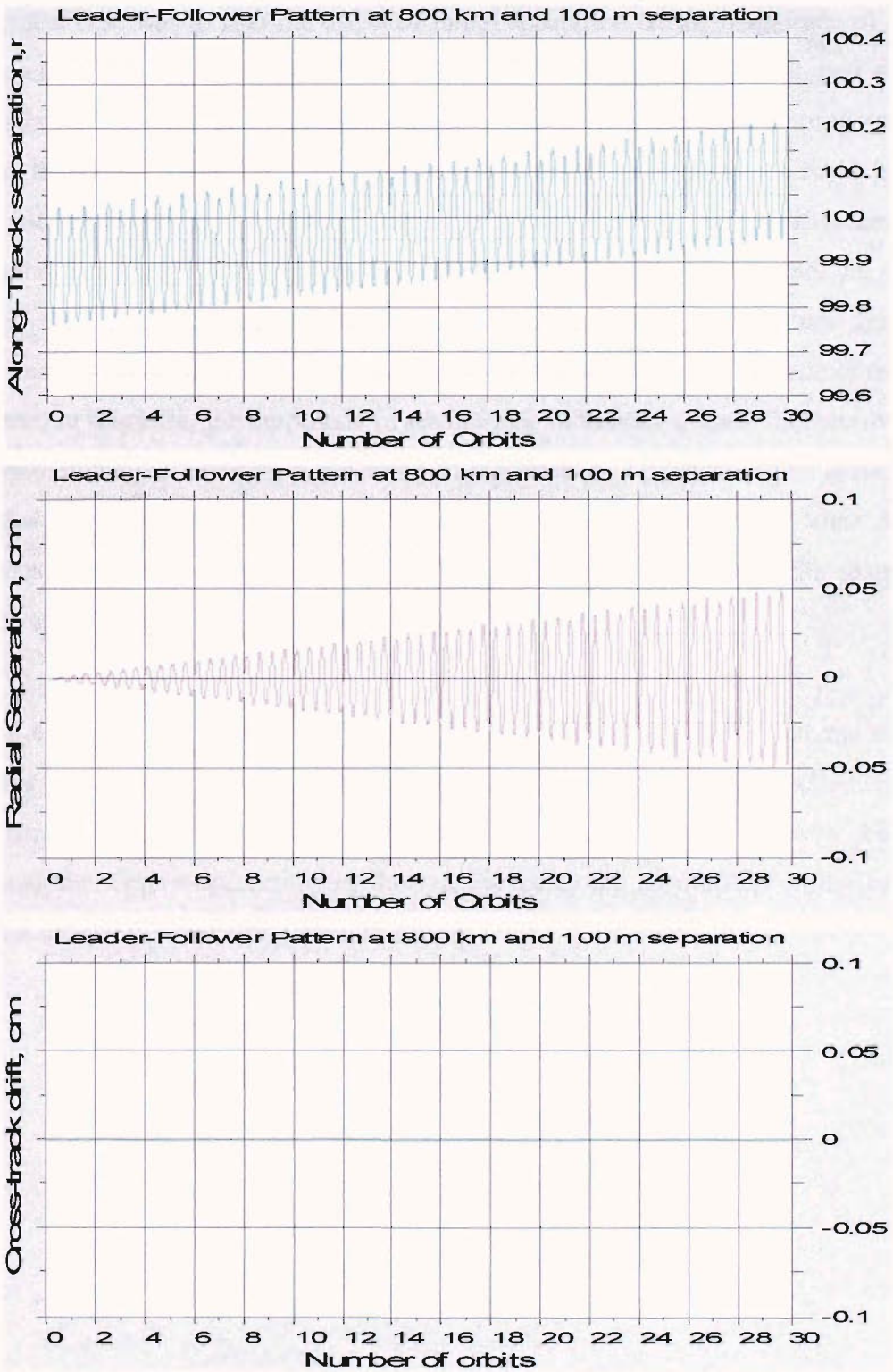

FIGURE 4.4.3 ALONG-TRACK, RADIAL AND CROSS-TRACK OFFSETS FOR LEADER-FOLLOWER FORMATION AT 800 KM POLAR ORBIT AND 100-M INITIAL SEPARATION

The next test case was to find the effect of initial separation on the magnitude of drifts and orbital oscillations. Figure 4.4.4 shows the results of simulation of a test case at 600-km altitude but for 1-km initial separation in the along-track direction. Results of the simulation show that the magnitude of the secular drift and the oscillations increases with the increase in the along-track separation distance. This is because of the growing differences of the gravitational accelerations experienced by the spacecraft with the increase in separation distances. As the along-track separation increases, the difference in the gravitational acceleration experienced by spacecraft increases and this causes the amplitude of oscillations to increase. In this case, the amplitude of oscillations in the along-track direction was found to be approximately 2.5 meters in the along-track direction. The secular drift induced by the differential J_2 effect was 0.5 m after 1 orbital revolution and 20 m after 10 orbital revolutions. There is no secular drift in the radial direction although the magnitude of periodic variations increases with time.

Figures 4.4.5 shows the evolution of relative trajectory for a case where both the master and deputy are in circular orbits. Simulations show that the magnitude of the oscillations and the drift is almost similar to that of the original case that considers near-circular orbits of the master and the deputy spacecraft. In the circular case, the oscillations within one orbital revolution are equal in the along-track direction.

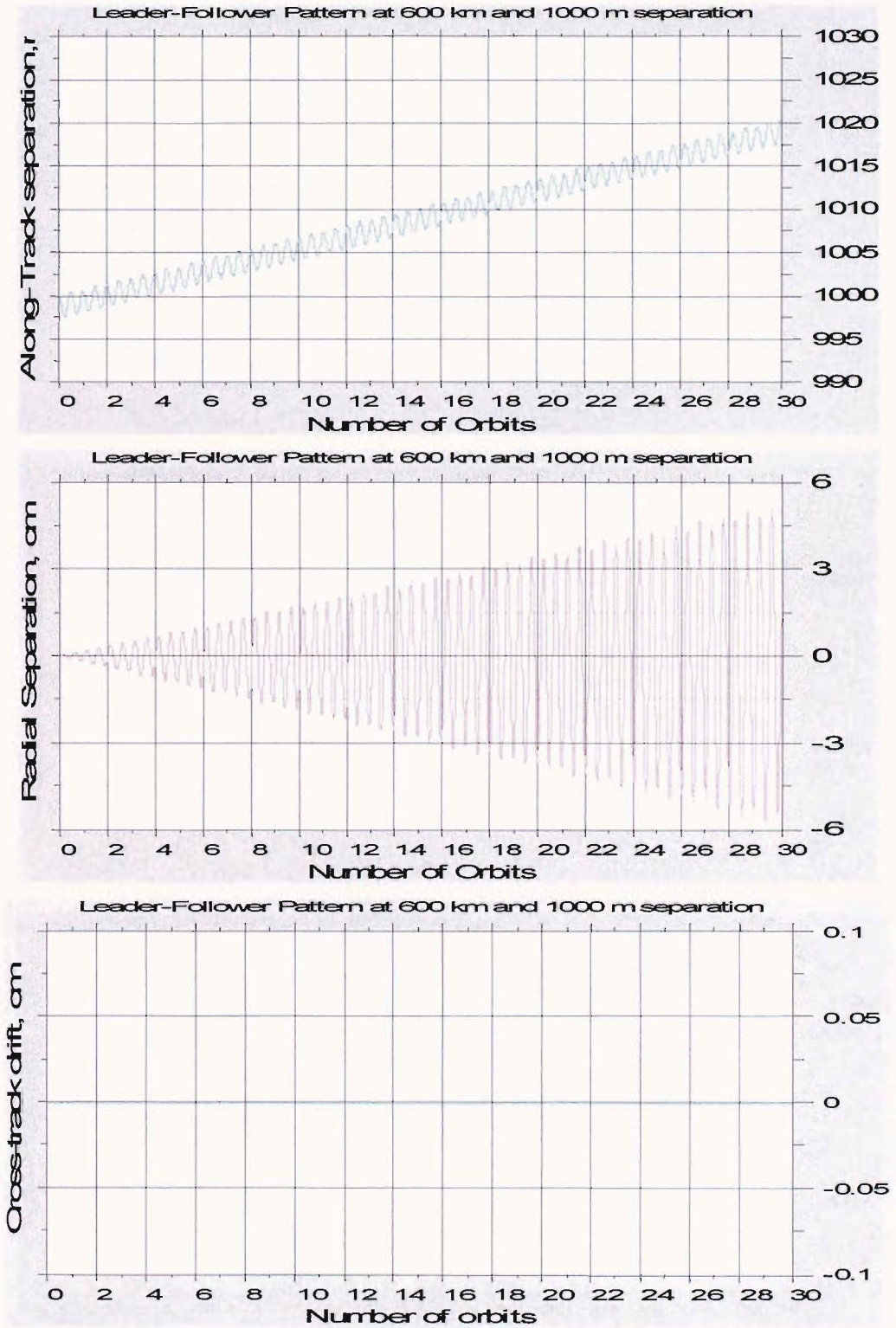

FIGURE 4.4.4 ALONG-TRACK ,RADIAL AND CROSS-TRACK OFFSETS FOR LEADER-FOLLOWER FORMATION AT 600 KM POLAR ORBIT AND 1-KM INITIAL SEPARATION

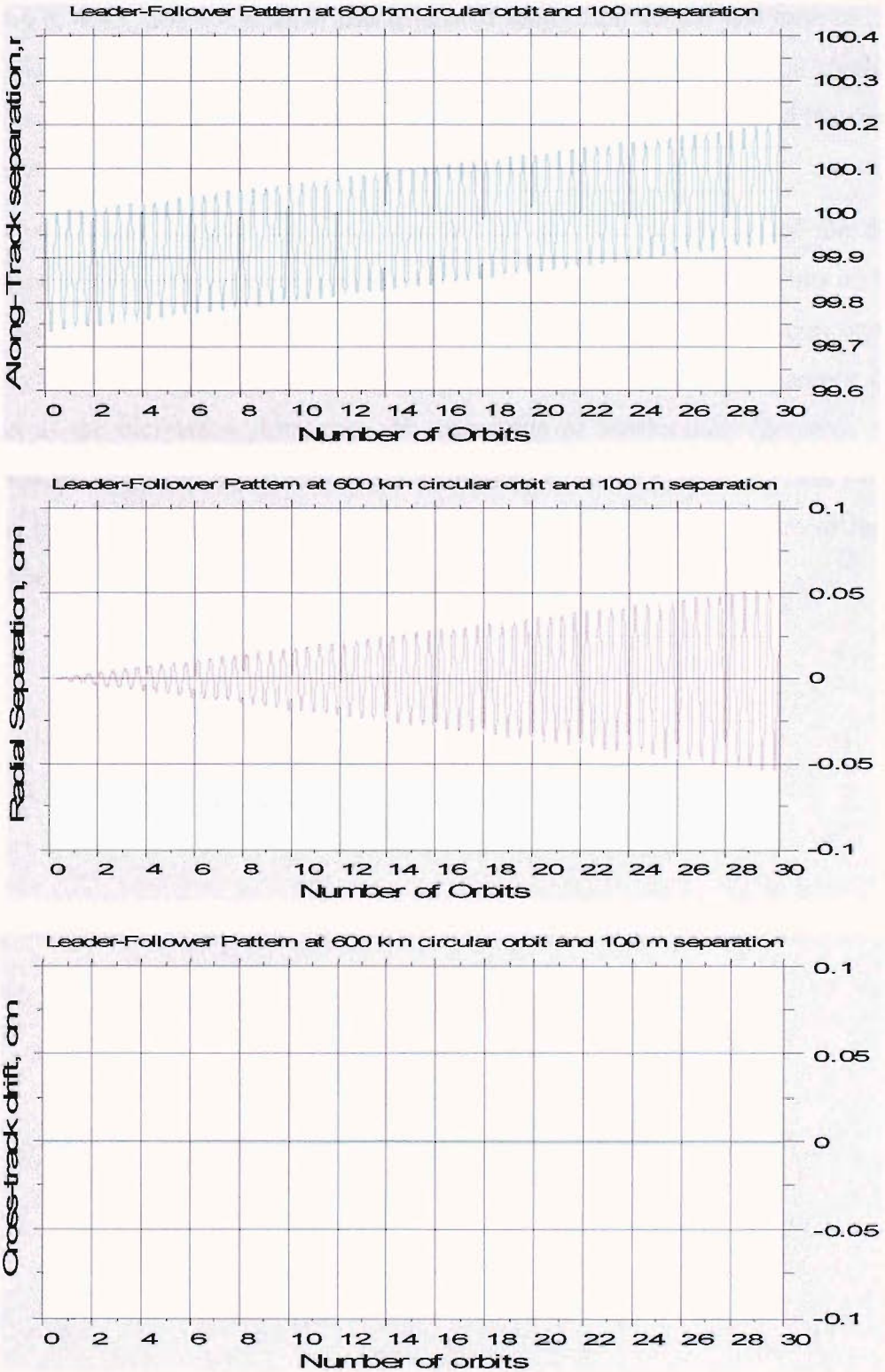

FIGURE 4.4.5 ALONG-TRACK, RADIAL AND CROSS-TRACK OFFSETS FOR LEADER-FOLLOWER FORMATION AT 600-KM CIRCULAR ORBIT AND 100 METERS INITIAL SEPARATION

Figures 4.4.6, 4.4.7 and 4.4.8 show the results of simulation of the test case to study the effect of inclination on the magnitude of drifts and oscillations. All the initial conditions are the same as given in table 4.4.1 except for the inclinations of the master and the deputy that are considered as 90 degrees, 45 degrees and 0 degrees.

It can be seen from Figures 4.4.6, 4.4.7 and 4.4.8 that the magnitude of the drifts and amplitude of oscillations decrease with the decrease in the inclination of orbits and become zero for equatorial orbits. The reason for this is the fact that the acceleration components induced by J_2 in all directions have the sine of the inclination in the numerator (equation 4.3.1) and as the inclination decreases, the magnitude of acceleration decreases in all the three directions. In reality, equatorial orbits also suffer from the effects of Earth's oblateness due to the presence of J_{22} components that are due to the ellipsoidal nature of the Earth's equator. The effects of J_{22} are not modeled in this thesis.

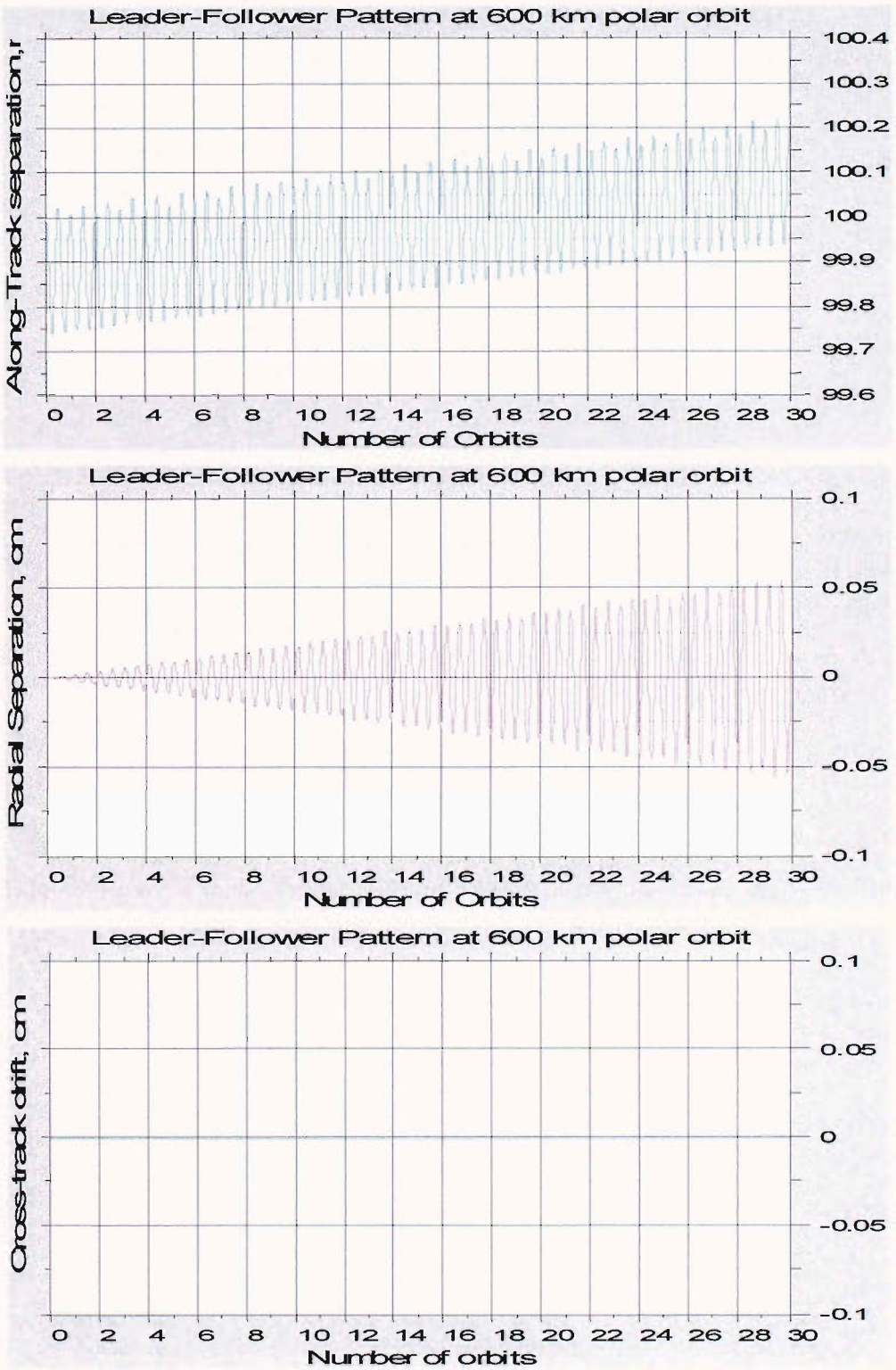

FIGURE 4.4.6 ALONG-TRACK, RADIAL AND CROSS-TRACK OFFSETS FOR LEADER-FOLLOWER FORMATION AT 600-KM ORBIT AND 90 DEGREE INCLINATION

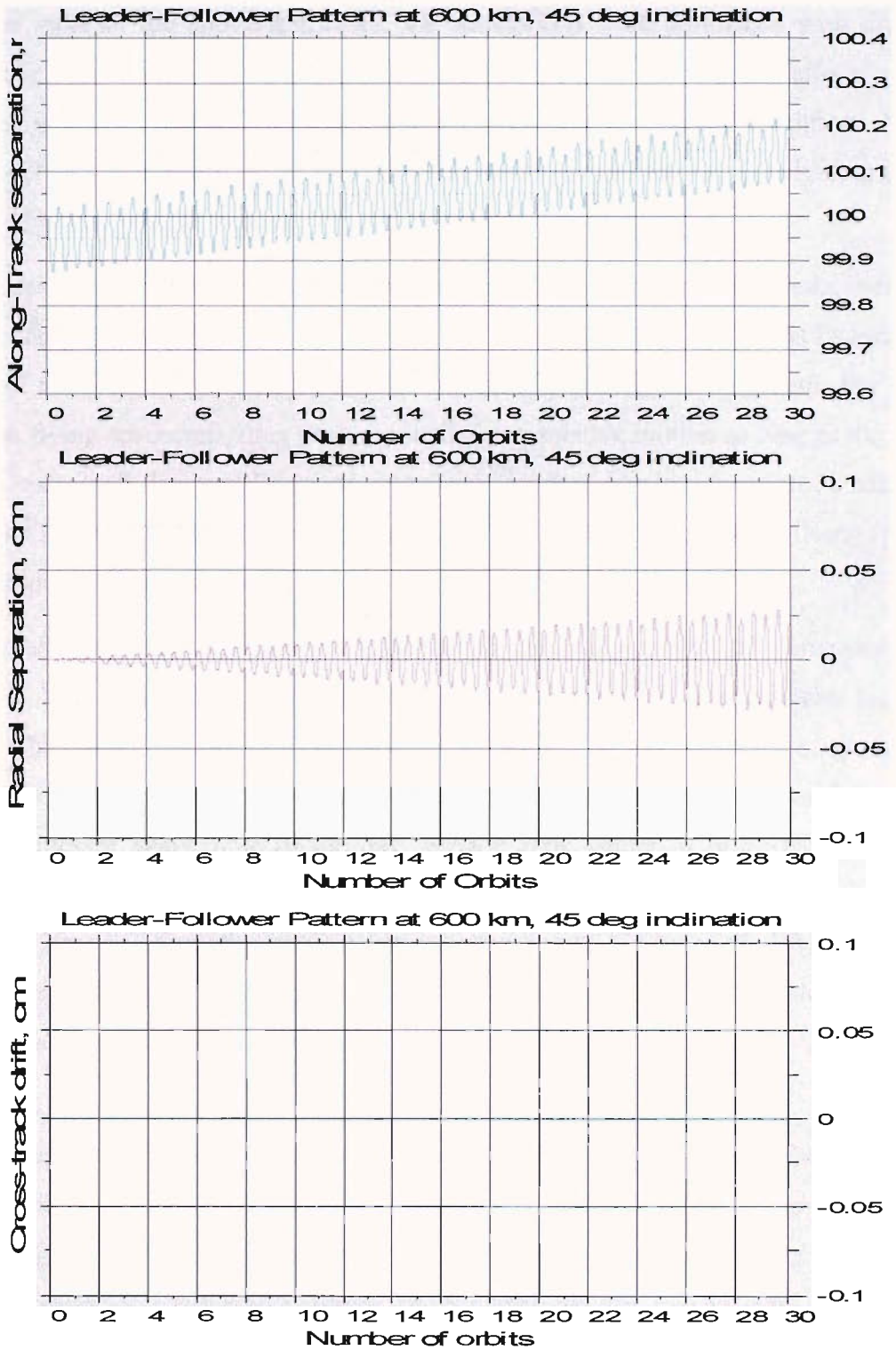

FIGURE 4.4.7 ALONG-TRACK, RADIAL AND CROSS-TRACK OFFSETS FOR LEADER-FOLLOWER FORMATION AT 600-KM EQUATORIAL ORBIT

In all the most of the above test cases, the simulations were performed with drag, solar radiation pressure and J_2-J_5 for identical formation flying spacecraft. The effects of earth's oblateness were analyzed for different test cases having different initial conditions. Now, the J_2-J_5 model will be disengaged and the effects of the other two forces, namely drag and solar radiation pressure will be studied.

Atmospheric drag, unlike J_2 is a non-conservative force and constantly depletes energy from the orbit. This causes orbits to decay and the rate of decay depends on several factors like the altitude of the orbit, mass of the spacecraft and surface area of the spacecraft. For identical formation flying spacecraft, drag does not induce any relative motion as long as the orbits of both the spacecraft decay at the same rate assuming drag is not a function of latitude and longitude. The effects of drag on relative motion for dissimilar formation flying spacecraft will be studied later in this thesis.

Solar radiation pressure also has an influence on the change of orbital parameters of any spacecraft. This influence is very significant for spacecraft orbiting at altitudes higher than 800 km. The effects of solar radiation pressure on satellite orbits depend on many factors like the surface area properties of the spacecraft, the time of year (as the solar flux varies at different times of year), time of the day, surface area, nature of orbit, etc. For identical formation flying spacecraft, the rates of change of orbital elements due to SRP are the same and hence there is no relative motion between spacecraft. However the SRP causes minor periodic variations and these variations are shown in figure 4.4.9. All other perturbative forces were disengaged from the model to get an insight of the effect of SRP on relative motion.

It can be seen from figure 4.4.9 that there is no secular drift due to differential solar radiation pressure effects and the amplitudes of oscillations for the 600-km altitude range from 10^{-4} m in the along-track direction and 10^{-6} m in the radial direction. Variations in the cross track direction due to solar radiation pressure was found to be very insignificant for the 600-km polar orbit and was in the order of 10^{-9} m in 1 orbit. The simulations were done for an initial spacecraft separation of 100 meters.

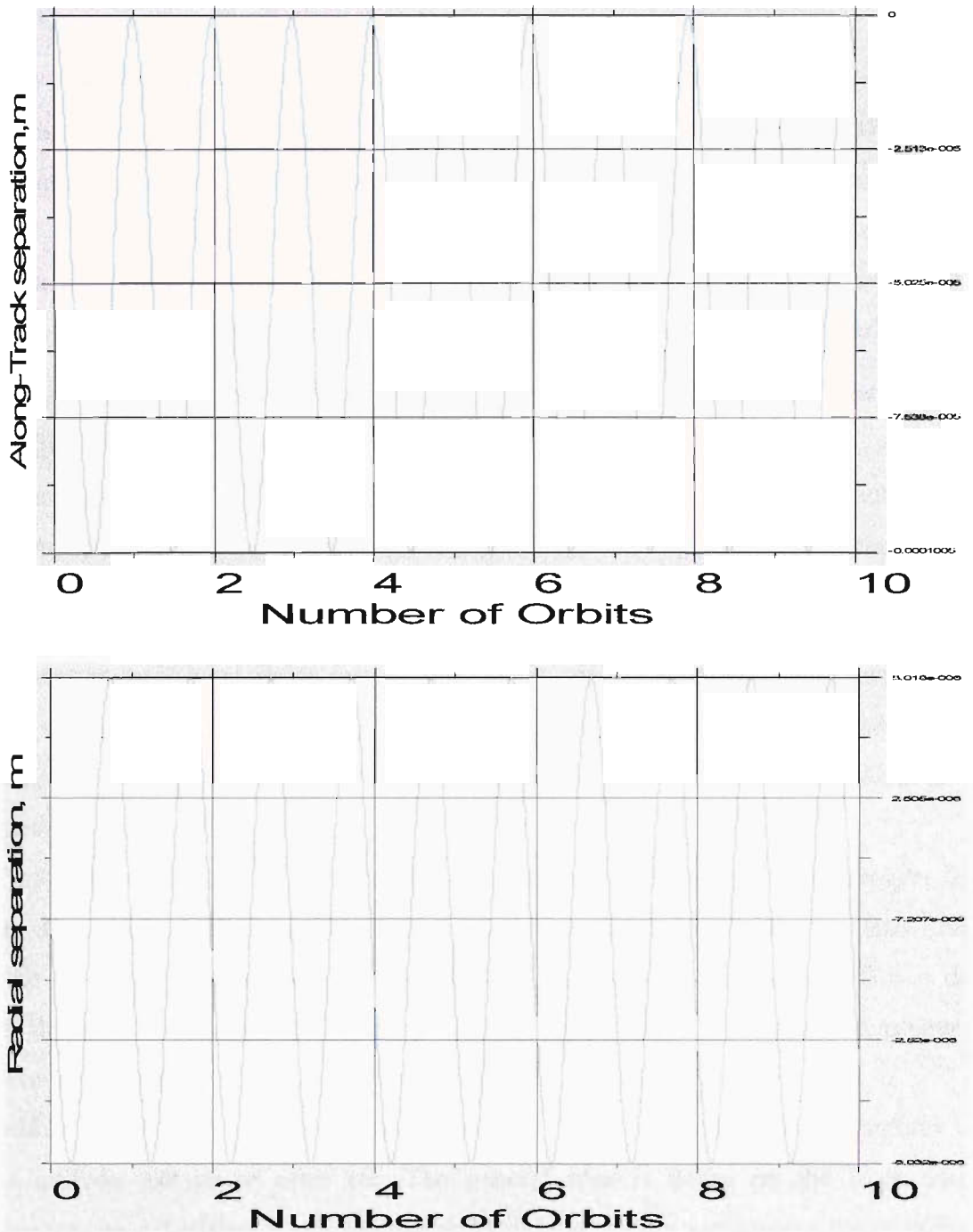

FIGURE 4.4.8 ALONG-TRACK AND RADIAL DISPLACEMENTS DUE TO SOLAR RADIATION PRESSURE EFFECTS FOR 600 KM ALTITUDE AND 100M INITIAL SEPARATION.

4.5 Fuel Consumption Prediction

In this section, the amount of ΔV required for station keeping purposes for the proposed 600-km circular polar orbit is estimated. This is done by calculating the amount of ΔV required to compensate for any secular drifts caused by the perturbing forces for a particular length of time and then integrating the value for one year. Note that these fuel requirements only provide a rough estimate of what will be needed and the real values entirely depend on formation keeping error bounds, precision of propulsion systems and navigational accuracy.

The along-track error growth induced by the various perturbing factors can be controlled via small adjustments in the semi major axis of the satellites. From Gauss's variation of parameter equations for keplerian elements in the normal tangential plane, the amount of ΔV required to compensate for a change in semi major axis can be found from the relation [27]

$$\Delta V = (\mu / 2a^2 V)\Delta a \tag{4.5.1}$$

where the changes in semi major axis Δa and velocity ΔV are assumed small compared to the nominal values. From Equation.(4.5.1), it can be shown that, to change the semi major axis by 1 cm, a velocity impulse of 0.0005424 cm/sec is required for a 600 km altitude near-circular orbit.

Table 4.5.1 shows the ΔV requirements for 1 year based on the frequency of thruster firings that are done at the end of an orbital revolution. It can be deduced from the table that the more the frequency of formation keeping, the less the total fuel expenditure. This is due to the fact that the drifts induced by the perturbative forces follow a non-linear pattern and their magnitudes vary after every single orbital revolution.

It should be noted that the values would vary for different types of formation patterns based on the altitude, nature of orbit etc. The general idea is based on the logic that ΔV requirements are calculated from values of drifts induced by the perturbative forces at the end of each orbit. In a real scenario, the values will depend on the control accuracy value as required for a specific mission.

Frequency of formation keeping	ΔV requirements for 1 year, m/sec	
	600-km altitude	800-km altitude
1 orbit	0.021	0.016
5 orbits	0.023	0.021
1 day	0.026	0.024
2 days	0.029	0.027

Table 4.5.1 ΔV requirements of the Leader-Follower formation pattern for 2 different altitudes for 1 year

Apart from formation keeping expenses, there might also be station-keeping expenses and a preliminary assessment shows a requirement of 1 m/sec for the proposed 600 km altitude and 0.15 m/sec for the 800 km altitude. Figures 4.5.1 and 4.5.2 show the altitude loss due to atmospheric drag for 600-km and 800-km altitude. The rate of loss in altitude in Figures 4.5.1 and 4.5.2 does not account for the density variation as a result of seasonal changes, solar-activity, change of latitude and longitude etc but could be programmed into the simulation with appropriate data. Infact, for the 600 km altitude, the atmospheric air drag is such a strong function of solar activity that the real loss of altitude may be 100 times greater that that shown in figure 4.5.1

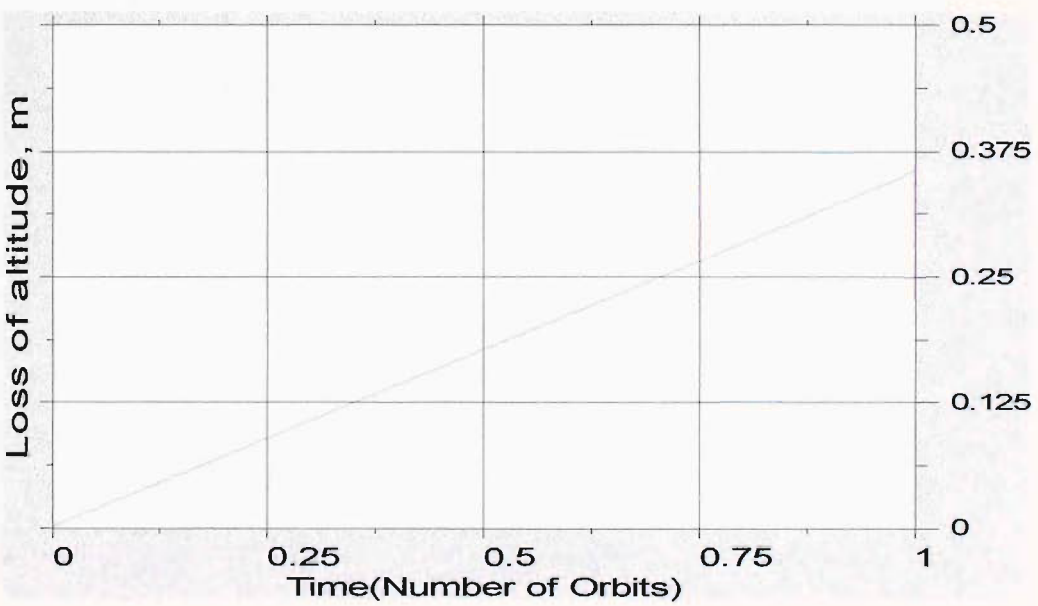

FIGURE 4.5.1 ALTITUDE LOSS IN METRES DUE TO ATMOSPHERIC DRAG FOR 600 KM ALTITUDE

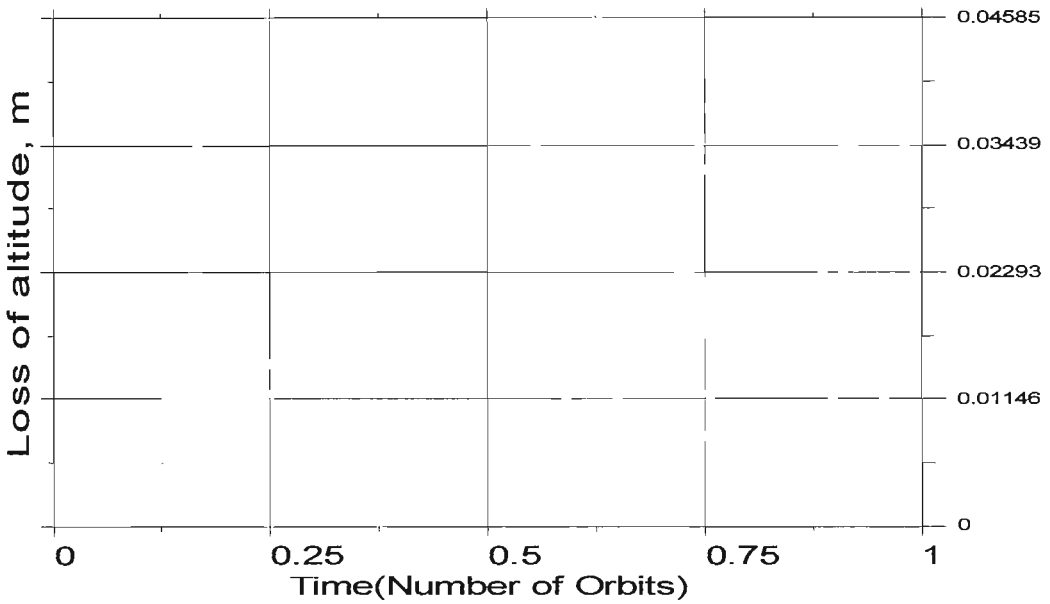

FIGURE 4.5.2 ALTITUDE LOSS IN METRES DUE TO ATMOSPHERIC DRAG FOR 800-KM ALTITUDE

4.6 Comparison With Closhessy-Wiltshire Equations and Other Methods and the Main Sources of Errors in the Orbital Element method

There are two different approaches in deriving the analytical solutions for Relative trajectory analysis. One is based on the dynamics of motion and the other on the geometry.

The dynamics method (CW method) uses the physics of motion to represent the relative motion. By doing so, the relative accelerations along the different coordinates are derived with respect to a rotating frame of reference. The analytical solutions of the relative positions are then obtained by solving the linearized differential equations.

In the Geometry methods (Orbital element, Gim and Alfriend and COWPOKE) the relative positions are directly obtained either by transforming the coordinates to the rotating master-spacecraft body frame or by direct relations from spherical trigonometry.

A close examination of the solutions of the CW method (equations 2.1.1.12a-2.1.1.12c) shows the cross coupling of the x and y coordinates with the x_0, y_0, $\dot{x}_0$ and $\dot{y}_0$ terms. This is very characteristic of the CW solutions as this cross-coupling property shows the consideration of the rotating frame of reference with the different accelerations such as the coriolis and the Euler that are characteristics of a rotating frame of reference.

In the Geometry methods, the x_0, y_0 terms are also present in the solution but are represented by the orbital elements. The initial value of the y coordinate is represented in the geometry methods including the orbital element method as a difference in the true anomalies of the master and deputy spacecraft. The true anomaly terms are present within the argument of latitude terms of the master and the deputy spacecraft, u ($u = \theta + \omega$) where θ is the true anomaly and ω is the argument of perigee. The initial value of the x coordinate is represented as a difference in the Radius of the master and deputy spacecraft R_m and R_d respectively. The initial velocity values in the Geometry methods including the Orbital element method are represented through the change of orbital elements. For example an initial velocity in the tangential direction can be represented as a change of semi-major axis and the eccentricity of the deputy spacecraft. Similarly any initial velocity in the radial direction can be represented as a change of argument of perigee and a change of eccentricity

of the deputy spacecraft. So a 1 m/s initial velocity in the along-track direction of the deputy spacecraft can be represented in the orbital element method by considering an initial eccentricity value of 2.645×10^{-4} of the deputy spacecraft. Since the eccentricity and the resultant change of the semi-major axis terms are present in both the x and y coordinates, a cross-coupling like that of the CW method is obtained

The dynamics method (CW method) and the Geometry methods (Orbital element, Gim and Alfriend and COWPOKE) are two different methods in approach but produce same results when simulated for a keplerian case with the same initial conditions. This has been verified analytically and is given in the plots below. The initial conditions for the simulations are given in table 4.6.1.

The simulations are carried for three different test cases. In the first of the two test cases, a velocity impact in the tangential direction is analyzed. A small velocity offset in the tangential direction causes the mechanical energy of the orbit to increase, which then causes the spacecraft to drift in the along-track direction. This type of relative motion is often related to thruster firings. The third test case is analyzed for periodic relative motion. There are two conditions where the relative motion can be periodic. The first condition is when both the master and the deputy have slight elliptical orbits whose eccentricities are the same but have their apogees and perigees 180 degrees apart. The second condition is when the master is in a circular orbit and the deputy is in an elliptical orbit or vice versa but their energies are matched (semi-major axes equal). This type of trajectory is often called as the Hill's trajectory[8]. For the first and the second test case, the deputy spacecraft is assumed to be deployed from the master spacecraft with an initial velocity of 0.001 m/sec and 0.03 m/sec respectively. For the third test case, the deputy spacecraft is assumed to be in a slightly elliptical orbit and the master spacecraft is assumed to be in a circular orbit but they have equal semi-major axis of 600 km. Due to the same energy of the orbits, the relative motion is an ellipse of 2 x 1 ratio as shown in figure 4.6.3. The initial conditions translated to appropriate orbital elements is given in table 4.6.1

The increase in velocity changes the deputy satellite's eccentricity. The eccentricity of the resultant orbit can be calculated from equation 4.6.1.

$$e = \left(1 - \frac{R_{perigee}}{a}\right) \tag{4.6.1}$$

where $R_{perigee}$ is equal to the initial radius of 600 km and a is the semi-major axis of the elliptical orbit. Equations 4.6.2 and 4.6.3 can be inturn used to calculate a, the semi-major axis.

$$a = \frac{-\mu}{2E} \tag{4.6.2}$$

$$E = \frac{(V_0 + \delta V + \delta V^*)^2}{2} - \frac{\mu}{R_{perigee}} \tag{4.6.3}$$

In equation (4.6.3), V_0 is the initial velocity of the deputy spacecraft, δV is the added velocity in the along-track direction and δV^* is the velocity that is due to perturbations like J_2, Drag or Solar radiation pressure. In reality $\delta V^* \neq 0$ as there are always perturbations present at any epoch time. But since a keplerian case is considered for simulations, δV^* is assumed to be zero. For a perturbed case, it is quite difficult to translate the addition of velocities in to exact change of orbital elements due to the presence of additional unknown velocity terms that are caused due to perturbations and this can be considered as one of the limitations of this model. This is also one of the sources of error in this model. Velocities are easier implement in the CW method than the Orbital element method and this can be attributed to the actual objective of derivation of the CW method; to solve the Spacecraft Rendezvous problem.

The other major source of error identified in the Orbital element method is the representation of true anomaly as a function of time. This is due to the fact that an approximated solution to the Kepler's equations is used in the simulations. The solutions to the Kepler's equations are given as

$$\theta(t) = M + 2e\sin(M \cdot t) + \frac{5}{4}e^2\sin(2M) + \frac{1}{12}e^3(13\sin(3M) - 3\sin(M)) \tag{4.6.4}$$

Where $M = \sqrt{\frac{\mu}{a^3}} \cdot t$

It can be seen that the true anomaly is expressed as a power series in terms of eccentricity. The higher the terms of eccentricity considered the more accurate is the resultant approximation. The simulations performed in the thesis have eccentricity terms of 6^{th} order to reduce the errors in the resultant approximation of the solutions to the Kepler's equations. Nevertheless, this is a source of error in the simulations. To improve the accuracy of the simulations, the Newton's method of successive approximations could be used which is given as[27]

$$E_{i+1} = E_i - \left(\frac{E_i - e\sin E_i - M}{1 - e\cos E_i} \right), E_0 = M \tag{4.6.5}$$

The true anomaly then could be found from equation

$$\tan\frac{\theta}{2} = \tan\frac{E}{2}\sqrt{\frac{1+e}{1-e}} \tag{4.6.6}$$

Since the successive estimates of E can be obtained only iteratively, the above technique was not used, as it doesn't provide a closed form solution to the Orbital element method.

As mentioned earlier, the effect of a radial impulse can be represented in the Orbital element method as a change of eccentricity and a change in the argument of perigee. A radial impulse will change the ellipticity of the orbit and the point at which the impulse is applied becomes one of the two points in the orbit that are the endpoints of the latus rectum. The impulse also changes the apogee that occurs 90 degrees from the point of the impulse (θ = 90 degrees), and perigee occurs 270 degrees from the point of the impulse (ω = 270 degrees). The change of orbital elements can be found using the algorithm given below.

After the radial impulse is applied the new velocity vector magnitude, V, is given

$$V = \sqrt{V_0^2 + \partial V_r^2} \tag{4.6.7}$$

The new specific mechanical energy is

$$E = \frac{V_0^2 + \partial V_r^2}{2} - \frac{\mu}{R_{perigee}} \tag{4.6.8}$$

The new semi-major axis is

$$a = \frac{-\mu}{2E} \tag{4.6.9}$$

and the eccentricity of the new orbit is

$$e = \left(1 - \frac{R_{perigee}}{a}\right) \tag{4.6.10}$$

It has to be noted that for a perturbed case, it is quite difficult to translate the addition of velocities in to exact change of orbital elements due to the presence of additional unknown velocity terms in the radial direction that are caused due to perturbations. This was mentioned earlier when the translation of tangential impulse in to appropriate orbital elements were calculated.

Initial Conditions for CW Equations							
	x_0	$\dot{x}_0$	y_0	$\dot{y}_0$	z_0	$\dot{z}_0$	ω
Fig. 4.6.1	0 m	0 m/sec	0 m	0.001 m/sec	0 m	0 m/sec	0.062 deg/sec
Fig. 4.6.2	0 m	0 m/sec	0 m	0.03 m/sec	0 m	0 m/sec	0.062 deg/sec
Fig. 4.6.3	-697.1m	0 m/sec	0 m	0.38 m/sec	0 m	0 m/sec	0.062 deg/sec

Initial conditions as Orbital elements							
		i_m	Ω_m	ω_m	e_m	θ_m	a_m
Master	Fig.4.6.1	90 deg	10 deg	0 deg	0	0 deg	6971 km
	Fig.4.6.2	90 deg	10 deg	0 deg	0	0 deg	6971 km
	Fig.4.6.3	90 deg	10 deg	0 deg	0	0 deg	6971 km
		i_d	Ω_d	ω_d	e_d	θ_d	a_d
Deputy	Fig.4.6.1	90 deg	10 deg	0 deg	2.645×10^{-7}	0 deg	6971.002 km
	Fig.4.6.2	90 deg	10 deg	0 deg	7.935×10^{-6}	0 deg	6971.055 km
	Fig.4.6.3	90 deg	10 deg	0 deg	0.0001	0 deg	6971 km

Time of Simulation : 30 orbits

Table 4.6.1 Initial conditions for the comparison of the CW equations with the orbital elements method.

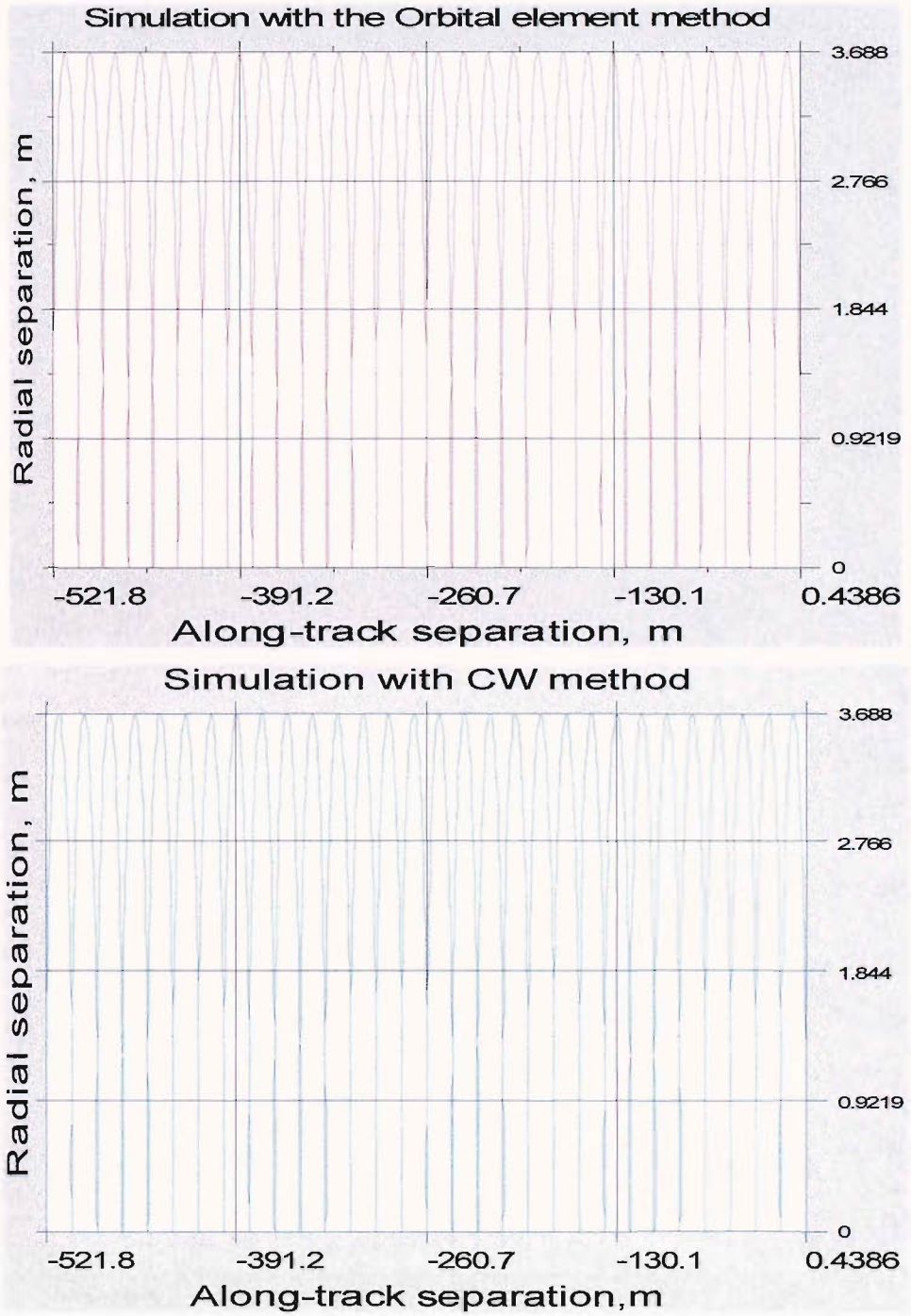

FIGURE 4.6.1. EFFECT OF AN INITIAL VELOCITY OF 0.001 M/SEC ON THE RELATIVE TRAJECTORY EVOLUTION AS PREDICTED BY THE ORBITAL ELEMENT METHOD AND THE CW METHOD

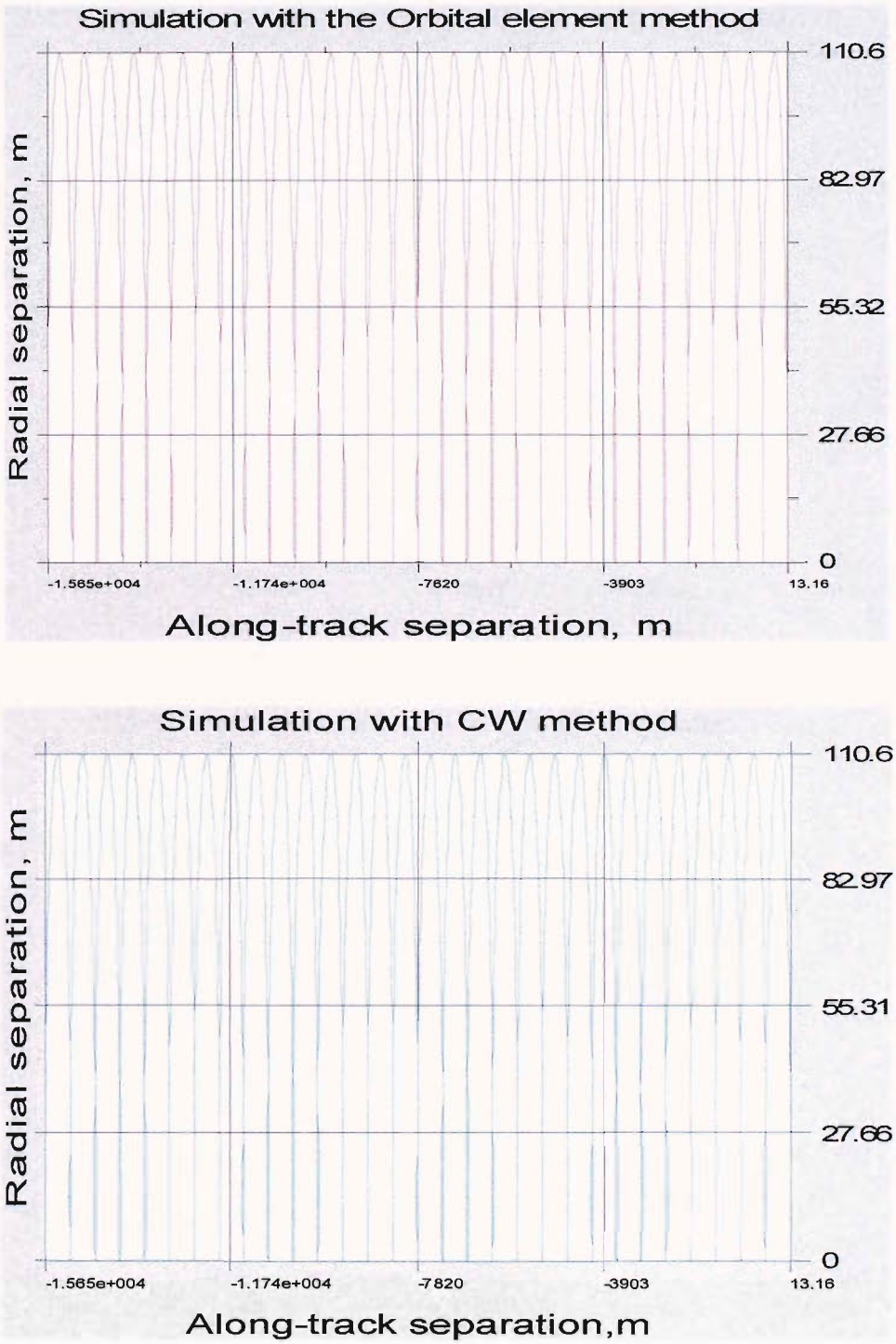

FIGURE 4.6.2. EFFECT OF AN INITIAL VELOCITY OF 0.03 M/SEC ON THE RELATIVE TRAJECTORY EVOLUTION AS PREDICTED BY THE ORBITAL ELEMENT METHOD AND THE CW METHOD

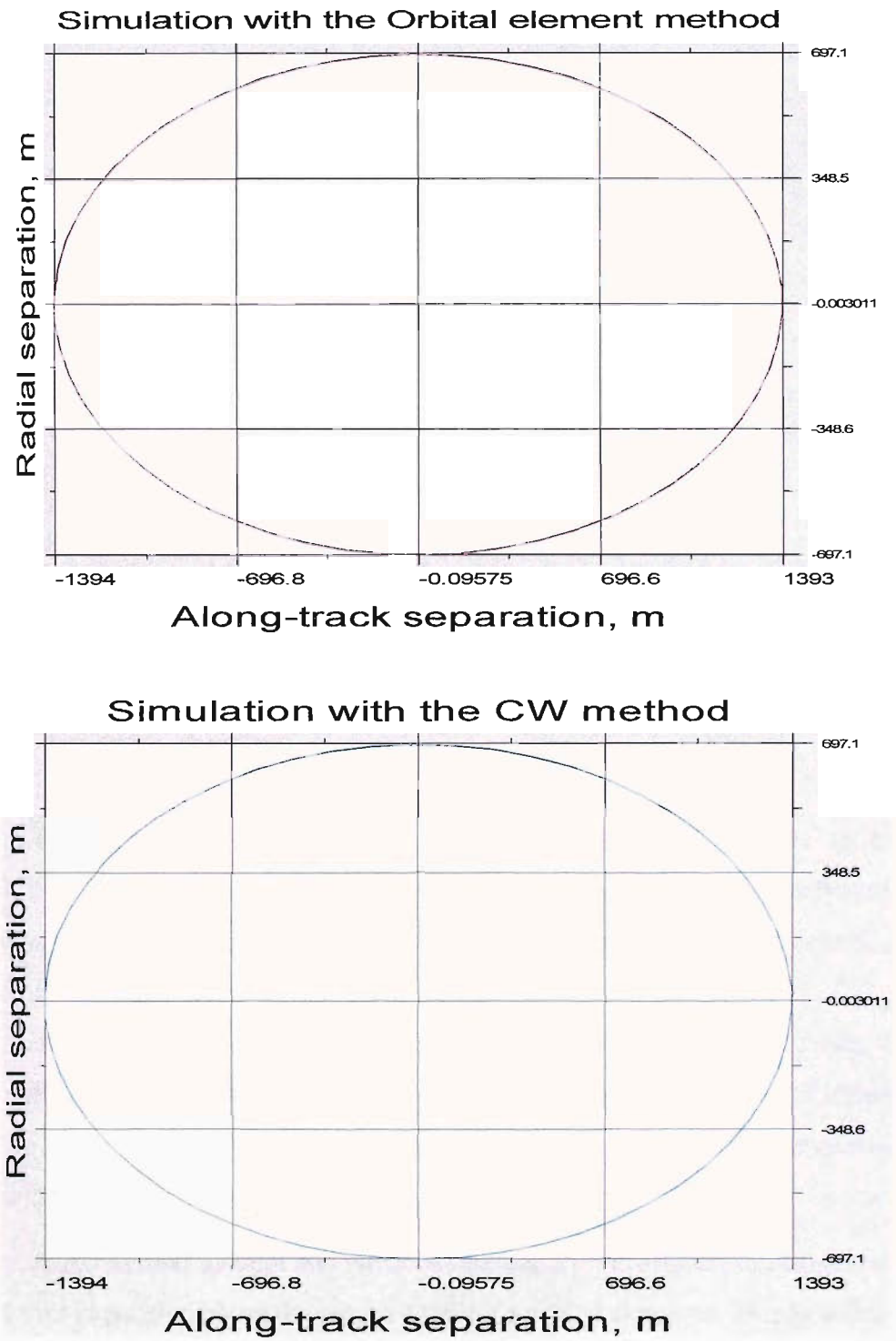

FIGURE 4.6.3. ENERGY MATCHED ORBITS WITH PERIODIC RELATIVE MOTION

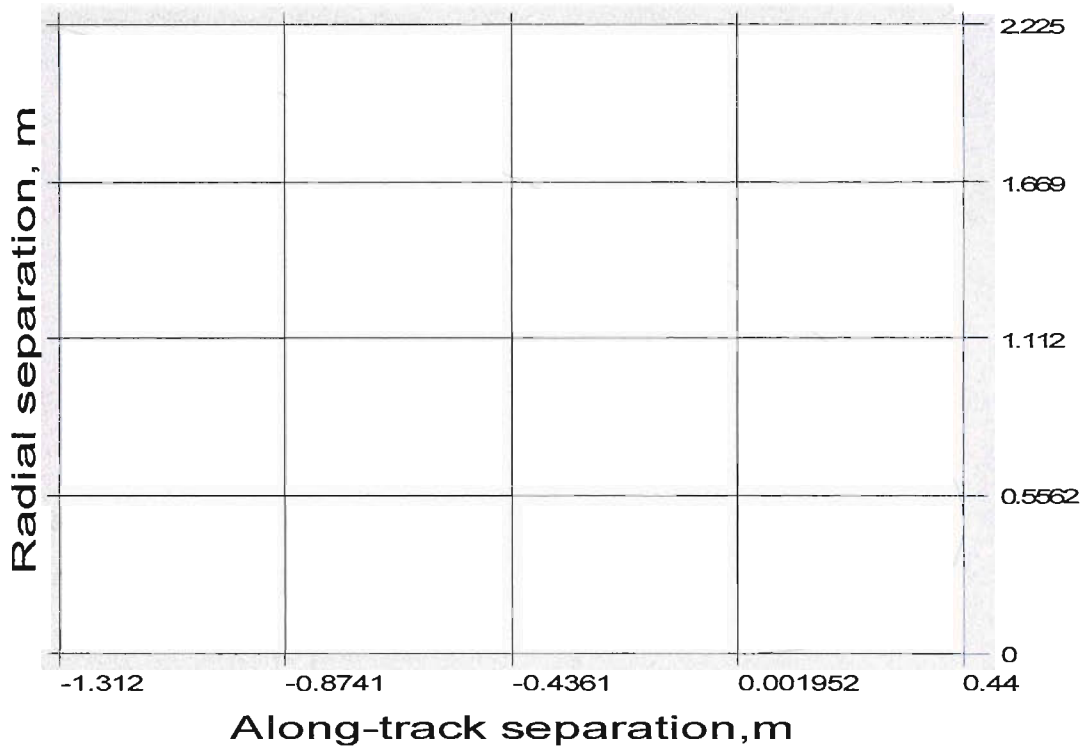

FIGURE 4.6.4. IMMEDIATE CONSEQUENCES OF A VELOCITY INCREMENT OF 0.001M/S TO THE RELATIVE MOTION

Figure 4.6.4 shows the immediate effects of adding a velocity impulse to the deputy spacecraft. The deputy spacecraft starts to move ahead of the master spacecraft for some time due to the velocity increment and then starts to drift behind the master spacecraft due to the slight eccentricity of its orbit.

The Geometry method and the COWPOKE methods also converge well with the orbital element method with some assumptions. In the Geometry and the COWPOKE methods, the solutions to the relative motion are derived with the assumption that the master and the deputy are closely placed to one another.

In the Geometric method by Gim and Alfriend, the deputy's orbital elements are expressed as a Taylor series expansion about the master satellite's orbital elements. This is under the very assumption that the initial separation distances are small and hence any orbital element of the master can be represented as[13]

$$e_d = e_m + \partial e \tag{4.6.4}$$

The same is true for a transformation

$$\vec{R}_d^C = T^{CE}(T^{EC} + \partial T^{EC}) \begin{pmatrix} R_c + \partial R_c \\ 0 \\ 0 \end{pmatrix} \tag{4.6.5}$$

The functions are then expanded by Taylor series that reads as

$$f(x + \partial x) = x + \ldots\ldots\ldots\ldots$$

The solutions of the Geometric method also show sign of assumptions. This can be particularly seen from the angles. The solutions to the Geometric method are[13]

$$\begin{bmatrix} x \\ y \\ z \end{bmatrix} = \begin{bmatrix} \delta R \\ (\delta u + \cos i_m \cdot \delta\Omega) \cdot R_d \\ (\sin u_d \cdot \delta i - \sin i_m \cdot \cos u_d \cdot \delta\Omega) \cdot R_d \end{bmatrix} \tag{4.6.6}$$

The COWPOKE method is derived in a different way. The angles subtended by the master and deputy satellites due to their initial positional differences are calculated and are multiplied by the projection of the positional vectors to give the solutions to the relative coordinates. The solutions are given as [14]

$$\begin{bmatrix} \delta r \\ \alpha \\ \beta \end{bmatrix} = \begin{bmatrix} x \\ \frac{y}{r} \\ \frac{z}{r} \end{bmatrix} = \begin{bmatrix} \dfrac{(a+\delta a)(1-(e+\delta e)^2)}{1+(e+\delta e)\cos(M+2e\sin(M)+\delta\nu)} - \dfrac{a(1-e^2)}{1+e\cos(\nu)} \\ [(\delta\omega+\delta\nu)\cos(\delta i)+\delta\Omega\cos(i)] \\ [-2\sin\dfrac{\delta\Omega}{2}\sin(i)\cos(\omega+\dfrac{\delta\omega}{2}+M+2e\sin(M)+\dfrac{\delta\nu}{2})+\delta i\sin(\omega+\delta\omega+M+2e\sin(M)+\delta\nu)] \end{bmatrix} \tag{4.6.7}$$

The COWPOKE method is also derived for small angular separations of the master and the deputy. An error analysis was presented in Section 4.1 of this thesis where the relative errors were plotted for different initial separations by changing only one orbital element, namely RAAN. In the following pages, the relative accuracy between the Orbital element method and the Geometry and the COWPOKE methods will be examined by changing more than one orbital element.

For the analysis, three different sets of orbital elements were selected and the initial relative coordinates were calculated using the COWPOKE equations (equation 4.6.7), the Orbital element method (equations 3.3.11) and the Geometry method (equation 4.6.6). The results are given in Table 4.6.3. Table 4.6.2 represents the initial conditions and Table 4.6.3 represents the results.

Master			
	Test case 1	**Test case 2**	**Test case 3**
a_m, km	6971	6971	6971
Ω_m, deg	10	10	10
i_m, deg	90	90	90
ω_m, deg	0	0	0
θ_m, deg	0	0	0
e_m	0	0	0
Deputy			
a_d, km	6972	6981	7071
Ω_d, deg	10.00005	10.005	10.5
i_d, deg	90.00005	90.005	90.5
ω_d, deg	0	0	0
θ_d, deg	0.008218	0.082	0.82
e_d	0	0	0

Table 4.6.2 Test conditions for comparison of different methods

Test Case 1			
	Orbital element method (Eqn.s 3.3.11a - 3.3.11c)	**COWPOKE method** (Eqn. 4.6.7)	**Geometry Method** (Eqn. 4.6.6)
x, meters	999.928	1000	1000
y, meters	1000.123	1000.123	1000.123
z, meters	6.078	6.078	6.078
Test Case 2			
x, meters	9992.790	10000	10000
y, meters	10014.144	10014.147	10014.378
z, meters	609.421	608.547	609.421
Test Case 3			
x, meters	997230	100000	100000
y, meters	101425.17	101428.650	101432.151
z, meters	625100	624214.278	625100.824

Table 4.6.3 Results of the comparison of different methods

The results show that the relative errors between the Orbital method and the other two compared methods increase with the separation distance. For a separation of a hundred kilometers, the relative errors are in the order of a few kilometers in the radial direction, a few hundred meters in the along-track direction and a few hundred meters in the cross-track direction. It should be noted that Table 4.6.3 only represents the relative errors calculated for initial positions. The magnitude of the relative errors is subject to increase with the progression of time.

Since the COWPOKE and the Geometry methods are represented as a function of the orbital elements similar to the orbital element method, the inclusion of J_2 dynamics is easily achieved by substituting the mean rate of change of orbital elements due to J_2 perturbations.

The mean rate of change of Orbital elements due to J_2 is given as[29]

$$\dot{\Omega} = -\frac{3nR_e^{\,2}J_2}{2p^2}\cos i$$

$$\dot{\omega} = \frac{3nR_e^{\,2}J_2}{4p^2}(4-5\sin^2 i) \qquad (4.6.8)$$

$$\dot{M} = \frac{3nR_e^{\,2}J_2\sqrt{1-e^2}}{4p^2}(2-3\sin^2 i)$$

The mean rate of change of orbital elements can be used to predict the long-term evolution of relative orbits due to the effects of J_2.

In the following pages, a direct comparison of the COWPOKE equations, as presented by Catlin[34], is made with the orbital element method, for a perturbed case with the same initial conditions. The relative orbits are simulated with the mean rate of change of elements due to J_2 in the both the methods. The resultant plots are consistent with the ones given by Catlin[34] and are shown in plots 4.6.5 and 4.6.6. Plots 4.6.5 are the ones simulated with the orbital element method and plots 4.6.6 are the ones simulated by Catlin[34].

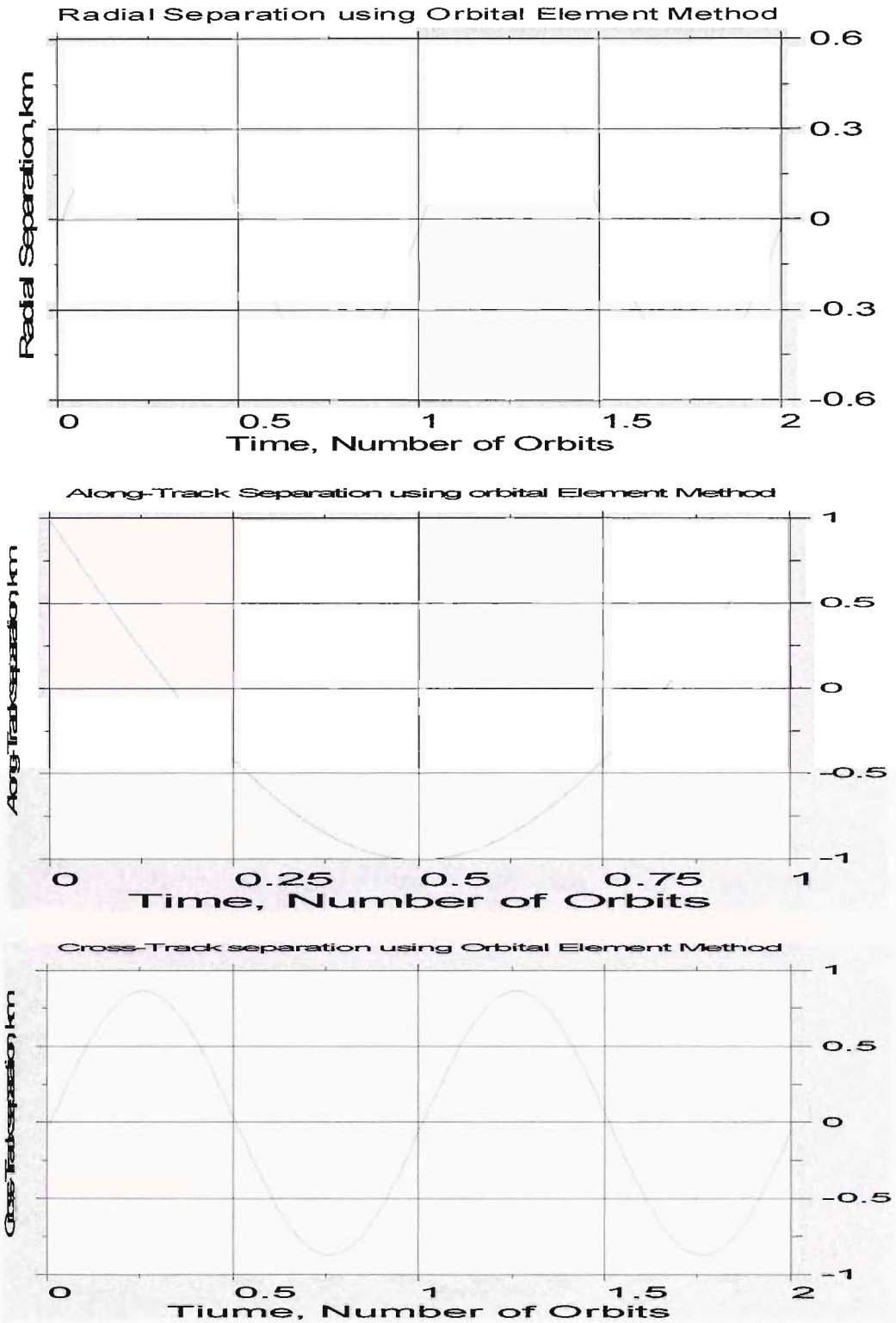

FIGURE 4.6.5 SIMULATION WITH J_2 WITH THE ORBITAL ELEMENT METHOD USING MEAN RATE OF CHANGE OF ORBITAL ELEMENTS

The plots below were extracted from Catlin[55] and shows the simulation with COWPOKE equations using mean rate of change of orbital elements

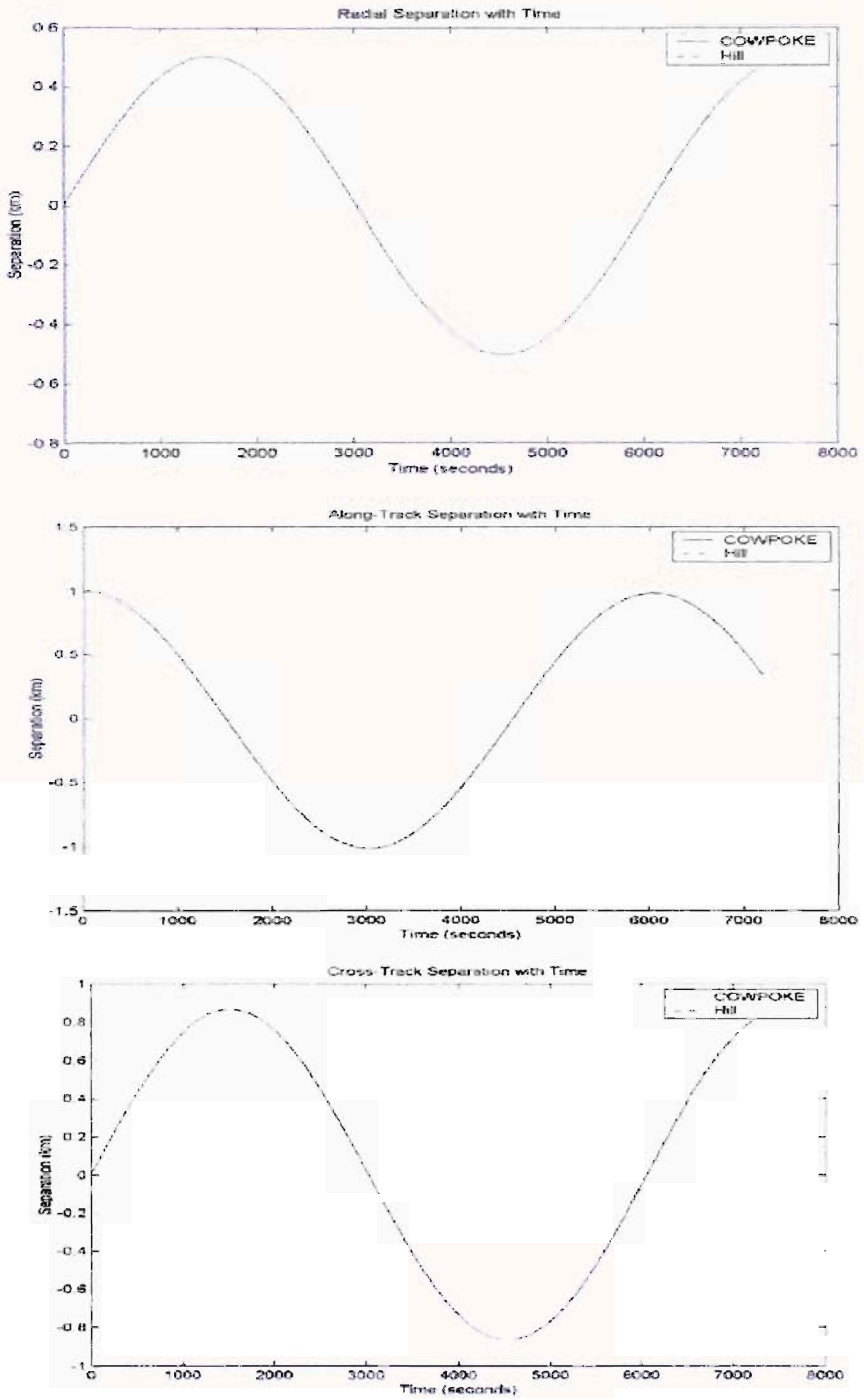

FIGURE 4.6.6 ACTUAL SIMULATION OF COWPOKE EQUATIONS USING MEAN CHANGE OF ORBITAL ELEMENTS EXTRACTED FROM A PUBLISHED PAPER BY CATLIN

Below is the table with the initial conditions used for simulation of the above plots.

	Master satellite	Difference
Semi major axis, km	7178.1363	0
Eccentricity	10^{-8}	6.964463×10^{-5}
Inclination, deg	45	0.00691260
RAAN, deg	0	1.4×10^{-6}
Argument of perigee, deg	0	270.02484058
Mean Anomaly, deg	0	89.97515845

Table 4.6.1 Conditions for Simulation using the COWPOKE equations

4.7 Numerical Integration off Differential Equations for Relative Trajectory Analysis

So far, In this thesis only the analytical methods for relative motion analysis of spacecraft were discussed. These analytical methods provide closed form solutions with or without perturbations and are useful for quite a number of applications like the fuel optimization problem. The amount of fuel needed to compensate the drifts caused by perturbations can be directly related to one another through closed form analytical solutions and in this way optimization of fuel is possible. Also the analytical solutions help to visualize the properties of possible relative trajectories even without having to simulate the analytical expressions as shown in section 4.2. This is quite impossible if we were to follow some type of numerical integration method. Infact before any of the analytical methods came in to existence, people were analyzing relative trajectories with numerical methods based on integrating relative motion equations. This method is based on integrating the differential equations of motion for both the satellites in the Earth Centered Frame and transforming the position and velocity vectors to the orbital frame of a reference orbit or the master satellite orbit and then by differencing them to obtain position and velocity vectors. This method of analysis is quite

straightforward and provides the relative position and velocities with a good level of accuracy. The level of accuracy depends only on the step size and the type of numerical method of integration used.

Gim and Alfriend[12] have done some comparisons of their method with the numerical method and the results show that their method is quite as accurate as the numerical method for the perturbed and the unperturbed case (with J_2). Their results also show that the Hill's equations when compared to the numerical method yield errors that are of significant magnitude for the perturbed and the unperturbed cases.

In this thesis, in section 4.1.1, the accuracy of the geometric method by Gim and Alfriend was compared with the orbital element method and it was shown that the Geometric method converged well with the orbital element method for conditions that had spacecraft close to each other. For large separation distances, the geometric method seemed to generate errors that were of significant magnitude.

The orbital element method developed in this thesis is consistent with the geometric method and that inturn has been shown to be consistent with the numerical method. This leads to a direct conclusion that the orbital element is indeed consistent with the numerical method of analysis and should provide the same or better level of accuracy than the geometric method. The comparison of the Geometric method with the numerical method and the Hill's method with the numerical method as of Gim and Alfriend[12] is shown in the plots below.

Chief	a (km)	e	i (deg)	Ω (deg)	ω (deg)	M_0 (deg)
	7,100	0.005	70	45	20	29.7144
Deputy	x (m)	$\dot{x}$ (m/s)	y (m)	$\dot{y}$ (m/s)	z (m)	$\dot{z}$ (m/s)
	0	0.264	500	0	0	0.528
	δa (m)	δe	δi (deg)	$\delta\Omega$ (deg)	$\delta\omega$ (deg)	δM_0 (deg)
	-1.272	1.7×10^{-5}	2.6×10^{-3}	3.2×10^{-3}	-0.3473	0.3462

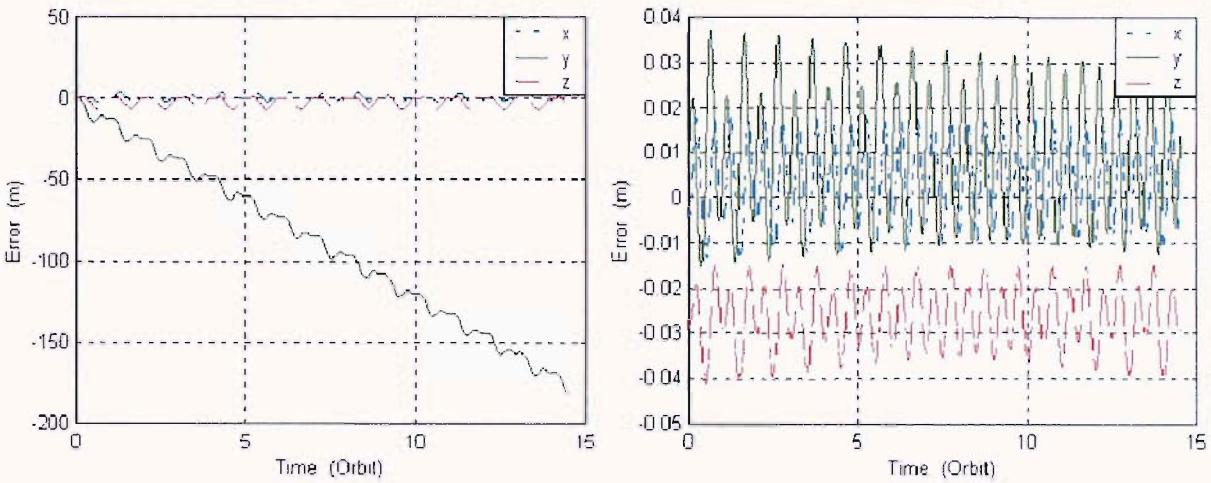

(a) Hill's Equations Errors

(b) Geometric Method Errors

FIGURE 4.7.1 COMPARISON OF THE GEOMETRIC METHOD AND THE HILL'S METHOD WITH THE NUMERICAL METHOD BY ALFRIEND[12] FOR AN UNPERTURBED CASE

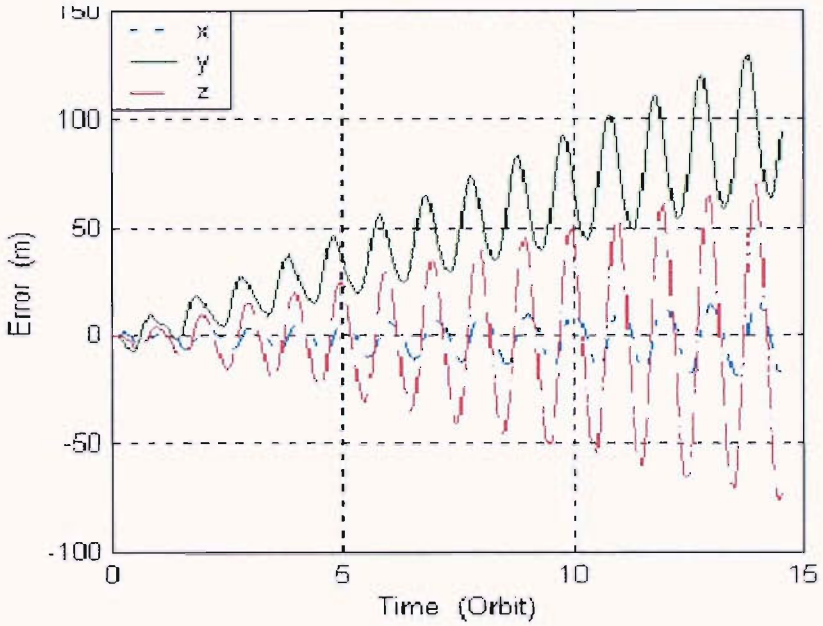

FIGURE 4.7.2 COMPARISON OF THE HILL'S METHOD WITH THE NUMERICAL METHOD BY ALFRIEND[12] FOR AN PERTURBED CASE

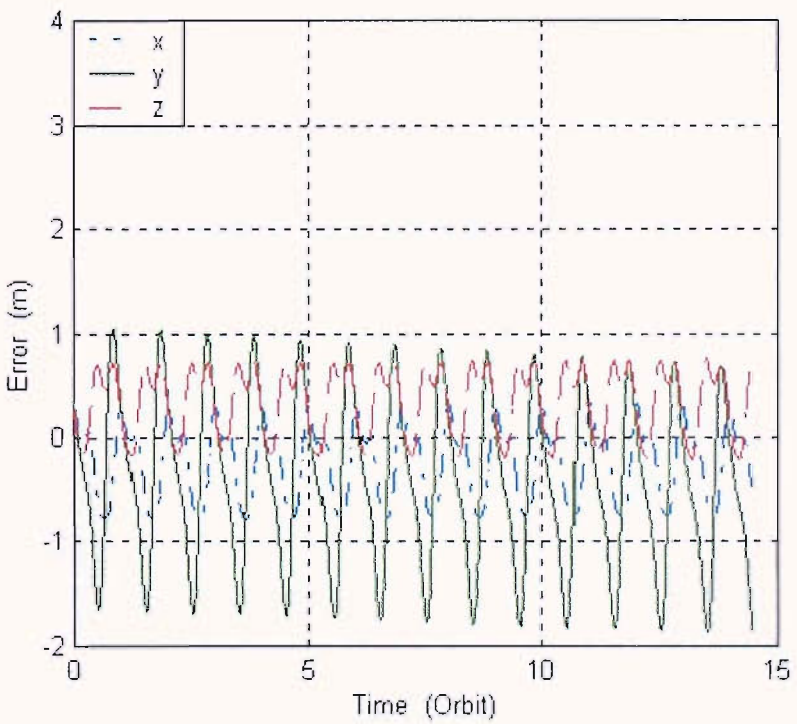

FIGURE 4.7.3 COMPARISON OF THE GEOMETRIC METHOD WITH THE NUMERICAL METHOD BY ALFRIEND[12] FOR AN PERTURBED CASE

Below is a table that compares the various models available for spacecraft relative dynamics analysis.

Method	**CW method** Section (2.1.1)	**Cowpoke method** Section (2.2.2)	**Geometry method** Section (2.2.2)	**Orbital Element method**
Is it a Nonlinear method of Analysis?	No	Yes	Yes	Yes
Is the master's spacecraft eccentricity included?	No	Yes	Yes	Yes
Is it valid for any separation distance?	No	No	No	Yes
Is it valid for longer simulation times?	No	No	No	Yes
Can all the perturbative forces be included with ease?	No	Yes	Yes	Yes
Has it got any simplifications in its derivation?	Yes	Yes	Yes	Yes
Can it be used to analyze effects of initial velocities in different directions?	Yes	No	No	No
Has it got a closed form solution for non-keplerian orbit analysis?	Yes	Yes	Yes	Yes

Table 4.7.1 Comparison of different formation flying mathematical models

Chapter 5
Simulation of Other Test Cases

5.1 Introduction

In the previous chapter, the Leader follower pattern was investigated and the behaviour of spacecraft in the presence of different forces was characterized. In this chapter, a few other formation patterns will be studied and the effects of differential drag on formation stability will be analyzed.

5.2 Formation Design Patterns

There are two general formation design configurations;

1. Formations that have spacecraft in the same orbital plane
2. Formations that have spacecraft in different orbital planes

An example of the first formation design configuration is the Leader-Follower pattern. The leader follower configuration has the satellites in the same plane and hence there is no cross-track separation of satellites. The second category of the formation design patterns is the one that has satellites in different orbital planes. The cross-track separation that arises as a result of the separation of the orbital planes can be attributed to two different individual conditions.

- Cross-track separation due to a difference in ascending nodes of the spacecraft
- Cross-track separation due to a difference in the inclination of the spacecraft

The maximum cross-track separation due to a difference in ascending nodes in achieved at the equator and due to an inclination difference is achieved at the poles. This is due to the intersection of orbital planes at the poles for the ascending node case and at the equator for the inclination difference case.

One of the practical implications of the formation with the difference in ascending node is the In-track formation. The In-track formation has two or more satellites orbiting in slightly different orbital planes and separated by shifts in true anomaly, $\delta\theta$, and right ascension, $\delta\Omega$.

The value of $\delta\Omega$ orients the orbits so that the spacecraft in the formation share the same ground track. This is especially good for remote sensing missions that plan to pass over the same point above the ground for close surveillance. The mathematical expression for such a Formation pattern would be

$$\delta\Omega = \omega_e \cdot \delta t \tag{5.2.1}$$

where ω_e and δt are the angular velocity of the earth and difference in time between satellite ground passes respectively.

Formations that have a cross-track separation due to a difference in the orbital inclinations, δi, can be named as Formation pattern with an inclination difference. Formations patterns such as circular formation flying pattern that has satellites in different planes can be designed with an inclination or ascending node difference. Figure 5.2.1 shows the in-track and inclination difference patterns.

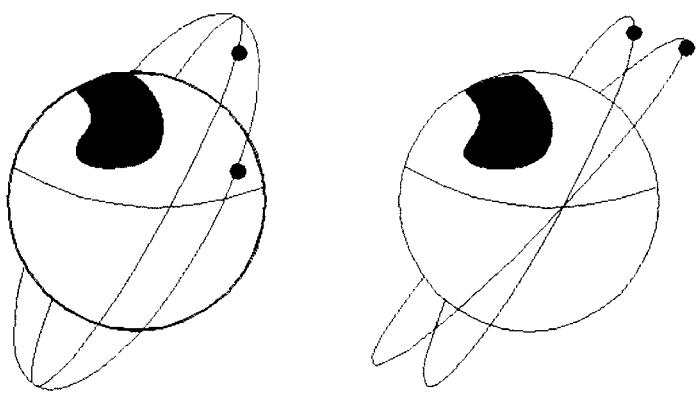

FIGURE 5.2.1. IN-TRACK AND INCLINATION DIFFERENCE FORMATION PATTERNS

5.3 Simulation Conditions of the Test Cases

To analyze the stability of the formations with a cross-track separation, test cases were simulated for the in-track and the inclination difference formation patterns using the orbital elements method. All the test cases were again considered to be near circular and polar with $\delta\Omega$ = 0.0005 deg, for the in-track formation and δi = 0.0005 deg, for the formation with an

inclination difference. The initial separation of the satellites was considered as 100 meters in the simulations and that corresponds to a $\delta\theta$ = 8.219 x 10^{-4} deg. Table 5.3.1 gives the summary of orbital elements of both the master and deputy spacecraft for the simulation test cases.

Orbital element	In-Track master/deputy	Inclination Difference master/deputy
a, km	600/600	600/600
e	0.0001 /0.0001	0.0001 /0.0001
i, deg	98/98	98/98.0005
Ω, deg	10/10.0005	10/10
θ, deg	8.219 x 10^{-4}/0	8.219 x 10^{-4}/0
ω, deg	0/0	0/0

Table 5.3.1 Orbital elements of the Deputy and master satellites

5.4 Simulation Results

The results of the numerical simulation of the in-track formation pattern are presented as figure 5.4.1. Figure 5.4.1 shows the along-track, radial and cross-track drifts for a period of 30 orbital revolutions. For the considered initial orbital elements the initial along-track separation is 108.45 meters. The magnitude of the drift and the amplitude of oscillations induced by J_2 *to* J_5 are almost similar to that obtained in figure 4.4.2 (leader-follower test case with 100 meters separation). The only difference is the periodic change in the cross-track separation distance and that is due to the intersection of the orbital planes at the poles. There are no secular drifts in the radial and cross-track directions for this formation pattern and the secular drift in the along-track direction is approximately 0.06 m/orbit.

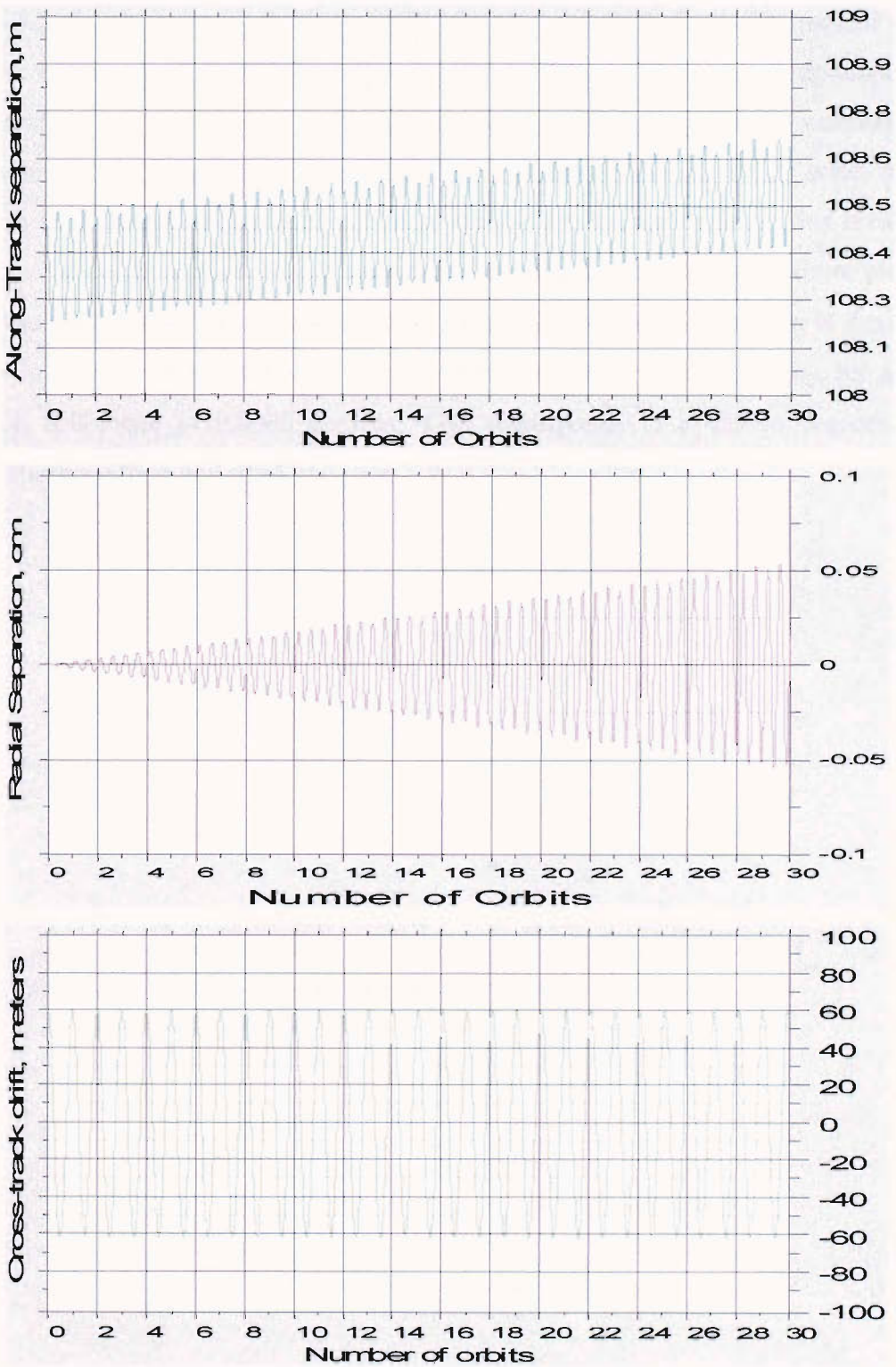

FIGURE 5.4.1. RELATIVE TRAJECTORY EVOLUTION FOR THE IN-TRACK PATTERN WITH A DIFFERENCE IN RAAN OF 0.0005 DEGREES

Figure 5.4.2 shows the evolution of relative trajectory for the formation pattern with the inclination difference of 0.0005 deg. The magnitude of the drifts in the along-track and the radial directions are the same as the formation pattern with a difference in ascending node. However unlike the formation pattern with the difference in the ascending node, there is a slight drift in the cross-track direction that gradually increases with time. This is due to the slow drift of the orbital planes from each other. J_2 induces a drift of the orbital planes and that is in turn caused by the differential rates of change of RAAN as shown in figure 5.4.3. The rate of change of RAAN was found to be $\delta\Omega = 1.25 \times 10^{-4}$ deg/day for an initial inclination difference of 0.0005 degrees. This corresponds to a 0.0456 degrees relative RAAN difference for a period of one year.

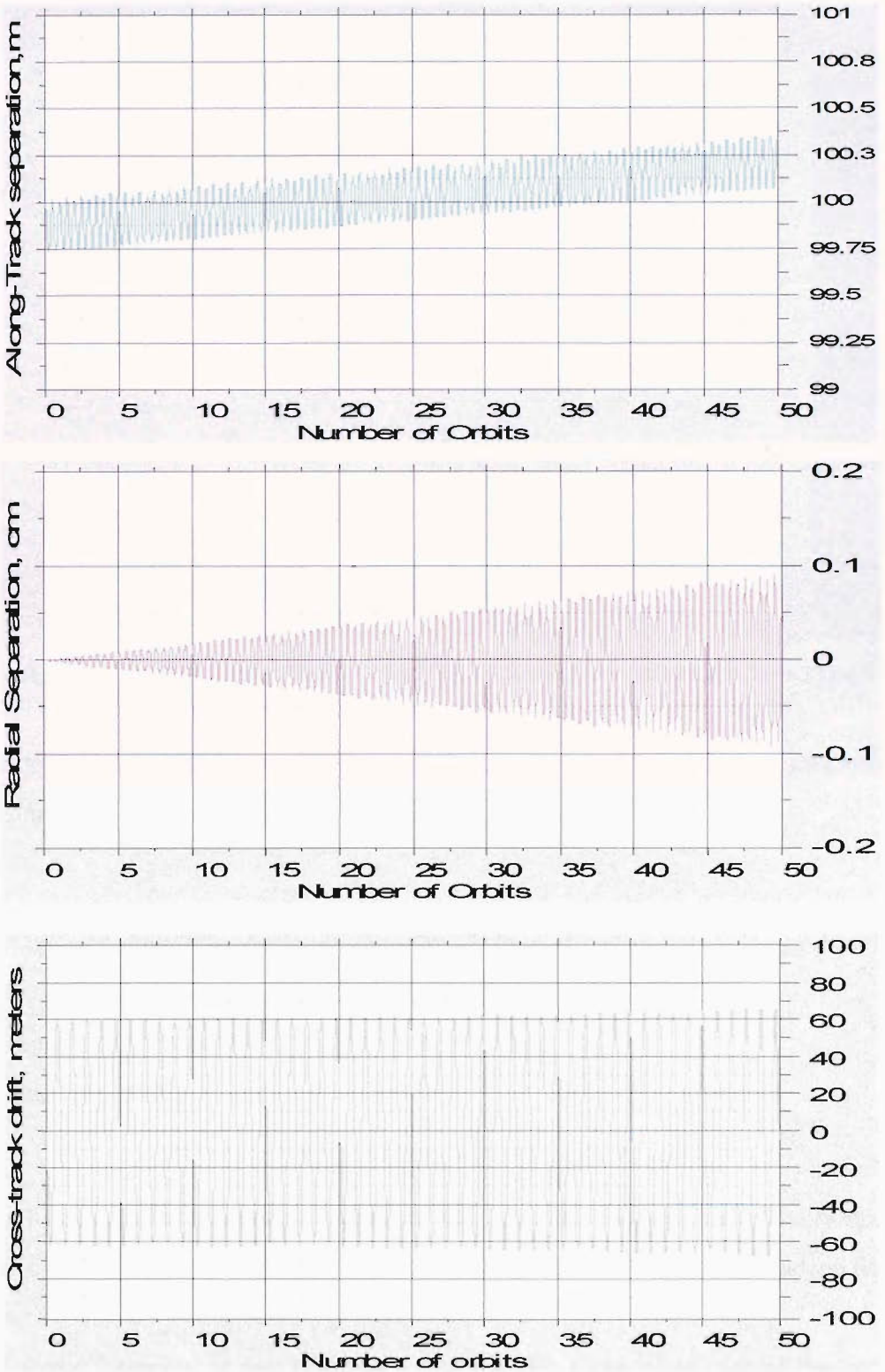

FIGURE 5.4.2 RELATIVE TRAJECTORY EVOLUTION FOR THE INCLINATION DIFFERENCE FORMATION PATTERN WITH A DIFFERENCE IN INCLINATION OF 0.0005 DEGREES

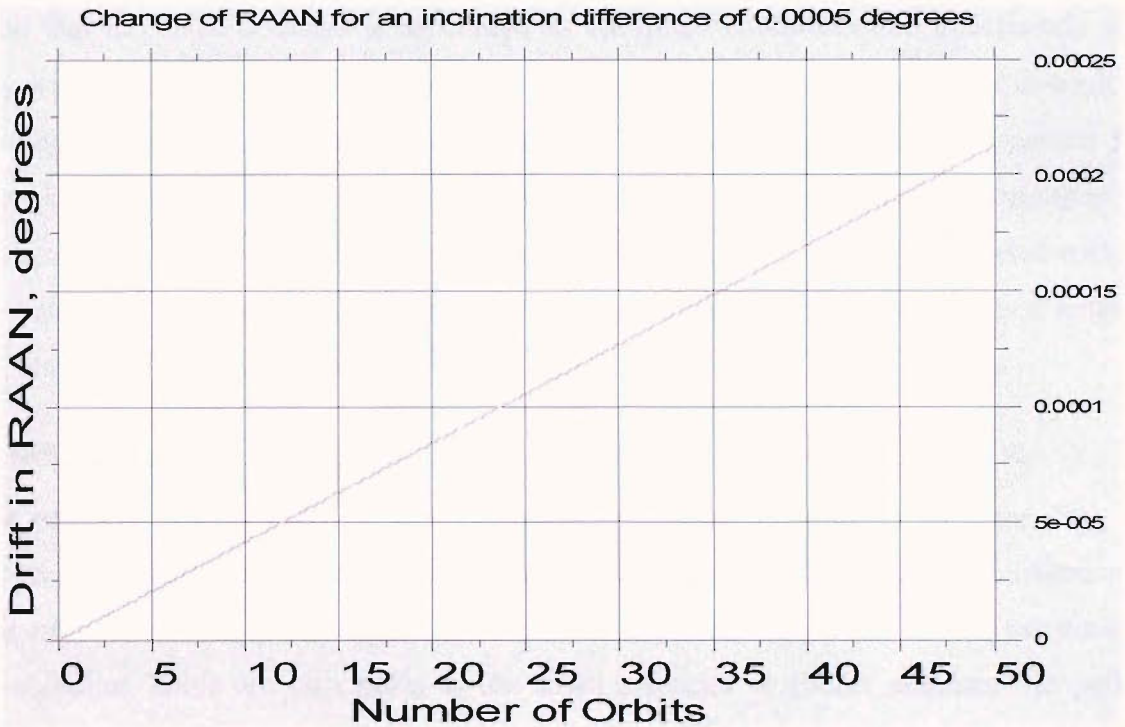

FIGURE 5.4.3 RAAN DIFFERENCE CHANGE FOR THE INCLINATION DIFFERENCE PATTERN

The velocity impulse required to compensate for a change in argument of the ascending node Ω and inclination i, can be found from the following relation [29]

$$\Delta V = 2V \sin\frac{\Delta\lambda}{2} \tag{5.4.1}$$

where

V is the circumferential velocity at the point of correction;

$\Delta\lambda$ = The total plane change and is given by [29]

$$\Delta\lambda = \cos^{-1}(\sin i_1 \sin i_2 \cos(\Omega_2 - \Omega_1) + \cos i_1 \cos i_2) \tag{5.4.2}$$

Subscripts 1 and 2 refer to conditions before and after the impulse respectively and in the simulation case it refers to the difference in change of inclination and ascending node respectively.

Using the above formulas, it was calculated that the ΔV required to correct the cross-track separation for 1 year is approximately 6 m/sec/year for the selected test case. It should be

noted that the value obtained is dependent on the initial conditions and is definitely set to vary with the initial angular difference of the planes. The ΔV requirements for in-track and the inclination difference patterns are almost the same as the leader follower pattern for a given separation distance for 1 year. This is based on the assumption that satellites pass through regions of the same atmospheric density. If the motion were to be modeled such that the atmospheric density not only varies with altitude but also with the latitude and longitude of a place then there would be some drift due to the difference in drag conditions.

5.5 Differential Drag Effects

In a practical formation-flying scenario, there is always a possibility of some drag area difference due to technical requirements like antenna pointing. Even a small difference in drag area will contribute to a significant secular change in distance between the satellites in a constellation. There are now plans to use small inspector or Escort satellites[35] to perform visual and thermal imaging of a Chief-target satellite. This enables diagnosis for repair in the case of a breakdown and helps to identify problems for similar missions. The relative trajectory of the escort satellite around the target would depend on the difference in drag area between the escort and the target, difference in masses and the altitude of their orbits. Also the difference in the ballistic coefficients caused due to any uneven depletion of fuel for formation or station keeping would cause a similar effect like the differential drag effect. So test cases with a difference in surface areas of the formation flying spacecraft will be considered. In particular the effects of altitude and differential drag on the station keeping requirements will be investigated.

Two test cases were simulated namely for the Leader-follower pattern at 600-km and the 400-km altitude with an initial separation of 100 m and the difference in drag was considered to be 10%. All the other perturbative forces were disengaged from the model and only atmospheric drag was simulated. Figures 5.5.1 and 5.5.2 represent the evolution of relative trajectory with differential drag for 600-km and 400-km altitudes respectively.

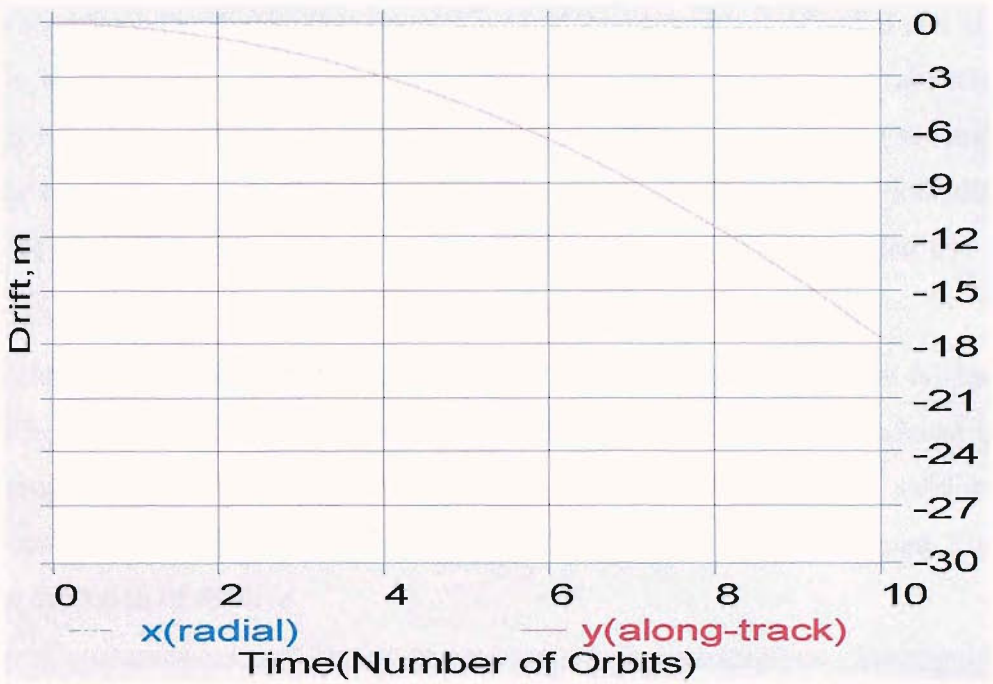

FIGURE 5.5.1 EFFECTS OF A 10% DIFFERENTIAL DRAG AREA ON THE EVOLUTION OF RELATIVE TRAJECTORY FOR A LEADER-FOLLOWER PATTERN AT 600 KM ALTITUDE

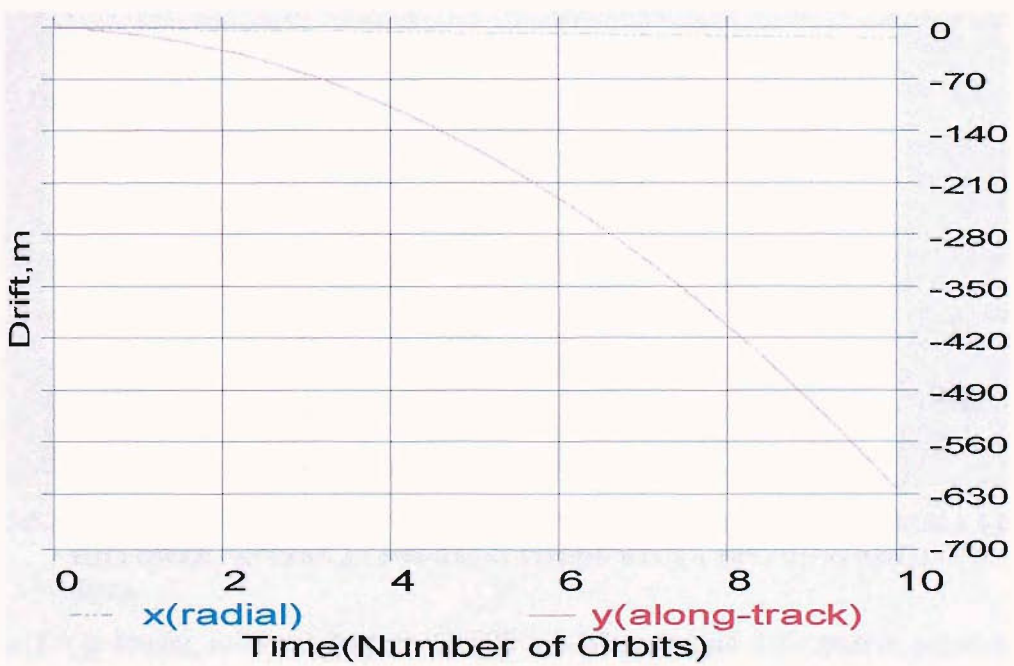

FIGURE 5.5.2 EFFECTS OF A 10% DIFFERENTIAL DRAG AREA ON THE EVOLUTION OF RELATIVE TRAJECTORY FOR A LEADER-FOLLOWER PATTERN AT 400-KM ALTITUDE

It can be seen from the figures that there is a considerable amount of radial and along-track drifts due to differential drag effects. As one can predict, the 400-km altitude has the maximum magnitude of drifts in both the directions. It is also interesting to note that the magnitude of the secular drifts induced by atmospheric drag for the 600 km altitude was found to be almost similar to the ones obtained with the preliminary method and shown in figure 3.2.3

It was decided to simulate a test case to find out the effects of SRP on the relative motion with a differential drag area. This is because of the fact the acceleration induced by SRP is directly proportional to the surface area and the surface properties of the satellites. So all other forces were disengaged from the model and only the SRP was simulated. Figure 5.5.3 shows the evolution of relative

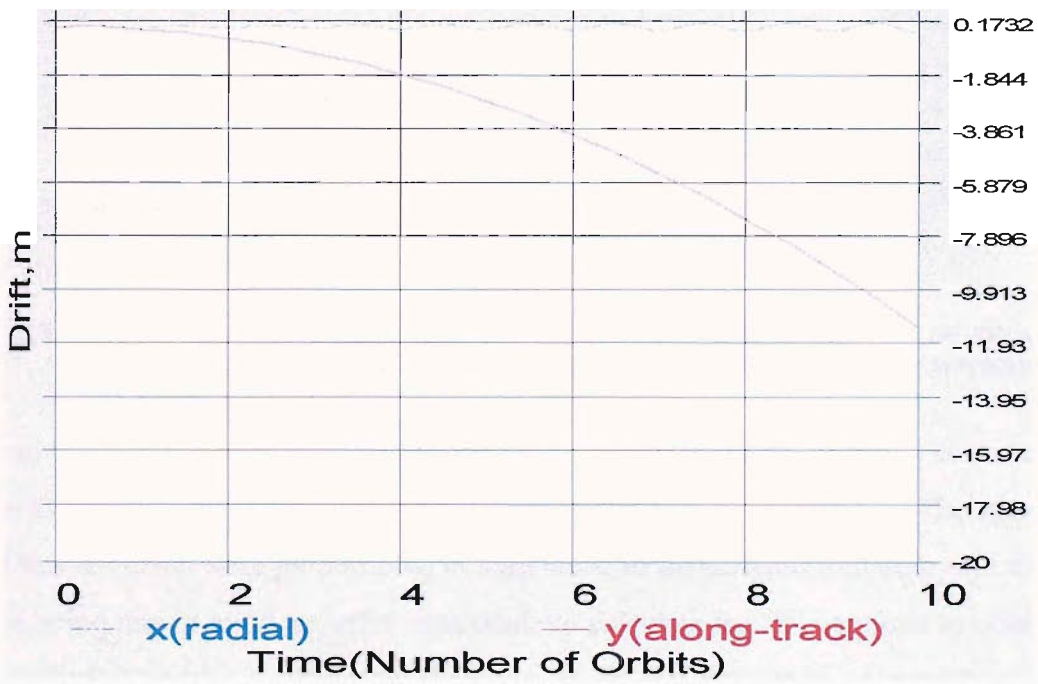

FIGURE 5.5.3 EFFECTS OF SRP ON THE EVOLUTION OF RELATIVE TRAJECTORY FOR A LEADER-FOLLOWER PATTERN AT 600-KM ALTITUDE WITH A 10% DIFFERENTIAL DRAG AREA

trajectory for a leader follower pattern at 600 km altitude and 100 meters separation with 10% differential drag area. It can be seen that SRP causes a drift of approximately 11 meters in the along-track direction and 0.4 meters in the radial direction for a 100 meters initial

separation in the along-track direction. For a 1000 meters along-track separation, the drifts would be more. Having analyzed the individual effects of atmospheric drag and the SRP, it was decided to analyze the combined effects of atmospheric drag and SRP on satellite relative motion with a differential drag area. The result of the simulation is shown in figure 5.5.4. The total drift due to the combined effects of SRP and atmospheric drag was found to be 28 meters in the along-track direction and 1 meter in the radial direction for a differential drag area of 10% for 10 orbital revolutions.

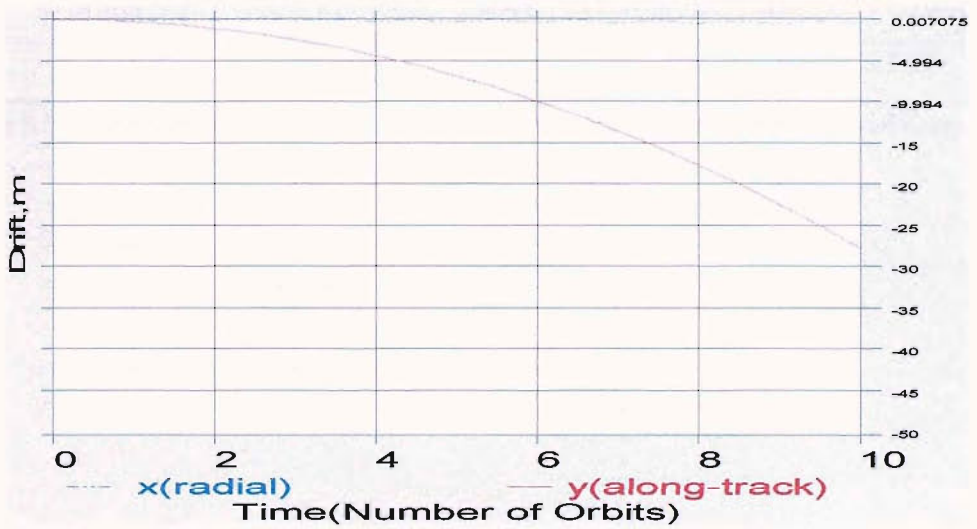

FIGURE 5.5.4 EFFECTS OF A 10% DIFFERENTIAL DRAG AREA ON THE EVOLUTION OF RELATIVE MOTION FOR A LEADER-FOLLOWER PATTERN AT 600 KM ALTITUDE WITH DRAG AND SRP

It should be noted that in a practical formation flying scenario, there is wide range of possible differences in drag area ranging anywhere from 1% to even 200%. The simulations showed that the drifts were proportional in magnitude to the difference in drag area assumed. So considering this in mind, an effort was made to calculate the ΔV required to compensate for the drifts induced by a differential drag area of 1% and the results are presented in table 5.5.1. The reason that lower frequencies of formation keeping require more fuel follows from the fact that the drift induced by Drag and SRP follows a nonlinear pattern. The magnitude of secular drifts increase with the orbital revolutions and is not proportional with time. So it is economical to fire thrusters more frequently than allowing a considerable growth of the secular drift before any thruster firings are done. In the above case considered, the magnitude

of secular drift after one orbital revolution is almost 30 times less than the magnitude of secular drift after 10 orbital revolutions in the along-track direction.

Frequency of formation keeping	ΔV requirements for 1 year, m/sec	
	600-km altitude	400-km altitude
1 orbit	0.44	5.32
5 orbits	0.49	11.20
1 day	1.2	23.62

Table 5.5.1 ΔV requirements for the Leader-Follower pattern with a differential drag of 1%

Chapter 6
Practical Issues of Formation Flight

6.1 Introduction

In this chapter, the system engineering issues of formation flight including issues concerning orbit establishment will be discussed.

6.2 Orbit Establishment for Formation Flying Spacecraft

The issue of assembling multiple spacecraft into a desired formation is the first challenge involved in a real formation-flying mission. For this, Mission planners need to know the orbital elements of each participating spacecraft based on their positional data in the formation. The method of determination of orbital elements for formations such as the In-plane formation pattern is simple and straightforward but complex for 3-dimensional formation patterns such as the triangular or circular formation pattern. There exists no direct method that gives the value of orbital elements from the initial relative positional data. However, without the knowledge of orbital elements of the spacecraft in formation, tasks such as orbit establishment, maintenance and orbit simulation is impossible. Here, in this section, the orbital elements will be represented as a function of the relative coordinates. This will be done for a closely placed formation scenario and will use three pieces of information, namely

1.The orbital elements of one of the spacecraft in formation

2. The initial values of relative displacement and

3. The formation geometry (if appropriate)

Once the orbital elements of all the spacecraft in formation are known the necessary maneuvers to establish a desired configuration pattern can be planned ahead.

6.2.1 Orbital Elements as a Function of Relative coordinates

The relationship between the orbital elements and the relative coordinates can be established by making the following assumptions in Equation (4.1.4).

- $\partial i = 0$;
- $cos\delta u \approx 1$ & $sin\delta u \approx \delta u$
- $cos\ u_d \approx cos\ u_m$

The first assumption follows from the fact that formation patterns with an inclination difference tend to be more expensive than the other formation patterns in terms of fuel consumption due to the differential drift of orbital planes. The second and the third assumptions are true for closely placed formation patterns when the relative displacement is very small compared to the distance of the spacecraft from the center of earth. Similarly, $\delta e \approx 0$ & $\omega \approx 0$ for closely placed spacecraft and that leaves us to find the other three significant orbital elements namely, the semimajor axis, RAAN and the true anomaly. By considering the above mentioned assumptions and rearranging terms in equation (4.1.4),

$$R_d = x + R_m \tag{6.2.1.1a}$$

$$\partial\Omega = \frac{-z}{(x + R_m)\sin i_m \cos u_m} \tag{6.2.1.1b}$$

$$\partial u = \frac{y \sin i_m \cos u_m + \cos i_m z}{(x + R_m)\sin i_m \cos u_m} \tag{6.2.1.1c}$$

The above equations for the angular orbital elements when evaluated and substituted in equations $\Omega_d = \Omega_m - \delta\Omega$, $u_d = u_m - \delta u$ yield the orbital elements of the deputy spacecraft. The above equations can also be simplified for specific cases as shown in table. (6.2.1).

	xy plane, *z=0*	*xz* plane, *y=0*	*yz* plane, *x=0*	*x,y,z =0*
$R_d =$	$x + R_m$	$x + R_m$	R_m	0
$\partial\Omega =$	0	$\frac{-z}{(x+R_m)\sin i_m \cos u_m}$	$\frac{-z}{R_m \sin i_m \cos u_m}$	0
$\partial u =$	$\frac{y \sin i_m \cos u_m}{(x+R_m)\sin i_m \cos u_m}$	$\frac{\cos i_m z}{(x+R_m)\sin i_m \cos u_m}$	$\frac{y \sin i_m \cos u_m + \cos i_m z}{R_m \sin i_m \cos u_m}$	0

Table 6.2.1 Formulas of orbital elements pertaining to different cases

6.2.2 Validation of the Results

It should be noted that the above results are not very accurate due to several assumptions made in their derivation. Nevertheless they can be used to predict the values of the orbital elements of the deputy spacecraft and with some iteration they can be also made to provide accurate results. This will be shown in the following paragraphs by considering the following formation-flying scenario.

It has been planned to use 2 spacecraft with the master spacecraft having the following orbital elements;

R_m = 6971 km, $e_m = 10^{-4}$, i_m = 90 deg, Ω_m = 10 deg, ω_m = 0 deg, θ_m = 0 deg and

The initial relative coordinates of the deputy are; x_0 = -1 km, y_0 = -1 km, z_0 = 1 km

The objective is to find the orbital values of the deputy spacecraft with the above known parameters. It will be shown in the following paragraphs that the problem of finding the accurate values of the orbital elements is an iterative process

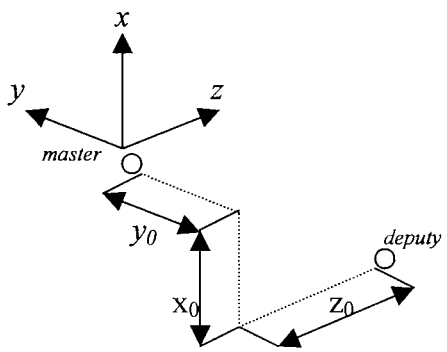

FIGURE 6.2.1 GEOMETRICAL REPRESENTATION OF A PRACTICAL FORMATION-FLYING SCENARIO

Figure (6.3.1) is the geometrical representation of the formation pattern. By substituting the known values in Equations.(6.2.1.1a-6.2.1.1c),

R_d = 6970 km (599 km altitude), $\delta\Omega = 8.347 \times 10^{-3}$ deg, $\delta u = 8.22 \times 10^{-3}$ deg,

Correspondingly, R_d = 6970 km, $e_d = 10^{-4}$, i_d = 90 deg, Ω_d = 10.0083 deg, ω_d = 0 deg,

u_d = -0.0082 deg

Now as discussed earlier, these values are just approximate values due to the several assumptions made in Equation (4.1.4). The difference can be estimated by substituting the obtained orbital element values in relative coordinate equations (3.3.11a –3.3.11c). The difference between the actual values of the orbital elements and those obtained with the formulas becomes higher with the increase in the values of the relative coordinates.

In our case, by substituting the orbital elements in equations (3.3.11a –3.3.11c),

x = -1000.146 m, y = 999.958 m, z = -1015.408 m

It can be seen that the cross track displacement differs by approximately 15 meters from its actual value and to correct it, the difference in RAAN might have to be reduced slightly. Similarly the value of the true anomaly needs to be slightly adjusted to tally the difference in the y direction. After a few iterations the correct values of RAAN and true anomaly of the deputy spacecraft corresponding to the desired values of x, y, z were found to be Ω_d = 10.0082203 deg and u_d = -0.0082203 deg. The same algorithm can be used to find the orbital

elements of any number of deputy spacecraft with just the knowledge of their positional data with respect to the master spacecraft.

6.2.3 Assembly and Control of Spacecraft Formation

In the previous subsections, the relationship between the orbital elements and the formation geometry was discussed. It was shown that the orbital elements of the deputy spacecraft could be determined with the knowledge of the formation geometry and the orbital elements of the master spacecraft. The next question that needs attention is the strategy involved in the actual assembly of the spacecraft into a formation. Different formations will need different strategies for spacecraft deployment and assembly. Also the total time taken for the assembly would depend on the final separation distance of the spacecraft, the complexity of the formation and the fuel budget. For formation patterns that have all spacecraft in the same orbital plane, the strategy for assembly should be relatively simple and straightforward when compared to complex formations with spacecraft in different orbital planes. Choosing the fuel optimal strategy is one of the main problems involved in spacecraft formation assembly and this is very important especially for nanosatellite formation assembly.

Let us consider a simple case of a proposed leader-follower formation-flying mission. Two spacecraft are planned to have an initial separation distance of 1000 meters. It is proposed to seek a strategy to assemble the spacecraft with the minimum amount of fuel spent and within a specified time. One of the possible strategies would be to eject one of the spacecraft with an excess velocity in the along-track direction relative to the other. The slight excess velocity would then cause the spacecraft to drift in the along-track direction. Once the desired separation distance is obtained, a drift stop maneuver can be performed to stop the relative drift between the spacecraft. To avoid any final radial separation distances, it is better to perform the drift maneuver at the perigee altitude where the radial separation will be the least. To execute this strategy, one needs to know three parameters in advance. These are the initial spacecraft distance, time for formation assembly and the velocity increment needed for the drift. In practice, two of the parameters are dictated by the mission requirements namely the initial separation distance and the formation assembly time. The third parameter, namely

the required velocity increment can be found from the algorithm developed by the author of this thesis and is given below. In the algorithm the deputy spacecraft is assumed to have the velocity increment.

The along-track separation distance, from equation 4.1.2 is given as

$$y = (\sin \delta u + \cos i_m \cdot \delta\Omega \cdot \cos \delta u) \cdot R_d$$

For spacecraft lying in the same orbital plane, the above equation can be written as

$$y = \sin \delta u \cdot R_d$$

$$\Rightarrow \delta u = \sin^{-1} \frac{y}{R_d}$$

$$\Rightarrow \frac{2\pi t}{T_m} - \frac{2\pi t}{T_d} = \sin^{-1} \frac{y}{R_d} \qquad (6.2.3.1)$$

Where t in the above equation is the time, R_d is the perigee radius and T is the Time period. Subscripts m and d refer to the master and the deputy spacecraft respectively.

In the above equation, parameters R_d, T_m and y are known and T_d is the unknown parameter.

Equation 6.2.3.1 can be rewritten as

$$\Rightarrow \frac{1}{T_d} = \frac{1}{T_m} - \frac{\sin^{-1} \frac{y}{R_d}}{2\pi t}$$

$$\Rightarrow \frac{1}{T_d} = \frac{2\pi t - T_m \sin^{-1} \frac{y}{R_d}}{2\pi t T_m} \qquad (6.2.3.2)$$

$$\Rightarrow T_d = \frac{2\pi t T_m}{2\pi t - T_m \sin^{-1} \frac{y}{R_d}} \qquad (6.2.3.3)$$

substituting $T_d = 2\pi \sqrt{\frac{a_d^3}{\mu}}$ in the above equation gives

$$\sqrt{\frac{a_d^{\,3}}{\mu}} = \frac{tT_m}{2\pi t - T_m \sin^{-1}\frac{y}{R_d}} \tag{6.2.3.4}$$

Substituting $a_d = \frac{R_{d0}}{1-e}$ in equation 6.2.3.4 gives

$$\sqrt{\frac{R_{d0}^{\,3}}{\mu(1-e)^3}} = \frac{tT_m}{2\pi t - T_m \sin^{-1}\frac{y}{R_d}} \tag{6.2.3.5}$$

In the above equations, R_{d0} refers to the perigee radius of the deputy spacecraft just before the addition of velocity increment. Also $R_{d0} = R_m$

$$\Rightarrow (1-e)^{\frac{3}{2}} = \frac{\left(2\pi t - T_m \sin^{-1}\frac{y}{R_d}\right)}{tT_m}\sqrt{\frac{R_m^{\,3}}{\mu}}$$

$$e = 1 - \left[\frac{\left(2\pi t - T_m \sin^{-1}\frac{y}{R_d}\right)}{tT_m}\right]^{\frac{2}{3}} \frac{R_m}{\mu^{\frac{1}{3}}} \tag{6.2.3.6}$$

In the above equation t can be represented as $t = n \cdot T_m$ where n is the number of orbits of the master spacecraft. So equation 6.2.3.6 can be written as

$$e = 1 - \left[\frac{\left(2\pi n T_m - T_m \sin^{-1}\frac{y}{R_d}\right)}{nT_m T_m}\right]^{\frac{2}{3}} \frac{R_m}{\mu^{\frac{1}{3}}}$$

$$\Rightarrow e = 1 - \left[\frac{\left(2\pi n - \sin^{-1}\frac{y}{R_d}\right)}{nT_m}\right]^{\frac{2}{3}} \frac{R_m}{\mu^{\frac{1}{3}}} \tag{6.2.3.7}$$

Equation 6.2.3.7 can be used to determine the resultant eccentricity of an orbit, which gives a drift of y after n orbits of the master spacecraft. The value of e can be then used to find the magnitude of the velocity increment needed for the specified conditions. For that the semi-major axis a_d of the deputy spacecraft can be found with the help of e obtained from equation 6.2.3.8.

$$a_d = \frac{R_{perigee}}{1-e} \tag{6.2.3.8}$$

where $R_{perigee}$ is equal to the initial radius of the deputy spacecraft before the velocity increment. The energy equation is written as.

$$\frac{(V_{d0}+\delta V)^2}{2} - \frac{\mu}{R_{perigee}} = \frac{-\mu}{2a_d} \tag{6.2.3.9}$$

The required velocity increment can then be found by rearranging the terms in equation 6.2.3.9. In Equation 6.2.3.9, V_{d0} refers to the initial velocity of the deputy spacecraft just before the velocity increment and is equal to V_m, the velocity of the master spacecraft.

$$\delta V = \sqrt{2}\left(\frac{-\mu}{2a_d} + \frac{\mu}{R_{perigee}}\right)^{\frac{1}{2}} - V_m \tag{6.2.3.10}$$

Substitution of equations 6.2.3.8 and 6.2.3.7 in equation 6.2.3.10 gives the final equation

$$\delta V = \frac{\mu}{R_{perigee}}\left(2 - \left[\frac{\left(2\pi n - \sin^{-1}\frac{y}{R_d}\right)}{nT_m}\right]^{\frac{2}{3}} \frac{R_m}{\mu^{\frac{1}{3}}}\right)^{\frac{1}{2}} - V_m \tag{6.2.3.11}$$

The above algorithm can be used to find the velocity increment needed to achieve an along-track drift of y meters in n orbits. An example is illustrated below to demonstrate the validity of the above algorithm.

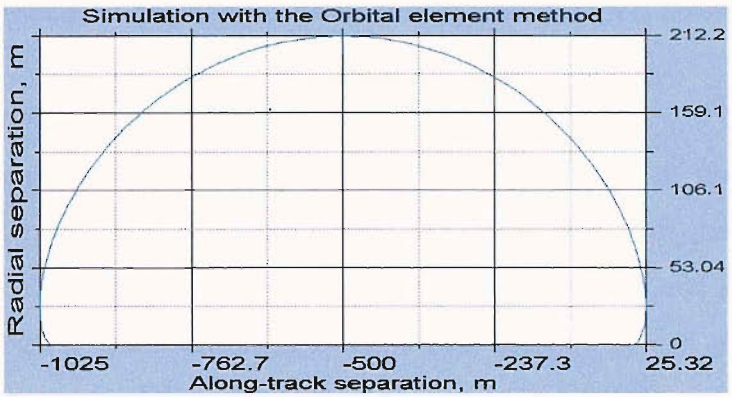

FIGURE 6.2.2 SIMULATION SHOWING THE CONSISTENCY OF THE ALGORITHM WITH THE DERIVED FORMULAE TO PREDICT THE REQUIRED δV

It is necessary to determine the δV to achieve an along-track separation of 1000 meters after1 orbital revolution of the master for a 600-km initial altitude. Using the given data, the eccentricity of the resultant orbit can be found from equation 6.2.3.7. The eccentricity computes to 1.522×10^{-5}. The δV can then be found from equation 6.2.3.10 and equals 0.058 m/sec. The results are then substituted in equations 3.3.11a-3.3.11b and the simulated plot is shown as figure 6.2.2. It can be seen that for the specified velocity increment, the along-track separation is 1000 meters after one orbit. This shows that the algorithm is valid and consistent with the derived formulas for the specified conditions. It should be noted that the algorithm presented is only valid for velocity increments made in the along-track direction. The above algorithm could also be used in the controller algorithm for fuel optimal formation reconfiguration with appropriate data from relative co-ordinate determination sensors. It should be noted that the algorithm presented might not represent the optimal method to assemble the formation but is just one of the possible ways to assemble a formation.

6.3 System Engineering Issues

Formation flying is undoubtedly a revolutionary concept that has many useful implications. However, to accomplish a successful mission using this concept, a number of challenges have to be overcome in the field of sensing, actuating and controlling of the spacecraft

involved. These challenges are a part of the requirements for a good systems design. In this section, the current status of the main focus areas of system design is discussed.

6.3.1 Formation Flying Sensors

Many of the currently proposed formation flying missions plan to use spaceborne GPS technology for determining and controlling the relative positions of the satellites. Several teams, including NASA, JPL and ESA, are working with university and industry partners to move this technology to the forefront[36]. Current GPS technology can provide information about the relative positions of the satellites to an accuracy of a few centimeters. It is expected to take three generations of receiver developments to achieve the GPS (transmit/receive) spacecraft cross-link sensor that is needed for future formation flying missions[36]. An alternative to GPS technology is the vision-based navigation (VISNAV) system under development by Texas A&M University. VISNAV has an optical sensor made up with a Position Sensing Diode (PSD) placed in the focal plane of a wide-angle lens. When the rectangular silicon area of the PSD is illuminated by the energy from a beacon, it generates electrical currents that are processed to determine position co-ordinates. The advantage of such a sensor is that the light sources can be put at the end of a deployed boom of a single spacecraft for determining alignment, or on other spacecraft in a formation to determine position and attitude.

6.3.2 Formation Flying Actuators

Formation control puts high demands on spacecraft actuators. New technologies are necessary to ensure sufficient resources are available onboard to maintain the formation. These technologies must support higher pointing constraints, provide greater precision thrust capability and significantly improve use of propellant expendables since a greater manoeuvring frequency can be expected to maintain precision relative positioning. Several initiatives that are of particular interest are micro-reaction wheels and micro-thrusters. These could be used to support very small micro and nanosatellites as well the extremely fine pointing needed to achieve the requirements for formation flying missions such as planet finder, interferometry, synthetic aperture radar, and relativity. Colloid microthrusters (with

thrust in the milli-Newton range) are a promising new technology in the field of small spacecraft propulsion. Because of their small size and low weight these devices are particularly interesting to missions incorporating formation flying and nanosatellites.

There are also proposals of using drag panels to control relative separation of spacecraft for coarse formation flying missions. This is achieved by creating a differential drag effect by either opening or closing the drag panels on the master or the deputy spacecraft. C.L.Leonard[37] proved in his paper that it is feasible to use differential drag as the means for controlling the spacecraft relative position. This is an advantage especially when different spacecraft in a formation have different masses due to uneven spending of fuel for formation and station keeping. However there are some limitations like the cross-track drifts are often not controllable.

6.4 Some General Issues Concerning Formation Flying

The costliest of all formation patterns in terms of fuel is the formation with the inclination difference. This is due to the fact that formation patterns with spacecraft in different orbital planes need additional fuel for compensating the cross-track secular growth error. It is also very expensive to maintain formations at low altitudes due to the atmospheric drag effects. For example it was found that the semi major axis decayed at a rate of 41 m/orbit for 400-km altitude. The worst case would be to have a differential drag-area that would require additional fuel for formation keeping. The effects of differential drag increase with the decrease in satellite altitude. Satellites flying in formation are likely to develop dissimilarities in mass during their entire lifetime due to the expulsion of mass as propellants. The quantity of the propellants used by each satellite directly depends upon the attitude accuracy requirement as defined by the mission and the frequency of formation maneuvering. The depletion of mass as fuel increases the ballistic coefficients of the satellites thereby increasing their drag deceleration. The extent of relative motion directly depends upon the difference in mass between the formation flying satellites. The greater the difference in mass, the more the satellites drift or come close to each other depending upon their positions in the formation. The dissimilarities in mass of the formation flying satellites, at different instances

of time, during the mission is variant as the satellites burn up fuel in different ratios as required by the mission control. The effects of dissimilarities in mass are almost identical to the effects of difference in drag area, as both the factors tend to change the net drag deceleration and the solar radiation pressure on the satellites. The effects of difference in mass can be reduced by the proper planning of the fuel usage between the satellites or by using drag panels as actuators for formation maneuvering and correction. For nano-satellite formation flying, it is desirable to use higher altitudes to reduce any differential drag effects and consequently minimize fuel spending.

Apart from the fuel expenses for formation keeping, station keeping and formation maneuvering, spacecraft may also need to carry extra fuel for any correction of velocity or position offsets that may arise after separation from the launch vehicle. The magnitude of the ΔV to compensate the velocity offset depends on the accuracy of the satellite deployment or separation mechanisms and also the direction of the velocity offset and can constitute a few meters/second if the velocity of offset is in the orbit normal direction.

Chapter 7
Summary, Conclusions and Recommendations

7.1 Summary

The main purpose of this thesis was to study and analyze the dynamics of spacecraft formation flight. In the first two chapters of this thesis, the concept of spacecraft formation flight and the different approaches available for the study of formation dynamics were discussed. The literature review in chapter-two reveals the fact that the existing methods are generally based on the CW equations and considerable improvement to the dynamics is needed for an accurate prediction of the relative positions of the spacecraft that will consequently minimize fuel consumption and maximize lifetime. Many of the existing methods also suffer from limitations like on eccentricity of the reference orbit, initial separation distance and simulation time. Chapter Three deals with the development of the mathematical model for the analysis of spacecraft formation flight dynamics. The method is based on a geometrical transformation of the coordinates from the Earth-centered co-ordinate frame to the spacecraft centered co-ordinate frame. The resultant is a system of relative coordinates dependant on the orbital elements of the reference spacecraft and the target spacecraft. This feature also allows dynamical modelling of perturbative forces with the help of the Gauss equations that relate the change of orbital elements as a function of the perturbations. The model is then improved to accommodate zero values of inclination and eccentricity by converting the classical orbital elements to modified equinoctial orbital elements. This model is then used to predict the dynamical behavior of spacecraft in different formation patterns under the influence of perturbative forces like $J_2 - J_5$, Solar Radiation Pressure and Atmospheric Drag. The effects of the different initial conditions like spacecraft separation, type and nature of orbit are studied. Based on the values of drift predicted, an estimate of the ΔV needed to compensate for the drifts for different frequencies of thruster firings is calculated. The effect of differential drag on the stability of the formation is analyzed for different altitudes. Analysis of different formation patterns show that the differential J_2 effects induces short time periodic variations in all the directions and these

periodic variations are dependent on the initial conditions. For example, the initial along-track separation of the formation pattern is one of the factors that affect the magnitude of the periodic variations. Another factor that influences the periodic variations caused by J_2 is the inclination of the orbits. It was found that the spacecraft in high inclination orbits were most affected by the differential J_2 effects than the spacecraft located in low inclination orbits. The maximum magnitude of oscillations induced by differential J_2 was in the range of 0.5% of the initial separation distance. So a control accuracy value of $\pm 0.5\%$ of the initial separation distance would not incur any fuel expenditure due to the differential J_2 effects. This is however not true for formation patterns having spacecraft with different orbital inclinations. The differential J_2 effects also induce secular drifts in the along-track direction that needs to be corrected. The magnitude of the secular drifts again depends on the initial conditions and the formation patterns with spacecraft located in different inclinations need more fuel for formation keeping than the formation patterns that have spacecraft located in the same orbital plane. A study is conducted to compare the results of the orbital element method with the CW method and the COWPOKE equations.

Finally, in chapter six, the equations of the relative coordinates and the geometry of the formation are utilized to predict the orbital elements of the deputy spacecraft for the formation assembly problem. This is done with the help of the simplified version of the relative coordinate equations for a closely placed formation scenario. Also in chapter six, some of the system engineering issues related to practical formation flying are discussed.

7.2 Recommendations

Due to the scope of this thesis, there are many interesting questions that have been identified as possible case studies for future research. They are listed in order below.

- Inclusion of tesseral harmonic coefficients and modelling gravitational perturbations as a function of the latitude and the longitude of the sub-satellite point as only zonal harmonic coefficients are modeled in this thesis. The zonal harmonic coefficients are only dependent on the latitude of the sub-satellite point.
- Modeling and the inclusion of third body perturbations like lunar and solar perturbations.

- Extend the relative motion equations for analysis of formation flying missions for deep space missions with the sun as a central attracting body. This will include analysis of relative motion with parabolic or highly elliptical reference orbits.
- Development of controller algorithm using the relative motion equations and finding fuel optimal trajectories for formation keeping and reconfiguration.
- Assembly of complex spacecraft formations and the dynamics of separation
- Modelling the dynamics with Brower's equations rather than Gauss perturbation equations. In this way the method of formation flight dynamics analysis can be made fully analytical.

The method of analysis of spacecraft formation flight dynamics presented in this paper is based on a semi-analytical method where the actual dynamics is analyzed using the Gauss perturbation equations that require numerical integration. Instead of using the Gauss perturbation equations, the Brower's [38] equations can be used to make the method fully analytical. However the Brower's equations are only approximate solutions to the Lagrange's planetary equations and only show the change of orbital elements due to the effect of J_2.

At the time of writing this thesis, one of the research students of the Astronautics Research group, namely Riaz Ahmed has proposed a method based on the basic concept of the method developed in this thesis but with some differences. Instead of using the Gauss perturbation equations to simulate the effect of perturbative forces, he proposes to use Cowell's method to include perturbations. The idea of his method is to find the rate of change of orbital elements using the Cowell's method of orbit propagation and then substitute the values of the orbital elements in equations 3.3.11a-3.3.11c of this thesis. The advantage of using the Cowell's method is that there is no need to worry about any singularities in eccentricity and inclination occurring like in the standard version of the Gauss perturbation equations. The only disadvantage is that it needs the prior knowledge of the relative coordinates x, y, z in terms of the Geo-centric coordinates X, Y, Z and that requires some computational effort. This method is currently being evaluated for its accuracy and consistency with the method given in this thesis.

7.3 Conclusions

This thesis investigates the dynamics of formation-flying spacecraft by analyzing their relative trajectory in the presence of perturbative forces. In order to be able to analyze the relative trajectory, a novel method otherwise known as the orbital element method has been developed in which the equations of relative coordinates are dependent on the orbital properties of the formation flying spacecraft. The derivation of equations is a result of a series of Euler transformations and a translation from the Earth centered body frame to spacecraft centered rotating frame.

Traditionally, CW equations have been used to simulate relative trajectories of spacecraft. The CW equations are a linearized solution to the Hill's differential equations and are only accurate for a very short period of time. Also the CW method does not support analysis of elliptical reference orbits unlike the orbital element method developed in this thesis that supports analysis of any type of reference orbits.

The orbital element method incorporates all the orbital elements of the deputy and the master spacecraft, allowing easy dynamical modeling with the help of Gauss perturbation Equations. For maximizing the mission lifetime and minimizing fuel consumption, precise determination of coordinates is imperative and the orbital element method provides the necessary solution. The orbital element method also provides closed form analytical solutions that can be used for fuel optimization, analysis of trajectories without actual simulations and determining the orbital elements from the geometry of the formation pattern.

There are other methods like the Geometry method by Gim[12] and the COWPOKE method by Sabol[14] that are better than the CW method and can used to analyze the relative trajectory but they also suffer limitations due to the various assumptions made in their derivation. The Geometry and the COWPOKE methods include the effects of master spacecraft eccentricity, which the CW equations fail to consider but have limitations on spacecraft separation as they are derived with the assumption that the spacecraft in a formation are closely placed to one another. The orbital element method is derived with the least of assumptions and can be used to analyze any type of formation thus giving a general approach to the problem of formation

flight dynamics. With proper modeling, the approach presented in this thesis can be utilized to analyze behaviour of any formation patterns and their stability in the presence of perturbative forces. The orbital element method can also be used for designing the orbit controller algorithm and for finding the optimal orbit transfer for reconfiguration of formation flying satellites using appropriate formation flying sensors.

Bibliography

[1]. Paul. S Visher, United States Patent Office Number 4,375,697, http://patent.tange.dk/ziki/EP/7/8/EP787387.html

[2] Zink. M., Definition of the TerraSAR-L Cartwheel Constellation, ESA TS-SW-ESA-SY-0002, ESTEC, Noordwijk, 2003.

[3] S. Chien, B. Engelhardt, R. Knight, G. Rabideau, R. Sherwood, E. Hansen, A. Ortiviz, C. Wilklow, S. Wichman , "Onboard Autonomy on the Three Corner Sat Mission," Proceedings of the 2001 International Symposium on Artificial Intelligence, Robotics, and Automation for Space, Montreal, Canada, June 2001

[4] J.A.M. Bleeker and others, 'X-ray Evolving-Universe Spectroscopy - The XEUS Mission Summary' SP-1242, ESA Publications Divison, ESTEC, The Netherlands, ISBN No.: 92-9092-564-7, May 2000

[5]. Clohessy, W. H. and Wiltshire, R. S., "Terminal Guidance System for Satellite Rendezvous,"*Journal of the Aerospace Sciences*, Vol. 27, No. 5, 1960, pp. 653–658, 674

[6] Hill, G. W., "Researches in the Lunar Theory," *American Journal of Mathematics*, Vol. 1, No. 1, 1878, pp. 5–26, 129–147, 245–260.

[7] London, H. S., "Second Approximation to the Solution of the Rendezvous Equations," *AIAA Journal*, Vol. 1, No. 7, 1963, pp. 1691–1693.

[8] Anthony, M. L. and Sasaki, F. T., "Rendezvous Problem for Nearly Circular Orbits," AIAA Journal, Vol. 3, No. 7, 1965, pp. 1666–1673.

[9] Werlwas, R. W., A New First Order Solution to the Relative Motion Problem with Application to Intercept and Rendezvous, PhD thesis, Virginia Polytechnic Institute and State University, Blacksburg, VA, 1968.

[10] Berreen, T. F. and Crisp, J. D. C., "An Exact and a New First-Order Solution for the Relative Trajectories of a Probe Ejected From a Space Station," Celestial Mechanics, Vol. 13, 1976, pp. 75–88.

[11] Garrison, J. L., Gardner, T. G., and Axelrad, P., "Relative Motion in Highly Elliptical Orbits," Advances in the Astronautical Sciences, Vol. 89, No. 2, 1995, pp. 1359–1376.

[12] D.W.Gim, and K.T. Alfriend., "The State Transition Matrix of Relative Motion for Formation Flying Satellites ", Paper AAS 02-186, *2002 AAS/AIAA Space Flight Mechanics Meeting*, San Antonio, Texas.

[13] Kyle T. Alfriend, Hanspeter Schaub, Dong-Woo Gim, 'Gravitational Perturbations, Nonlinearity and Circular Orbit Assumption Effects on Formation Flying Control Strategies' Presented at the AAS/AIAA Space Flight Mechanics Meeting, 2000, Paper AAS 00-012

[14] Chris Sabol, Craig A. McLaughlin and K. Kim Luu. " Meet the Cluster Orbits With Perturnations of Keplerian Elements (COWPOKE) Equations. ''AAS/AIAA Space Flight Mechanics Meeting, Ponce, Puerto Rico, 9-13 February 2003, Paper AAS 03-138

[15] Chris Sabol, Rich Burns and Craig A. McLaughlin, " Satellite Formation Flying Design and Evolution", *Journal of Spacecraft and Rockets*, Vol. 38, No. 2. Mar.-Apr. 2001.

[16] Badesha, S. S., Heyler, G. A., Sharer, P. J., and Strikwerda, T. E., "Development of Formation Deployment and Initialization Concepts," In Flight Mechanics Symposium, Goddard Space Flight Center, May 1999.

[17] David F. Chichka, " Satellite Clusters with Constant Apparent Distribution", *Journal of Guidance, Control, and Dynamics*, Vol. 24, No. 1. Jan.-Feb. 2001.

[18] S. A. Schweighart, R. J. Sedwick, "A Perturbative Analysis of Geopotential Disturbances for Satellite Formation Flying," Presented at the IEEE Aerospace Conference, 2001.

[19]. Vadali, S. R., Vaddi, S. S., and Alfriend, K. T., "New Concept for Controlling Formation Flying Satellites," In *Space Flight Mechanics Conference*, Santa Barbara, California, February 2001.

[20]. Shankar K. Balaji, Adrian Tatnall 'System Design Issues of Small Formation Flying Spacecraft', *IEEE Aerospace Conference proceedings*, Montana, United States, March 2003

[21]. Shankar K. Balaji, Adrian Tatnall ' Relative Trajectory Analysis of Dissimilar Formation Flying Spacecraft', *Advances in the Astronautical Sciences, Vol.104, pages 531-544,* 2003

[22] Shankar Kumar Balaji, Adrian Tatnall, 'Precise Modelling of Relative Trajectory for Formation Flying Spacecraft' Paper No. IAC-03-A.P..15, *54th International Astronautical Congress,* Bremen , Germany, September 2003

[23] Shankar K. Balaji, Adrian Tatnall, ' Determination of Orbital Elements for Formation Assembly Problem' Paper No. 1515, IEEE Aerospace Conference, Montana, United States, March 2004

[24] Shankar K. Balaji, Adrian Tatnall and Riaz Ahmed, ' Closed Form Analytical Solutions For Spacecraft Formation Flying Relative Trajectory Analysis'. *4th International Conference on Satellite Constellations and Formation Flying'* Sao Paolo Brazil, February 2005.

[25]. Kraft A Ehricke.,*Space flight dynamics 11,D.V an Nostrand company,inc,*1962. page 678

[26] R.G. Melton, "Time-Explicit representation of relative Motion Between Elliptical Orbits," *AAS/AIAA Astrodynamics Specialists Conference,* Sunvalley, ID, Aug.1997.

[27] R.H.Battin, " An introduction to the Mathematics and Methods of Astrodynamics", *AIAA Education series*, Washingtion D.C. 1987.

[28] Figure showing the orbital element extracted from www.nasa.gov

[29] Vladimir.A.Chobotov, "Orbital Mechanics Second edition ", *AIAA Education series*, Washingtion D.C. 1996

[30] George W. Collins, 'The Foundation of Celestial Mechanics' *Pachart Foundation Publishing House,* June 1988

[31] Bo J. Nassz, 'Classical Element Feedback Control for Spacecraft Orbital Maneuvers'Presented as a Master's Thesis to the Virginia Polytechnic University, 2002

[32] Chao, C. C., Pollard, J. E., and Janson, S. W., "Dynamics and Control of Cluster Orbits for Distributed Space Missions," *Advances in the Astronautical Sciences*, Vol. 102, No. 1, 1999, pp. 355–374.

[33] Peter Fortescue, John Stark and Graham Swinerd., Spacecraft Systems Engineering, Third edition, *John Wiley & Sons Ltd*, 2003, pages 103-104

[34] Catlin, Kathryn A. "Satellite Formation Flight Using the Perturbed COWPOKE Equations." *AIAA Region V Student Conference*, Minneapolis, MN, April

[35] Jacobovits Vaneck, AeroAstro's Escort – A Microsatellite for On-Orbit Inspection of Space Assets, *17th Annual AIAA/USU Conference on Small Satellites*, 2003

[36] F.H. Bauer, K. Hartman, E.G. Lightsey, " Spaceborne GPS: Current Status and Future Visions," ION GPS-98, Nashville, TN, September 1998.

[37] C.L.Leonard, " Orbital Formation-Keeping with Differential Drag", *Journal of Guidance, Control, and Dynamics*, Vol. 12, No. 1. Jan.-Feb. 1989.

[38] Brouwer D., and G. Clemence, *Methods of Celestial Mechanics*, Academic Press, New York, 1961.

[39] Steve Chien, Paul Zetocha, '*The Techsat-21 Autonomous Space Science Agent*' International Conference on Autonomous Agents, Bologna, Italy 2002.

[40] D. E. Lencioni and D. R. Hearn, "New Millennium EO-1 Advanced land Imager" *International Symposium on Spectral Sensing Research*, San Diego, Dec. 13-19, 1997

[41] J.A.M. Bleeker and others, 'X-ray Evolving-Universe Spectroscopy - The XEUS Mission Summary' SP-1242, ESA Publications Divison, ESTEC, The Netherlands, ISBN No.: 92-9092-564-7, May 2000

[42] M. Warhaut, S. Matussi & P. Ferri, Cluster 11; Evolution of the operations Concept, ESA Bulletin, Volume 102, 2000

[43] Jesse Leitner, Hardware-in-the-loop testbed for spacecraft formation flying applications 2001 IEEE Aerospace Conference, Mar 10-17 2001
Volume 2, pp.615-620

[44] M. Campbell and T. Schetter, "Formation Flying Mission for the UW DawgStar Satellite," IEEE Aerospace Conference, Big Sky MT, March 2000

[45] M. Warhaut, S. Matussi & P. Ferri, Cluster 11; Evolution of the operations Concept, ESA Bulletin, Volume 102, 2000

[46] Steve Chien, Paul Zetocha, '*The Techsat-21 Autonomous Space Science Agent*' International Conference on Autonomous Agents, Bologna, Italy 2002.

[47] Chao, C. C., Pollard, J. E., and Janson, S. W., "Dynamics and Control of Cluster Orbits for Distributed Space Missions," Advances in the Astronautical Sciences, Vol. 102, No. 1, 1999, pp. 355–374.

[48].Kazuhisa Mitsuda, Hajime Inoue, 'Study of formation flying for the XEUS mission and the ISAS design of the ISAS design of the detector spacecraft' *Proceedings of SPIE*, March 2003

Appendix A

The following is the Algorithm for the Runge-Kutta Fehlberg Method.
Each Runge-Kutta-Fehlberg step requires the use of the following six values:

$$k_1 = h\, f(t_j, y_j)$$

$$k_2 = h\, f\left(t_j + \frac{1}{4}h,\ y_j + \frac{1}{4}k_1\right)$$

$$k_3 = h\, f\left(t_j + \frac{3}{8}h,\ y_j + \frac{3}{32}k_1 + \frac{9}{32}k_2\right)$$

$$k_4 = h\, f\left(t_j + \frac{12}{13}h,\ y_j + \frac{1932}{2197}k_1 - \frac{7200}{2197}k_2 + \frac{7296}{2197}k_3\right)$$

$$k_5 = h\, f\left(t_j + h,\ y_j + \frac{439}{216}k_1 - 8k_2 + \frac{3680}{513}k_3 - \frac{845}{4104}k_4\right)$$

$$k_6 = h\, f\left(t_j + \frac{1}{2}h,\ y_j - \frac{8}{27}k_1 + 2k_2 - \frac{3544}{2565}k_3 + \frac{1859}{4104}k_4 - \frac{11}{40}k_5\right)$$

Then an approximation is made using a Runge-Kutta method of order 4:

$$y_{j+1} = y_j + \frac{25}{216}k_1 + \frac{1408}{2565}k_3 + \frac{2197}{4104}k_4 - \frac{1}{5}k_5$$

And a better value for the solution is determined using a Runge-Kutta method of order 5:

$$z_{j+1} = y_j + \frac{16}{135}k_1 + \frac{6656}{12825}k_3 + \frac{28561}{56430}k_4 - \frac{9}{50}k_5 + \frac{2}{55}k_6$$

The optimal step size sh can be determined by multiplying the scalar s times the current step size h. The scalar s is

$$s = \left(\frac{\epsilon h}{2\,|\,z_{j+1} - y_{j+1}\,|}\right)^{1/4} = 0.840896\left(\frac{\epsilon h}{|\,z_{j+1} - y_{j+1}\,|}\right)^{1/4}$$

where ϵ is the specified error control tolerance.

Appendix B

Section 3.2.2 (Page 42)

$$x(t) = \left[\cos\left(\theta_{a0} + \int_t \frac{2\pi}{\left(2 - \left[\frac{v_a(t)}{v_0}\right]^2\right)^{-\frac{3}{2}} T_{a0}} dt\right) \cos\left(\theta_{b0} + \int_t \frac{2\pi}{\left(2 - \left[\frac{v_b(t)}{v_0}\right]^2\right)^{-\frac{3}{2}} T_{b0}} dt\right) + \sin\left(\theta_{a0} + \int_t \frac{2\pi}{\left(2 - \left[\frac{v_a(t)}{v_0}\right]^2\right)^{-\frac{3}{2}} T_{a0}} dt\right) \sin\left(\theta_{b0} + \int_t \frac{2\pi}{\left(2 - \left[\frac{v_b(t)}{v_0}\right]^2\right)^{-\frac{3}{2}} T_{b0}} dt\right) \right]$$

$$\frac{\mu / r_{b0}}{v_{b0}^2}\left[2\frac{F}{m}\frac{r_{b0}}{\mu / r_{b0}^2}(\omega_{b0}t - \sin\omega_{b0}t) + \left(\frac{v_{b0}^2}{\mu / r_{b0}} - r_{b0}\right)(1 - \cos\omega_{b0}t)\right] - \frac{\mu / r_{a0}}{v_{a0}^2}\left[2\frac{F}{m}\frac{r_{a0}}{\mu / r_{a0}^2}(\omega_{a0}t - \sin\omega_{a0}t) + \left(\frac{v_{a0}^2}{\mu / r_{a0}} - r_{a0}\right)(1 - \cos\omega_{a0}t)\right]$$

$$y(t) = \left[-\sin\left(\theta_{a0} + \int_t \frac{2\pi}{\left(2 - \left[\frac{v_a(t)}{v_0}\right]^2\right)^{-\frac{3}{2}} T_{a0}} dt\right) \cos\left(\theta_{b0} + \int_t \frac{2\pi}{\left(2 - \left[\frac{v_b(t)}{v_0}\right]^2\right)^{-\frac{3}{2}} T_{b0}} dt\right) + \cos\left(\theta_{a0} + \int_t \frac{2\pi}{\left(2 - \left[\frac{v_a(t)}{v_0}\right]^2\right)^{-\frac{3}{2}} T_{a0}} dt\right) \sin\left(\theta_{b0} + \int_t \frac{2\pi}{\left(2 - \left[\frac{v_b(t)}{v_0}\right]^2\right)^{-\frac{3}{2}} T_{b0}} dt\right) \right]$$

$$\frac{\mu / r_{b0}}{v_{b0}^2}\left[2\frac{F}{m}\frac{r_{b0}}{\mu / r_{b0}^2}(\omega_{b0}t - \sin\omega_{b0}t) + \left(\frac{v_{b0}^2}{\mu / r_{b0}} - r_{b0}\right)(1 - \cos\omega_{b0}t)\right]$$
